UNIVERSIDADE DA BEIRA INTERIOR
Engenharia

Airframe Assembly, Systems Integration and Flight Testing of a Long Endurance Electric UAV

Afonso Santos Rodrigues

Dissertação para obtenção do Grau de Mestre em
Engenharia Aeronáutica
(ciclo de estudos integrados)

Orientador: Prof. Doutor Pedro Vieira Gamboa

Covilhã, Fevereiro de 2017

Intentionally left blank

To Adelino and Elsa, my parents.

To Joaquina and Sofia, my sister and girlfriend.

Intentionally left blank

“Once you have tasted flight, you will forever walk the Earth with your eyes turned skyward, for there you have been and there you will always long to return.”

Leonardo Da Vinci

Intentionally left blank

Acknowledgments

This thesis is the result of 9 months I spent as a student in the Structures and Vibrations Laboratory of Prof. Pedro Gamboa in the Department of Aerospace Sciences at University of Beira Interior. This period was a very interesting and rewarding time, with many collaborations, and it was a pleasure to work in such environment.

First, I would like to thank my thesis advisor Doctor Pedro Gamboa of the Engineering Faculty at University of Beira Interior. The door to Prof. P. Gamboa office was always open whenever I ran into a difficult step or had a question about my work or writing. He consistently allowed this thesis to be my own work, but steered me in the right direction whenever he thought I needed it.

This thesis would not have been possible without the great help of Eng. Pedro Santos, and Eng. Alexandre Duarte. I would like to thank them very much because during the entire duration of this project, they taught me thousands of things in the domain of model aircraft.

I would also like to thank in particular my fellow Pedro Moutinho for conducting the majority of the LEEUAV flight tests performed and also for helping me throughout this work.

Finally, I must express my very profound gratitude to my parents and to my girlfriend for providing me with unfailing support and continuous encouragement throughout my years of study and through the process of researching and writing this thesis. This accomplishment would not have been possible without them. Thank you.

Intentionally left blank

Resumo

A necessidade de adoção de novas técnicas e práticas no ramo da Indústria Aeronáutica é uma consequência do desenvolvimento tecnológico. O presente trabalho aborda o uso de energia solar como principal fonte de energia na aviação, com enfoque num voo de grande autonomia de uma aeronave não tripulada. Esta tese de mestrado surge na sequência de trabalhos anteriores relativos ao LEEUAV, nos quais se efetuou o projeto e construção de uma aeronave não tripulada de grande autonomia. Assim, o principal objetivo deste trabalho é a integração de sistemas, testes de voo e validação de conceitos.

O UAV Solar LEEUAV é um protótipo de 4.5 metros de envergadura e de estrutura ultraleve parcialmente coberto de células fotovoltaicas sendo projetado para cumprir uma missão de voo contínuo de pelo menos 8h no equinócio. O avião de 5.42kg foi testado com sucesso mostrando a concordância com os cálculos teóricos já elaborados. O voo mais longo conseguido foi de 3.13 horas correspondendo a uma distância total percorrida de 96.265 km.

De modo a validar o conceito de aeronavegabilidade do LEEUAV foram efetuados vários voos de teste e recolhidos dados de voo (pressão estática e dinâmica, temperatura do ar, velocidade no solo e ângulo de arfagem) para posterior análise, utilizando um controlador de voo com múltiplos sensores a bordo. A análise dos resultados obtidos permitiu precisar o desempenho geral da aeronave, os principais defeitos, concordância com os resultados teóricos assim como determinar os valores reais dos coeficientes aerodinâmicos (C_L, C_D) através de um algoritmo de leitura e processamento de dados de voo, em Software MATLAB.

Por fim, são referidas algumas sugestões para o desenvolvimento de novos trabalhos com o objetivo de tornar O LEEUAV num veículo aéreo não tripulado de referência.

Palavra-chave

UAV Solar, Energia Solar, Voo Sustentável, LEEUAV, Indústria Aeronáutica, Células Fotovoltaicas, Propulsão Elétrica, Validação de Conceitos, Desempenho Aerodinâmico.

Intentionally left blank

Abstract

The need to adopt new techniques and practices in the Aerospace Industry branch is a consequence of technological development. The present work aims to study the use of solar power as a main energy source in the aviation, in this case for a flight of long endurance of an unmanned air vehicle. This master thesis follows on previous works of the LEEUAV, where it was done the design and construction of a long endurance unmanned aerial system. Thus, the main objective of this work is the systems integration, flight testing and concepts validation.

LEEUAV, a prototype of 4.5 meters' wingspan and ultralight structure partially covered by solar cells was designed to fulfil a continuous flight mission of at least 8 hours on the equinox. The 5.42Kg remotely piloted aircraft was successfully tested showing the agreement with theoretical calculations already made. The longest flight achieved lasted more than 8.5 hours' resulting in a total distance travelled of more than 75 km.

In order to validate the airworthiness concept of the LEEUAV several flight tests were performed and their respective data (static and total pressure, air temperature, ground speed and pitch angle) was collected for further analysis, using a flight controller with multiple sensors on board. The results obtained allowed to study the general performance of the aircraft, the main defects, agreement with the theoretical results as well as determine the real values of aerodynamic coefficients (C_L, C_D), through a reading and processing flight data algorithm in Software MATLAB.

Finally, some future expectations for upcoming work are suggested in order to make the LEEUAV an Unmanned Aerial Vehicle of reference.

Keywords

Solar UAV, Solar Energy, Sustainable Flight, LEEUAV, Aeronautical Industry, Photovoltaic Cells, Electric Propulsion, Concepts Validation, Aerodynamic Performance.

Intentionally left blank

Contents

Intentionally left blank

List of Figures

List of Tables

Intentionally left blank

Nomenclature

η_{prop}	Propeller Efficiency
C_D	Drag Coefficient
C_{Dind}	Induced Drag Coefficient
C_{Dpar}	Parasite Drag Coefficient
C_f	Friction Coefficient
E_{Diss}	Dissipative Energy [J]
E_{Kin}	Kinetic Energy [J]
E_{mec}	Mechanical Energy [J]
E_{pot}	Potential Energy [J]
F_{form}	Form Factor
I_{max}	Maximum Sun Irradiance [W/m^2]
M_{plr}	Resistance Moment [Nm]
P_e	Electric Power [W]
P_{req}	Required Power [W]
P_{shaft}	No-load Power [W]
S_{ref}	Reference Wing Area [m^2]
S_x	Surface Deflection Angle [°]
v_G	Ground Speed [m/s]
v_{air}	Airspeed [m/s]
h	Altitude [m]
AR	Aspect Ratio
C	Charge/Discharge Rate
C	Battery Capacity [mAh]
Ch	Transmission Channel
D	Drag Force [N]
I	Current [A]
L	Lift Force [N]
P	Power [W]
Q	Interference Factor
RC	Rate of Climb [m/s]
Re	Reynolds Number
T	Thrust Force [N]
T	Torque [Nm]
U	Voltage [V]
W	Weight [N]
b	Wingspan [m]
c	Wing chord [m]
e	Oswald Efficiency Factor
m	Mass [kg]
t	Time [s]
V	Speed [m/s]
α	Angle of Attack [°]
β	Slideslip Angle [°]
γ	Path Angle [°]

δ	Thrust Setting
η	Efficiency
μ	Air Dynamic Viscosity [Ns/m^2]
ρ	Air Density [kg/m^3]
ω	Angular speed [rad/s]

Acronyms

A.C.	Aerodynamic Centre
AEROG	Aeronautics and Astronautics Research Centre (UBI)
AGL	Above Ground Level
ALT	Altitude
AM	Air Mass
AM	Amplitude Modulation Signal
ARM	Advanced RISC Machines
BET	Blade Element Theory
BFS	Backward Facing Step
BLDC	Brushless Direct Current
CAD	Computer Aided Design
CATIA	Computer Aided Three-Dimensional Interactive Application
CCTAE	Centro de Ciências e Tecnologias Aeronáuticas e Espaciais (IST)
C.G.	Centre of Gravity
CNC	Computer Numerical Control
DARPA	Defense Advanced Research Projects Agency
DC	Direct Current
DCA	Department of Aerospace Sciences
DDD	Dull, Dirty or Dangerous Category
DLR	German Research Institute for Aviation and Space Flight
DoD	U.S. Department of Defense
DVR	Digital Video Recorder
EMI	Electromagnetic Interference
ERAST	Environmental Research Aircraft and Sensor Technology
ESC	Electronic Speed Controller
FAA	Federal Aviation Administration
FBWA	Fly by Wire A
FEM	Finite Element Method
FEUP	Faculdade de Engenharia da Universidade do Porto
FFS	Forward Facing Step
FM	Frequency Modulation Signal
FPV	First Person View
GCS	Ground Control Station
GLONASS	Global Navigation Satellite System
GNSS	Global Navigation Satellite System
GPS	Global Positioning System
GUI	Graphical User Interface
HALE	High Altitude Long Endurance
HALSOL	High Altitude Solar Project
HUD	Head Up Display
IAS	Indicated Airspeed
IDMEC	Instituto de Engenharia Mecânica (IST)
INEGI	Instituto de Ciência e Inovação em Engenharia Mecânica e Industrial

INS	Inertial Navigation System
IR	Infrared Radiation
IST	Instituto Superior Técnico
JST	Japan Solderless Terminal
LAETA	Laboratório Associado de Energia, Transportes e Aeronáutica
LCD	Liquid Crystal Display
LEEUAV	Long Endurance Electric Unmanned Aerial Vehicle
MALE	Medium Altitude Long Endurance
MIT	Massachusetts Institute of Technology
MP	Mission Planner Software
MPP	Maximum Power Point
MPPT	Maximum Power Point Tracker
NASA	National Aeronautics and Space Administration
NATO	North Atlantic Treaty Organization
NREL	National Renewable Energy Laboratory
OSD	On Screen Display
PDU	Power Distribution Unit
PM	Power Module
PPM	Pulse-Position Modulation Signal
PWM	Pulse-Width Modulation Signal
RC	Radio Control
RPAS	Remotely Piloted Aircraft System
RPM	Rotations Per Minute
RSSI	Received Signal Strength Indication
RTL	Return to Launch
SBAS	Satellite Based Augmentation System
SBUS	Serial BUS
SCC	Solar Charge Controller
SD	Secure Digital (Card)
SIT	System Integration Testing
TAF	Tests After Flight
TAS	True Airspeed
TBF	Tests Before Flight
TIF	Tests In Flight
TOW	Take-off Weight
UAS	Unmanned Aerial System
UAV	Unmanned Aerial Vehicle
UBEC	Ultimate Battery Eliminator Circuit
UBI	Universidade da Beira Interior
UHF	Ultra-High Frequency
USA	United States of America
USB	Universal Serial Bus
VDC	Video Diversity Controller

Chapter 1

1 Introduction

1.1 Motivation and Objectives

The demand for more efficient means of transport is an increasingly widespread reality due to the need to preserve the environment for the sustainability of future generations. It is known that the long-term consumption of energy derived from fossil fuels will become unsustainable.

The ability for an aircraft to fly during an extended period of time has become a key issue and a target of research all over the world. Both manned and unmanned aviation is taking an increasingly important place in our society, to meet the needs of civilian and military areas. Regarding the unmanned aviation, the required endurance for law enforcement, border surveillance, forest fire fighting or power line inspections are in the range of a couple of hours. However, for other applications at high altitudes, such as communication platforms for mobile devices, weather research and forecast, environmental monitoring, require the craft to remaining airborne for days, weeks or even months.

At present, external sources of power are required for this type of flight endurance, using for example, solar powered platforms or refuelling the aircraft.

Using photovoltaic modules to collect energy from the sun, during the day time, allows solar aircraft to use part of the energy to fly and store the surplus of energy for the night flight.

Using cutting-edge technology some recently solar powered airplanes are being designed to fly near space, i.e., above the common atmospheric flight region and below the spacecraft flight region (approximately 20–100 km). Future solar unmanned aircraft vehicles (UAVs) projects claim that they will be able to fly continuously for months, or even years, depending on the reliability of the airplane system and sunlight conditions, something which is impossible with traditional, fossil-fuelled airplanes. Solar-powered airplanes can function as complement to low-altitude satellites, with the advantage of having a relatively low altitude, free deployment, high resolution, high frequency of coverage, and low cost.

Solar-powered airplanes can also function as an alternative to high-altitude balloons and airships, with the advantage of having free-manoeuvre capability, high resilience to weather, as well as being easy to launch and recover. Compared with low-altitude airplanes, solar-powered airplanes have the advantage of reaching relatively high altitudes and covering large areas [1].

The present work is a result of a three-year collaborative research project involving two higher education universities, UBI and IST, which form part of three research units that follow the line of research of Aeronautics and Space of Associated Laboratory for Energy, Transports and Aeronautics (LAETA), namely Centre for Aerospace Science and Technology (CCTAE), Aeronautics and Astronautics Research Centre (AEROG), Institute of Mechanical Engineering

(IDMEC) and Institute of Science and Innovation in Mechanical and Industrial Engineering (INEGI). The LEEUAV was decided upon in a consortium meeting, having in mind the ultimate goal of creating a vehicle capable of flying for at least 8 hours at the equinox with low power requirements and carrying a payload of up to 1kg. The mission profile also requires a short take-off and landing distance, high flight altitude (at least 1000 meters) and a descent without power.

This work follows the need to search for, test and validate new techniques and practices in the aviation area such as the use of solar energy in UAVs. This thesis aims to validate the concept of an unmanned airplane that gets most of its energy from solar irradiance.

The main objectives of this work are to:

- Learn about the concepts inherent to unmanned solar flight aircraft;
- Finish the LEEUAV airframe and systems integration;
- Plan LEEUAV missions;
- Perform flight and ground tests;
- Analyse LEEUAV's aerodynamic performance;
- Compare the theoretical results with practical results;
- Draw conclusions about the results achieved.

1.2 History of Solar Powered Flight

1.2.1 Photovoltaic effect and solar cell

Since the 7th century B.C. solar energy has been used in different ways, such as the use of bronze shields, to focus the sunlight onto wooden ships so that they were set alight or for astronomical and illumination purposes. In 1839 Edmond Becquerel discovered the photovoltaic effect while experimenting with electrolytic cells and later in 1921 Albert Einstein received the Nobel Prize for explaining this process [2].

The first photovoltaic cell based on the photoelectric effect was created in 1888 by Aleksandr Stoletov, but it was unpractical. Then in 1954 Bell Laboratories announced the invention of the first practical silicon cell with an efficiency of 4%, converting enough energy of the sun's irradiance to power some electrical equipment, but it was unused until the 1960's, when NASA began to use it to power its space craft's [2].

As the space industry evolved so did the photovoltaic technology and both efficiency and reliability was improved. During the oil crisis in the 1970's photovoltaic cells became recognized as an alternative energy source but sadly the interest for greener energy alternatives declined as the price of oil fell.

1.2.2 The Combination of Electric Flight and Solar Cells

Electric flight was not discovered in this century neither in the last decades but it has currently been on the radar of researchers. In the 1880s a couple of French army officers named

Renard and Krebs equipped a hydrogen-filled dirigible, La France, with huge batteries and an 8-horsepower electric motor that enabled it to do what no balloon had ever done before: return to its launch site at the end of a flight, taking the lead over the existing steam engine [3]. Since La France, many other flights of model electric aircraft were attempted, as with German pioneer Fred Militky, who first achieved a successful flight with an uncontrolled model aircraft in October 1957 [4]. Since then, better model airplanes have been developed with the improvements in the field of motors and batteries [5]. Electric propulsion in manned airplanes was abandoned for the following 90 years.

The combination of electrical flight and solar cells was just made in 1970 decade by Robert Boucher, a pioneer that used electric motors for model airplanes, building a couple of pilotless solar-powered aircraft under contracts with the Defence Advanced Research Projects Agency [4].

Despite the existence of solar powered RC aircraft, the first manned electrically powered flight was made in 1973, where Fred Militky and Heino Brditschka converted a Brditschka HB-3 motor glider to an electric powered aircraft, the Militky MB-E1. The full size manned aircraft flew solely under electric power for 14 minutes, with a 10kW electric motor powered by Ni-Cd batteries [6].

At present, the endurance of an electric aircraft is very low, when compared to the internal combustion engine. This fact lies in the high energy required by electrical flight, which in turn, results in weight and space restrictions as well as high density batteries. The combination of electric flight and solar cells has become very useful once that the battery's size and weight can be reduced by applying solar cells, and thus, allowing long endurance flights.

Following the re-introduction of the electric powered flight, many experimental and commercial electric aircraft have been created since the 70's, searching for better results, namely in the endurance and efficiency fields. In world history, before 90's, the inexistence of high density batteries had led to the abandonment of electric aviation.

However, as soon as the high-density lithium-ion batteries were commercialized the existence of electric aircraft flying without any external source of power become a reality. Presently, the average maximum flight endurance of an electric aircraft, without external sources of power, is about 3 hours on gliders.

1.2.3 Early stages of Solar Aviation

After two more decades since the invention of the first photovoltaic cell, in November 4th 1974 R.J. Boucher from Astro Flight Inc. achieved the first solar powered flight with the airplane Sunrise I. Since that day many more solar powered aircraft have been built and improved but very few have been put into commercial use. The Sunrise I had a wingspan of 9.76m and weighed 12.25kg with 4096 solar cells over the wings capable of producing a 450W power output [3]. The inaugural flight lasted 20 minutes at an altitude of 100m, but further flights achieved almost four hours of continuous flight. Despite the short lifetime of the Sunrise

I caused by a serious damage during a sandstorm, the Sunrise II was even better weighting less and containing more efficient solar cells. After weeks of testing the Sunrise II also got damaged due to a failure in the command and control system. Despite all these incidents with the first solar aircraft, the solar flight has proved to be reliable.

Figure 1 - Sunrise I (1974) and Solaris (1976) [3]

In Europe, Fred Militky developed a solar aircraft project named Solaris in 1976 and on 16th of August of the same year, it successfully completed three flights of 150 seconds at an average altitude of 50m [4]. With the foundations implemented, the solar flight era was launched. Since then, thanks to technology development and the emergence of more efficient solar cells, many solar powered model aircraft have been built. Nevertheless, the general flight endurance of model aircraft was short until the 1990s when Wolfgang Schaeper achieve the official record with Solar Excel aircraft: flight duration of (11h34m), total distance of (190 km), at an altitude (2065 m) with medium speed of (62.15km/h) [7].

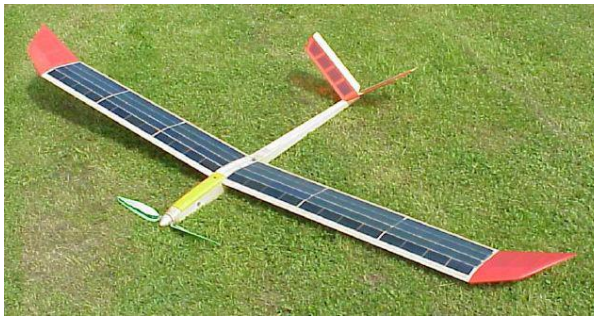

Figure 2 - Solar Excel (1990) [3]

1.2.4 Manned Solar Flight

After all the efforts to successfully produce the solar powered aircraft, the new challenge that fascinated the pioneers at the end of the 70's was manned flights powered solely by the sun.

As stated above, the first manned electrical flight, completed in 1973 by Fred Militky and Heino Brditschka, had a very low flight endurance and it eventually became unusable [6]. In order to accomplish the feat of increasing the endurance of the electrical powered flight, on 29th of April 1979, Larry Mauro built Mauro Solar Riser, the first solar-powered man-carrying aircraft. Solar Riser was an UFM Easy Riser biplane hang-glider, that used photovoltaic cells

capable of producing 350W at 30V. The solar charge of 1.5 hours was enough to power the aircraft for 3-5 minute, enabling it to reach a gliding altitude [3].

On the 19th of December 1978, Britons David Williams and Fred To launched Solar One on its maiden flight at Lasham Airfield, Hampshire. The Solar One was a motor-glider aircraft originally built as a pedal-powered airplane to attempt the Channel crossing. The airplane proved too heavy to be successfully powered by human power and was then converted to solar power, using an electric motor driven by batteries that were charged before flight by a solar cell array on the wing. The maiden flight of Solar One took place at Lasham Airfield; Hampshire on June 13, 1979 [6,8].

Figure 3 - Gossamer Penguin (1980) and its successor, Solar Challenger (1981) [3]

Looking for better endurance results Dr. Paul B. MacCready and Aerovironment Inc demonstrated, on August 23, 1977, the first sustained and manoeuvrable human-powered flight with the Gossamer Condor. After that , on the 12th June 1979, they completed the crossing of the English Channel with the human-powered Gossamer Albatross (second version of Gossamer Condor), Dr. MacCready created the third version of Gossamer, the Gossamer Penguin, which resulted in a 3/4 scale version of the original Gossamer, converted it into a man-carrying solar plane. On the 18th of May 1980, the Gossamer Penguin, with MacCready's 13 years old son Marshall on board, realized what can be considered as the world's first piloted solar powered flight in Europe.

Despite the Gossamer Penguin having shown good results in the early stages of solar aviation, flying at high altitudes was not safe for the pilot. In order to conquer the English Channel crossing with a solar powered airplane, with some sponsors, MacCready built the Solar Challenger which was a 14.2m wingspan, high-wing aircraft with 16128 solar cells producing 2500W at sea level. On July 7, 1981, the Solar Challenger flew for 5 hours traveling a total distance of 163 miles from Paris to London, under solar-power at an altitude record of 14.300 feet.

At the same time of the English conquest with Solar Challenger, a competitor in Germany Günther Rochelt constructed a canard design aircraft with 2499 wing-mounted solar cells, which produced an output power of 1.8kW. His objective was to accomplish exactly the same performance (crossing the English Channel), but he only succeeded on the 21th of August 1983

[3]. The Solair I crossed the English Channel using electric power mostly from solar energy and thermals, which are currents of hot air that help the aircraft to climb.

In 1986, after a meeting with Günther Rochelt, in the United States, Eric Raymond started designing the Sunseeker, which has become his own manned solar powered aircraft in 1989. In August 1990, Sunseeker crossed the USA in 21 solar powered flights with 121 hours in the air [9].

Figure 4 - Icaré 2 (1996) and Solair II (1998) [3]

In Ulm, Germany, there is a competition named Berblinger Prize in tribute to the first aeronautical pioneer to employ the principle of gliding flight. The Berblinger Prize [10] is awarded for special efforts, developments and innovative ideas in the construction of aviation devices in the field of general aviation. In the 1996 event, the prize to develop a real, practically usable solar aircraft, capable of staying airborne with at least half of the solar energy in a clear summer day, was won by Prof. Rudolf Voit-Nitschmann from Stuttgart University with Icaré 2, a world record breaking solar plane [11]. Through the years there have been several other solar powered airplanes to participate in this competition, as Solair II and Sole Mio, demonstrating the new technological applications and improvements in the various areas.

1.2.5 Long Endurance Platforms and Eternal Flight

With the purpose of creating a long endurance flight aircraft, AeroVironment Inc. funded by US government, created the first prototype HALSOL but the project was abandoned once seeing that the existing system technology, mainly the energy storage, was inadequate for this type of mission. Thus, the project took the direction of solar propulsion with the Pathfinder which achieved its first flight at Dryden in 1993. In 1994, the Pathfinder became part of NASA's Environmental Research Aircraft Sensor Technology (ERAST) and in 1995, it exceeded Solar Challenger's altitude record for solar powered aircraft when it reached an altitude of 15392m. In 1998, Pathfinder was upgraded for Pathfinder Plus, which had a larger wingspan and new solar, aerodynamic and propulsion systems technologies. The purpose of Pathfinder Plus was to validate the concept of its successor, the Centurion.

The Centurion was considered to be the base prototype technology for the following years of solar aviation [12]. With the double wingspan of Pathfinder, it was capable of carrying

45kg of remote sensing and data collection instruments for use in scientific studies and also 270kg of sensors, telecommunications and imaging equipment for up to 24400m of altitude. The Pathfinder lithium battery provided enough energy to power the airplane for a five-hour flight after sunset, but this was insufficient to fly during the entire night.

Figure 5 - Centurion (1997-1999) and Helios (1999-2003) [13]

The last prototype of the series designated as Helios was intended to be the ultimate "eternal airplane", incorporating energy storage for night-time flight. For NASA, the two primary goals were to demonstrate sustained flight at an altitude near 30480m (100000ft) and flying non-stop for at least 24 hours, including at least 14 hours above 15240m (50000ft). In 2001, Helios achieved the first goal near Hawaii with an unofficial world-record altitude of 29524m (96863 ft) and a 40-minute flight above 29261m (96000 ft). Unfortunately, it never reached the second objective as it was destroyed when it fell into the Pacific Ocean on June 26, 2003 due to structural failures [13].

In Europe, some developments were also made, for example the Solitair aircraft developed by DLR Institute of Flight Systems which had the particularity of having adjustable solar panels for optimum solar radiation absorption [14]. On the other hand, to prove the feasibility of high altitude long endurance (HALE) flight, more aircraft such as the Heliplat and the Solong were tested, the last in June of 2005 with just 4.75m wingspan and 11.5kg of MTOW flew for 48 hours and 16 minutes in California's Colorado Desert [15].

In 2001, a British company named QinetiQ proved to be very active in the field of solar HALE platforms with its Zephyr 6 aircraft that broke the official world record flight time of an unmanned aircraft with a 54-hour flight in New Mexico on the 10th of September 2007, reaching a maximum altitude of 17786m (58355ft) [16]. After Zephyr 6 established the record of the longest flight time, it did not take long for the British company to present more ambitious goals, in particular, the creation of a HALE platform with a capacity of carrying a 100kg payload in order to fulfil some missions such as forest monitoring, urban mapping, coastal monitoring, electric cable inspections and others.

After 2009 more amazing feats were achieved, in 2003, a well-known project named Solar Impulse started in Switzerland, aiming to be the first manned aircraft making the circumnavigation of the Earth using just solar energy as its source of power. In December 2009, it flew for the first time and in July 2010 Piccard and Borschberg completed successful solar-

powered flight from Switzerland to Spain lasting 26 hours. Shortly afterwards, in 2016, the manned solar-powered airplane Solar Impulse 2, completed the circumnavigation of the Earth [17].

1.3 State of the Art

To establish the state of the art of solar airplane field, in this section of the document the most advanced current practices, projects and future ambitions for solar powered airplanes are listed.

In 2007, The Defence Advanced Research Projects Agency (DARPA) of United States with the cooperation of Boeing Phantom Works proposed a featured HALE project, named DARPA's Vulture air vehicle program intended to create a solar aircraft weighting 453kg which would be able to fly for periods of up to five years [18]. The big advantage of this project lay in the capacity to operate as a very low altitude satellite platform allowing dramatic increases of sensors resolution, better mapping capacities as well as improving the communications range and feasibility as it circumnavigates the Earth several times during its 5-year journey. However, the DARPA Vulture project was cancelled in 2012 [19].

Figure 6 - DARPA Vulture (2012) and Solar Impulse II (2014) [17,19]

Even before the Solar Impulse I had successfully completed its first intercontinental flight in 2012, the Solar Impulse II had started being built in 2011, but a structural failure of the aircraft's main spar occurred during static tests in July 2012, delaying the flight tests. On 2nd June 2014, the Solar Impulse II, a 71.9m wingspan aircraft weighting 2300 kg completed its first flight and months later on 9th March 2015 it set off on its circumnavigation of the Earth, composed by 17 stages starting and finishing at Abu Dhabi. On 26th July 2016, the Solar Impulse II completed its 43041km journey around the world and set many records, such as the 5663km flight and the longest non-stop solo flight of 117 hours without refuelling [17].

The Solar Flight company is a solar powered aircraft producer that has already proved its value with the Sunseeker Duo, which is a two-person airplane that is able to cruise directly on solar power with two people on board for at least 12 hours, thanks to its 1510 high efficiency solar cells. The same company is also developing another manned solar aircraft, the Sunstar aiming to achieve the lowest power requirements to fly for months or even years. After reaching

cruise altitude, the Sunstar's three motors stop and the propellers fold back to decrease the drag [20].

Figure 7 - Sunseeker Duo (2013) and Sunstar (under development) [9]

After buying the program from QinetiQ in 2013, Airbus Defence & Space is now working on the Zephyr 8, the latest version of a record-breaking series aircraft with an ultra-lightweight airframe designed to loiter slowly over an area of interest at up to 70000ft. The Zephyr 8, like its previous version has the capability to fully charge its batteries from the sunlight during the day and maintain the same altitude at night. With 30% less weight and 50% more battery capacity, Airbus says that the Zephyr 8 can stay airborne for at least a month [21].

The giant social media Facebook has unveiled a prototype of a solar-powered UAV designed to fly above 60000ft for more than three months. Aquila is a carbon-fibre light weight aircraft whose mission is to provide Internet connectivity, through a laser-based communication, to remote locations of the world. On 21th July of 2016 the full-scale Aquila prototype made its first 90-minute flight allowing the verification of the general aircraft performance through several tests [22,23].

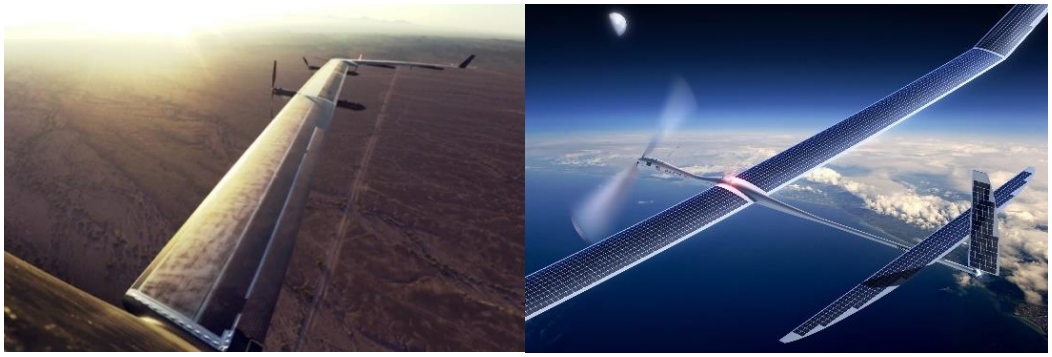

Figure 8 – Facebook Aquila (2016) and Google's Solara 50 [23,24]

It did not take much time before the giant Google bought out the American company, Titan Aerospace, which is currently working on Solara 50 and 60 aircraft. The Solara is a solar powered UAV project which intends to create a HALE platform that works as a satellite, allowing to monitor a significant number of meteorological events as well as provide solutions for agricultural applications, asset tracking, pipeline monitoring, search and rescue, disaster recovery, fire monitoring, etc. [24].

In the Autonomous Systems Lab (ASL) of ETH Zurich an unmanned solar aircraft project, the AtlantikSolar was created with the main objective of being the first fully solar powered aircraft to cross the Atlantic Ocean, a journey of 5000km and 7 days of continuous flight. This 5.6m wingspan aircraft has already proved its value by successfully completing an 81-hour continuous flight [25]. On the other side of the world, a USA company named Silent Falcon, has been developing the Silent Falcon UAV. With a wingspan of 4.4m and a MTOW of 142N, the Silent Falcon is capable of flying continuously for 7h [26].

Figure 9 - Silent Falcon UAV and AtlantikSolar [25,26]

1.4 Present and Future UAV Applications

In order to highlight the importance of solar powered UAVs, this section includes some applications that clearly justify all the research around the world in this particular area of aviation.

Solar-powered airplanes are suitable to perform various missions and applications not only for civilian recreation but also in military and commercial fields. Following this line of thinking the UAV applications can be subdivided into three main areas: Civilian, Commercial and Military area.

The most diffused area is probably the Civilian one, where the small UAVs commonly known as “drones”, are in an exponential growth. Although there is no exact data for the “commercialization boom” of civilian UAVs, they have been seen on the market since early 2008. The applications in the civilian world are mainly focused on personal entertainment, however, other uses such as mapping, private surveillance, aerial photography, shows and events also form part of civilian applications.

In regards to the commercial field, the UAV market is under development and the applications are growing remarkably. Each day new applications are found or suggested by the companies. Presently, UAVs can be seen in areas of agriculture where they are used for sowing, spraying of insecticides, plant growth verification and problems identification. Even though the Federal Aviation Authority (FAA), European Aviation Safety Agency (EASA) and other aviation authorities are stablishing restricted rules in relation to unmanned aviation, some companies continue to join efforts in order to improve the applicability of UAVs in our daily lives by using them as fast air-mail carriers for small packages, for inspection of electric lines, ground recognition or mapping applications.

Figure 10 – DHL Package delivery and medical emergency drones [30]

Still within commercial area, UAVs have proven to be very helpful in some social and community security applications such as combat and fire monitoring, anti-theft control, coastal surveillance, surveillance of crowds, disaster monitoring mapping, pollution, nuclear observations and accident contamination measurement, tracking of volcanic ash clouds, Illegal activity control and maritime surveillance. Many of these applications fall within the category of dull, dirty, or dangerous (DDD) aerial work and are associated with high risks and costs [27], making the UAVs a problem-solving application.

Although today there is a widespread use of UAVs in our daily lives, it all started in the military area in 1849 when the Austrian Army sent unmanned bomb-filled balloons to attack Venice. Since then, improvements and enhancements have been made in the field of UAVs [28]. Today they are used by the majority of air forces armies all over the world and according to Unmanned Aerial Vehicles Systems Association (UAVS), the UAVs applications can be separated in security (serial crowd monitoring, traffic and security watch), search and rescue (maritime and mountain), monitoring (waterways, oil and gas pipeline, fishery protection, surveillance missions and borders monitoring), disaster management (disaster effects management and damage estimation and rescue) and communications and munitions [29].

Speaking a bit of the UAVs future applications, they are expected to be found in humanitarian work, delivering vaccines and other critical medical supplies to remote locations in the developing countries as is the case of Bill and Melinda Gates Foundation UAV project, currently under development at the Massachusetts Institute of Technology (MIT). Expanding internet access is another amazing goal, Facebook Inc. is financing a project whose main objective is to create a perpetual solar flight aircraft capable of amplifying the internet signal from satellites to some remote areas in the world where internet access is very weak or inexistent.

In Netherlands, a student has revealed a prototype of an “ambulance drone”, a flying defibrillator able to reach heart attack victims within precious life-saving minutes, making it a probably future application.

From a long-term point of view, there are other ambitious challenges for UAVs applications, such as [30]:

- Early warning systems (the use of UAVs to prevent and warn about natural disasters as earthquakes, hurricanes, tornados, avalanches, tsunamis and forest fires);

- Emergency services (acting as a tracking device using different sensors to find a missing child, tracking animals in danger or just looking for danger situations in a city);
- News reporting (accident monitoring, weather time-lapse, aerial photography and direct interview ability);
- Delivery (medical, mail, package and grocery deliveries and send-it-back returns);
- Business activity monitoring (construction monitoring, topological surveying, instant environmental impact assessment, power line monitoring and geological surveying);
- Marketing (spot advertising, multimedia formations, etc.);
- Policy UAVs (domestic violence monitors, neighbourhood watch and surveillance);
- Smart home UAVs (home security);
- Science and discovery (animals watching, ocean currents monitoring, aurora borealis inspecting, archaeology among others);
- Gaming, entertainment, educational, health care and sport, among others.

The purpose of composing this rather exhaustive list is not an attempt to cover everything, but to show the enormous versatility of this platform.

1.5 LEEUAV Project

This small section is intended to contextualize the current work in the LEEUAV project timeline through a short review of each phase.

It all started with the idea of creating a long flight and environmentally reliable platform, capable of flight for more than 8 hours at the equinox with the minimum environmental impact. In LAETA, with the co-operation of CCTAE and IDMEC from IST, the AeroG from UBI and INEGI, the LEEUAV's preliminary and conceptual design was carried out by UBI whose main objectives and tests were successfully achieved by Luís Cândido [31]. In that work the main aircraft characteristics and structures, including the fuselage, tail and wing were suggested and designed. In a second phase of Luís Cândido work a pre-prototype with a polystyrene wing was built in order to analyse the behaviour of the conceived aircraft flight structures and the performance of the wing airfoil.

The work of Tiago Ferreira [32] from IST, comprised the design, test and evaluation of a possible LEEUAV propulsion system. In 2015, Joana Sousa's master thesis [33] proposed to validate the LEEUAV's solar propulsion system, as well as simulate the possible flight conditions and determine the global efficiency to predict the best fixing position of the solar panels on the wing. A work done by Alexandre Duarte [34] consisted of design, analyse and built the carbon fibre fuselage, tail boom and control surfaces of LEEUAV.

With the airframe and wing built, the present work is about to test and analyse the LEEUAV's flight performance. However, before flight there were a set of tasks that have to be performed in order to safely fly the LEEUAV, such as the integration of all electronic components and their functional tests. Furthermore, several hazards, such as the loss of roll

control at low airspeeds, tip stall tendency while turning and unstable spiral mode were detected during pre-prototype flight which forced to modify the existing wing tip by applying a washout of 4.5 degrees and an adequate endplate preventing the detected wing tip stall.

At the same time, two other works were done, namely the influence of the solar panels thickness in the low speed airfoil of the LEEUAV by Luís Freitas [35] and the real-time streaming of solar energy system data by Pedro Moutinho [36]. The first work provided the most suitable position for the fixation of the solar panels in the wing, i.e., the position where the drag caused by solar panels is lower and consequently the lift-to-drag ratio is higher for the designed LEEUAV cruise speed. The second one, also very important, aimed to stream the energy consumed by the motor/systems and the energy produced by photovoltaic panels during the flight to the ground control station and further based on the on-board stored energy estimate the remaining flight time.

1.6 Structure of this Work

After a quick introduction of the main goals of this work, the document was written with a logical order to facilitate the comprehension of the proposed goals. In order to contextualize the reader in the document, a brief introduction is presented at the beginning of each chapter.

This document comprises five main sections:

- **Basic Concepts:** A brief introduction of the main UAV concepts and an explanation of the theoretical principles behind a solar airplane were given in chapter 2;
- **Aircraft Description:** In this section the LEEUAV specifications and other main aspects of the aircraft are described and justified (chapter 3);
- **Systems Integration:** The third section includes the electronic, navigation and control systems integration. This section also covers a part dedicated to the solar cells integration (chapter 5);
- **Mission and Flight Testing:** The fourth section starts by defining the mission objectives for this Solar UAV, followed by the ground tests and flight experiences (chapter 6);
- **Results:** After retrieving the flight data from LEEUAV, a performance analysis was carried out using a Mechanical Energy Method. In this section the good and bad aspects of LEEUAV are described as well as the hazards found and the corrective actions taken to solve them (chapter 7).

Intentionally left blank

Chapter 2

2 Basic Concepts

2.1 Introduction

The objective of chapter 2 is to give a small explanation of the basic principles inherent to the flight of any fixed wing aircraft, in particular, unmanned solar aircraft. The systems and technologies involved and the knowledge required for the comprehension of this thesis are also addressed in this chapter. Much more information about the aviation principles could be included in this section, but that would extend the document considerably.

2.2 Main Forces of an Aircraft and Energies

A fixed wing aircraft flies thanks to the action of the four main forces during the majority of the flight phases (figure 11).

During a level or steady flight, the propeller, jet or fan in case of turbojet engines is responsible for creating the thrust force which pulls the aircraft forward. Thrust force is directly proportional to the power of the engine and inversely proportional to speed of the aircraft.

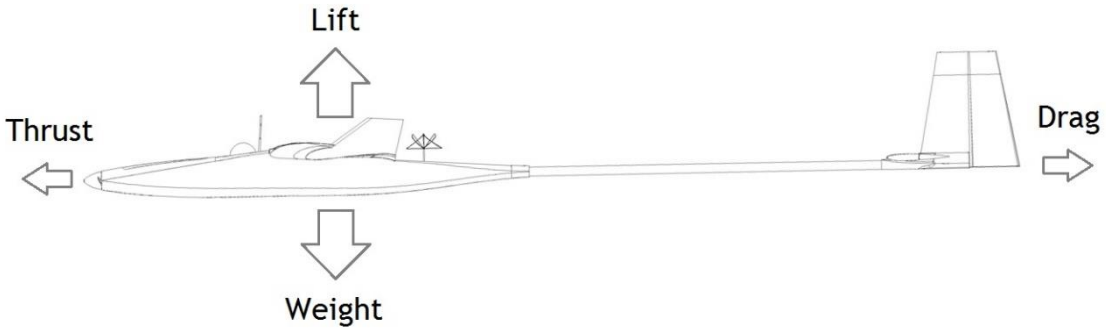

Figure 11 - Forces acting on an airplane at level flight

When the aircraft is moving, there is a flow of air in its airframe that creates an opposite force called drag. The drag force can be subdivided into many types (pressure drag, friction drag, parasite drag and induced drag) that are created by different physical phenomena, flight conditions and components of the airplane, such as wings, airframe, control surfaces and other external parts of the aircraft.

Besides the two main horizontal forces applied on an aircraft during its flight, another two vertical forces are present, namely, lift and weight. The weight force is the sum of weight of all components and systems of the aircraft at any moment of the flight. For the same aircraft, a higher weight requires a higher flight speed and usually higher power consumption. The last force and probably the most important is the lift. Lift force is created by the airflow in the wings, and its appearance is explained in the section 2.4 below.

To further understand the method applied in the LEEUAV performance analysis in chapter 6, it is necessary to clarify some physical energies that are present in everything on Earth and in this case in an aircraft. The mechanical energy E_{mec} of an object is the sum of all physical energies presented in the same object. Despite the variety of energies, for this work only the potential, kinetic and dissipative energies were considered, so the mechanical energy is given by:

$$E_{mec} = E_{pot} + E_{kin} + E_{dis} \tag{1}$$

The potential energy E_{pot} is the energy that an object has because of the gravitational field of the Earth. Mathematically, is the result of the object mass times gravity acceleration times relative altitude to the Earth's surface.

$$E_{pot} = mgh \tag{2}$$

The kinetic energy E_{kin} is the energy possessed by an object in motion and its value depends on the object mass and velocity.

$$E_{kin} = \frac{1}{2}mv^2 \tag{3}$$

The dissipative energy is the result of an irreversible process that takes place in all non-conservative systems. In those situations, the energy (internal, kinetic or potential) is transformed from an initial form to some final form. In the aerodynamic domain, the dissipative energy is represented by drag, which is a force, opposite to the relative motion of any object in a fluid.

2.3 Unmanned Aerial Vehicle

An unmanned aerial vehicle (UAV) commonly known as remotely piloted aircraft system (RPAS) or as a drone, is an aircraft that does not require the presence of a pilot on-board. The UAV's flight is monitored by a remote-control station operator on the ground or in another vehicle. The existing state of the art technology allows a fully autonomous flight capability, processed by on-board computers inside the UAV [37].

Despite the existence of controversial assignments for the weight categorization of UAVs the United States Department of Defense (DoD) has divided the unmanned aircraft systems (UAS) in 5 distinct groups shown in table 1.

Table 1 - Categorization of UAVs according to U.S. Department of Defense [38]

UAS Group	Maximum weight (lbs)	Nominal operating altitude (ft)	Speed (kts)
Group 1	0–20	< 1,200AGL	100
Group 2	21–55	< 3,500AGL	< 250
Group 3	< 1,320	< FL 180	< 250
Group 4	> 1,320	< FL 180	Any airspeed
Group 5	> 1,320	> FL 180	Any airspeed

With respect to the range/altitude categorization, the UAVs can be divided into 6 categories, from the smallest to the largest (altitude, range): hand-held (<600m, <2km), close (1500m, 10km), NATO type (3000m, 50km), Tactical (5500m, 160km), medium altitude long endurance (MALE) (9000m, 200km) and High-Altitude Long Endurance (HALE) (9100m, infinite range) [38]. Considering table 1, the LEEUAV aircraft fits into the category of close and possible in Group 1 (DoD).

Concerning the UAV typical structures and working principles, the general UAVs have a solid airframe that sustains all the components inside providing them the best working conditions. These conditions comprise a good cooling, adequate disposition and fixation of all components. The general structure of an UAV comprises at least one communication module that receives and sends information to a remote-control station via a data link connection. In turn, the communication module is connected to the flight controller (if present) whose function is to receive the operator inputs, process and send them to all components, such as motor, control surfaces (servo-motors), etc. Further, the motor and actuators are responsible to change the aircraft attitude. In some cases, the flight controller has the auto-flight function that uses on-board sensors and a computer module to control the airplane. Figure 12 shows the main system components of an Unmanned Aircraft System (UAS).

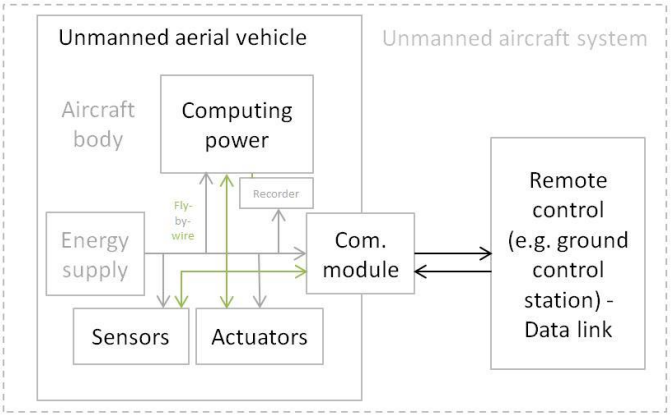

Figure 12 - Main components of an Unmanned Aerial System[56]

In addition to the UASs described, the aircraft portrayed in this work has another module, once it is powered by photovoltaic cells during flight. Solar aircraft usually have solar panels above the wings or covering other potential parts like tail or fuselage which collect solar energy from the sun's irradiance during the day and convert it into electric energy through the photovoltaic effect (figure 13).

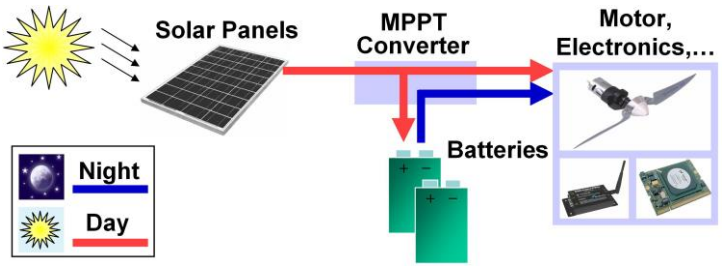

Figure 13 - Solar airplane basic principle [39]

Although it is not the case of the LEEUAV, whose maximum designed mission flight time is 8 hours at the equinox and always under sun light, other solar aircraft are forced to have enough on-board stored energy to ensure all the aircraft energy requirements for the night flight until the next morning, where a new cycle starts (figure 13).

2.4 Wing Aerodynamics

There are two types of aircraft configurations, the fixed wing aircraft and the rotary wing aircraft. The LEEUAV fits into the first category and its working principles are discussed in this chapter.

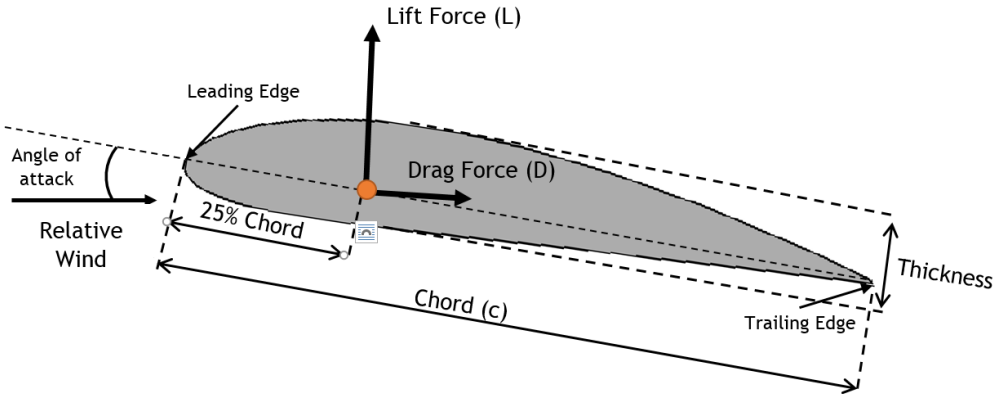

Figure 14 - Section of an airfoil

In order to understand the working principles that occur on a wing, figure 14 shows the cross section of a wing in a laminar airflow with a constant speed V. This airflow creates a different pressure distribution on the upper and lower side of this section, that once integrated is represented by two forces, lift and drag. These forces can be calculated using the following equations:

$$L = \frac{1}{2}\rho V^2 S C_L \quad \text{and} \quad D = \frac{1}{2}\rho V^2 S C_D \tag{4,5}$$

Where C_L and C_D are respectively the lift and drag coefficients, ρ is the air density, *S* the wing area and *V* the relative airspeed. C_L and C_D heavily depend on the airfoil, the angle of attack and the Reynolds number (*Re*) which represents the air flow viscosity.

$$Re = \frac{\rho V c}{\mu} = \frac{V c}{V} \tag{6}$$

Here, μ is the dynamic viscosity that once divided by the air density gives the kinematic viscosity and c represents the chord of the airfoil. The dependency on the angle of attack is depicted in figure 15. Increasing it makes C_L increase, but progressively the flow separates from the airfoil starting at the trailing edge and this gives rise to a turbulent zone that makes the C_D increase. At stall, the lift is maximum but the drag is high too. After this point, the behaviour is more difficult to predict or simulate, but basically the drag still increases but

without being followed by the lift that drops. Thus, the interesting and safe zone for an airplane is before the stall point, for glider especially at the point where the glide ratio C_L/C_D is maximum.

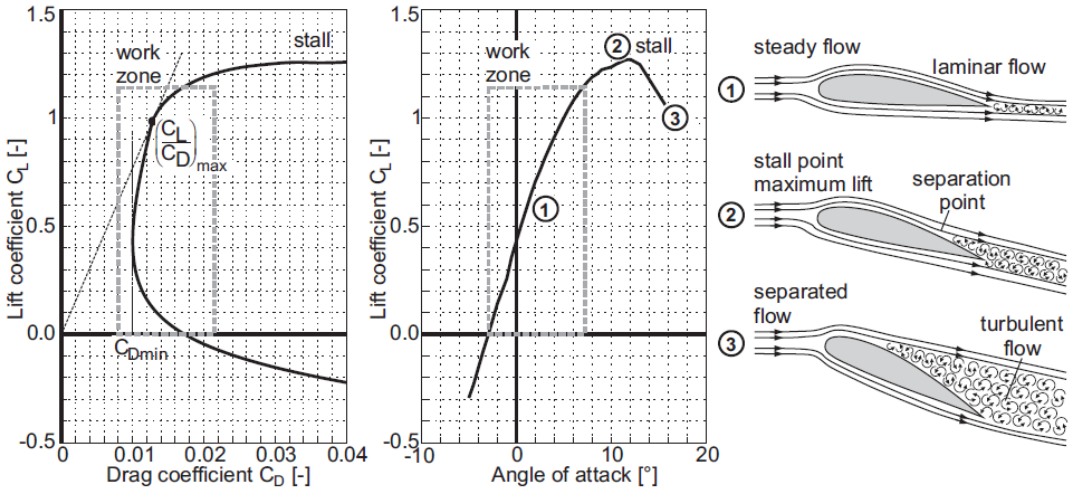

Figure 15 - Lift and drag coefficients depending on the angle of attack [39]

What was described so far is the case of an infinite length wing, but for a real wing, vortices are produced at the wing tips and airflow is redirected for other directions as a result of lift force creation, which induce an additional drag called the induced drag. It represents the energy spent for producing the wake behind the wing and follows:

$$C_{Dind} = \frac{C_L^2}{e\pi AR} \tag{7}$$

AR is the aspect ratio, i.e. the ratio between the wingspan b and the chord length *c* that can also be expressed with the wing area using $AR = \frac{b}{c} = \frac{b^2}{bc} = \frac{b^2}{S}$. The variable *e* is the Oswald efficiency factor that has a value between 0 and 1, being 1 the ideal case where the load distribution on the wing is elliptical. In many cases, its value is between 0.75 and 0.85. This induced drag has to be taken into account especially for small aspect ratio airplanes as it becomes more important.

Finally, there is the parasitic drag coming from non-lifting parts, like the fuselage, tail, surface irregularities and bumps, flaps, landing gear, etc., the parasitic drag also called by friction drag is the resistance force that is created when a solid body moves through a fluid, in this case, the air.

$$C_{Dpar} = (CfF_{form}QS_{wet})/S \tag{8}$$

Cf is the friction coefficient, F_{form} is the form factor, Q is the interference factor and S_{wet} is the wet surface area of the airplane.

Despite the existence of other drags sources, for this particular subsonic aircraft the value of the final drag coefficient can be approximated by the sum of the induced drag with the parasite drag coefficients [39].

$$C_D = C_{Dind} + C_{Dpar} \tag{9}$$

Other important parameters of gliders and long endurance flight aircraft, is the aircraft aerodynamic efficiency, glide ratio or lift-to-drag ratio (L/D). The glide ratio is the amount of lift generated by a wing or vehicle, divided by the aerodynamic drag it creates by moving through air.

A higher or more favourable L/D ratio is typically one of the main goals in the design stage of an aircraft, once that the required lift is set by aircraft's weight, delivering that lift with lower drag leads directly to better fuel/energy economy, climb performance and glide ratio (without thrust).

The aerodynamic efficiency of an aircraft is then given by:

$$\frac{L}{D} = \frac{Wcos(\gamma)}{Wsen(\gamma)} = \frac{1}{\tan(\gamma)} = \frac{\Delta X}{\Delta Z} \tag{10}$$

Considering zero wind conditions and no lateral disturbances, L/D only depends on the path angle (γ) which is the angle between the horizontal plane of the aircraft and relative wind. It is also equal to the distance travelled divided by the altitude lost. Achieving the maximum distance for altitude lost in windy conditions requires further modification of the best airspeed, as does alternating cruising and thermaling. Presently the best efficiency reached by sailplanes is around 35. This means that the aircraft can fly forward 35 units of distance, without thrust, for each unit of descent.

Knowing the lift and drag formulas (4,5), it is easy to understand the influence of the airspeed, altitude and aircraft configuration on the aerodynamic efficiency during the flight. The typical drag variation along airspeed for a fixed wing aircraft is depicted in figure 16 and it is possible to see that there is an optimal airspeed value where the total drag is minimum and in turn the required thrust.

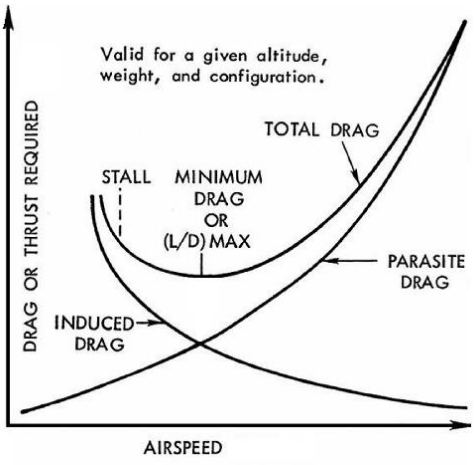

Figure 16 - Total drag vs Airspeed [1]

Working the formulas 4, 5 and 7, for non-powered flight (gliding flight) and symmetric drag polar, the airspeed for minimum power/drag is also the maximum endurance airspeed and it can mathematically be estimated by:

$$V_{Emax} = \sqrt{\frac{2W}{\rho S C_{Lminpower}}} = \left[\frac{4}{3}\left(\frac{W}{S}\right)^2 \frac{1}{\rho^2}\frac{1}{C_{D0}}\frac{1}{\pi e AR}\right]^{1/4} \quad (11)$$

The V_{Emax} can also be seen by finding the maximum point in "$L^{3/2}/D$ vs Airspeed" graph. On the other hand, the best gliding speed, i.e., the airspeed where the aircraft have the longest range without thrust, corresponds to the intersection point between the tangent and total drag curve or the maximum point in "L/D vs Airspeed" graph and it can be defined by:

$$V_{Rmax} = \sqrt{\frac{2W}{\rho S C_{Lmindrag}}} = \left[4\left(\frac{W}{S}\right)^2 \frac{1}{\rho^2}\frac{1}{C_{D0}}\frac{1}{\pi e AR}\right]^{1/4} \quad (12)$$

However, these airspeeds only concern the aerodynamic point of view and are only relevant for gliders or non-powered flight. For the cases where the aircraft is being thrusted it is necessary to consider the real propulsive system efficiency in order to determine the airspeeds where the power consumption and specific power (power produced per unit of weight) are minimum to maximize endurance and range, respectively.

After a brief introduction of the mechanisms that occur in a wing, it is easy to realize the importance of airfoil selection for a given interval of Reynolds number as well as the characteristics of a wing, namely, the wing tip, angle of incidence, aspect ratio and surface finishing quality.

2.5 Flight Control of an Unmanned Aircraft

As already mentioned, LEEUAV belongs to the fixed wing aircraft category and the attitude of this airplanes is controlled/changed through the adjustment of the primary control surfaces, such as ailerons, elevators and rudder and controlling the power given to the electric motor/propeller.

There are three axes of motion in an aircraft: lateral, longitudinal and vertical. All of them meet the aircraft's Centre of Gravity (C.G.), which is the average location of the weight of an object. The rotation of the aircraft around these three axes is usually named pitch, roll and yaw, respectively.

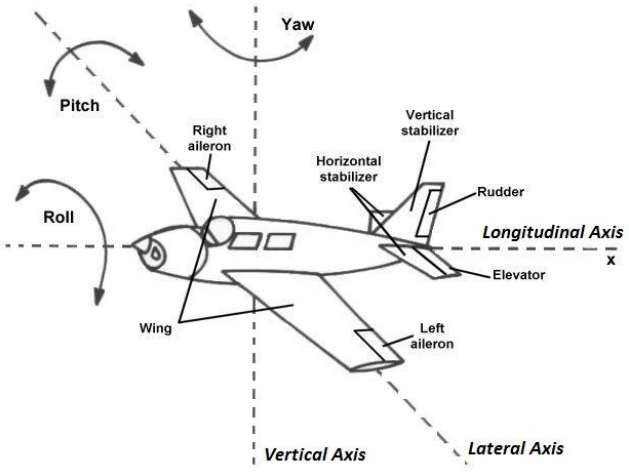

Figure 17 – Aircraft principal axis and control surfaces [57]

The rotation about the lateral axis (pitch) changes the vertical direction that the aircraft's nose is pointing and the primary control surfaces to control it are the elevators. The elevator is a moveable part of the horizontal stabilizer, hinged to the back of the fixed part of the horizontal tail. Whenever the elevators go up and down together a lift force is created on the tail of the aircraft changing its longitudinal attitude.

To control the side bank angle (angular displacement about the longitudinal axis), aircraft uses ailerons. The ailerons are mounted at the trailing edge of each wing near the wing tips and move in opposite directions. A raised aileron reduces lift on that wing and a lowered one increases lift, so moving the stick left causes the left wing to drop and the right wing to rise. This causes the aircraft to roll to the left and begin to turn to the left. The rudder also has a secondary effect on bank angle of the aircraft.

In order to control the direction where the aircraft's nose is pointing, left or right (Yaw movement), the rudder surface has to be changed. The rudder is typically mounted at the trailing edge of the vertical stabilizer, forming part of the empennage. As well as rudder influence the roll of an airplane the ailerons also have a secondary effect on yaw.

There are other secondary control surfaces such as spoilers, flaps, slats, air brakes, but they are not present in this aircraft so they will not be discussed here.

The mechanical working principles to actuate the control surfaces can be mechanical using steel cables or other high strength materials, hydraulic which requires hydraulic pumps and a very complex system (suitable only for huge control surfaces/airplanes), and the most recently and reliable technology, the servomotors.

The servomotors are actuators that use small direct current (DC) motors and high gear ratio mechanisms for steering an axis which in turn is controlled by an electronic circuit, based on measurement of an angle with a potentiometer, producing high torques allowing to change the position of the control surfaces, even under aerodynamic forces.

The justification for the use of this kind of actuator in LEEUAV is in the light weight, the reliability, precision and the very low power consumption when compared to the power required for the propulsion system.

The thrust of a propeller-driven aircraft is controlled varying on its propeller speed. In LEEUAV this is done with an electronic speed controller (ESC) whose functionality is explained below in section 2.6.

The control of the servomotors and ESC is done directly from ground control station (GCS) inputs or autonomously by the on-board flight controller. A detailed explanation about LEEUAV's flight control system is given in chapter 5.

2.6 Electric Propulsion

Concerning the propulsion methods currently available for unmanned aircraft applications there are two groups, gas propulsion using liquid fuel and electric propulsion using electric energy stored in batteries. The second is by far the most appropriate and widespread way to thrust a model or small aircraft where the power requirements are small. The main advantages of use this type of propulsion are the high efficiency, low weight and noise and above all, the lack of pollution. The necessity of carrying huge batteries to ensure high endurance results is the major problem that the electric propulsion is currently facing. However, the use of solar cells as an external source of power has come to temporarily solve this problem seeing that they allow to downsize the battery capacity and weight.

The typical electric propulsion system of an UAV involves a sequence of 4 base components, namely the battery, electronic speed controller, electric motor and propeller. For solar powered UAV cases, another two components have to be addressed, the solar panels and the solar charger. The complete circuit applied on LEEUAV is shown in the figure 18.

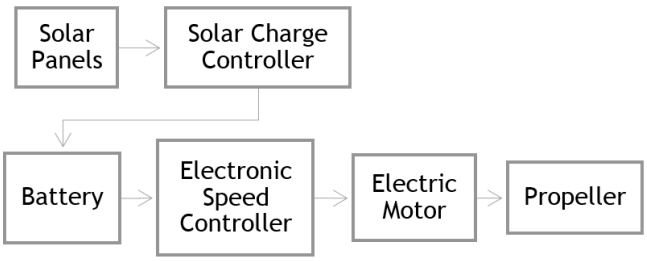

Figure 18 - Architecture of the propulsion system

When the sun's irradiance strikes the solar panels, the solar charger controller (SCC) gets on and redirects the energy to firstly supply the propulsion system and/or on-board electronics and further charge the battery with the surplus energy. This SCC is a device whose function is converting the voltage and current of the solar panels output to correctly charge the batteries and at the same time ensure the solar panels are working at their maximum power point MPP. This solar charger is also called Maximum Power Point Tracker Converter (MPPT Converter) and its detailed operation is explained in section 2.9.

Whenever the pilot or autopilot increase the throttle, the electric energy stored in batteries or directly coming from solar panels will power the ESC, which is an electronic circuit that controls the electric motor speed by varying the electrical current from the batteries to

the motor inputs in different ratios and at a defined frequency (frame rate). When the electrical energy reaches the electric motor it is converted into mechanical power which rotates the propeller. In order to obey the pilot/autopilot orders, the ESC is connected to a receiver or a fight controller.

The large variety of electric motors on the market is justified by its wide range of different applications. Depending on the supply source, size, torque and speed required, the most suitable electric motor for some application may have a different working principle when compared to another application.

By far the most common types are the brushed and brushless types, figure 19, which use mechanical and electronic commutation respectively to create a rotating magnetic field vector that pulls an electromagnet or a permanent magnet.

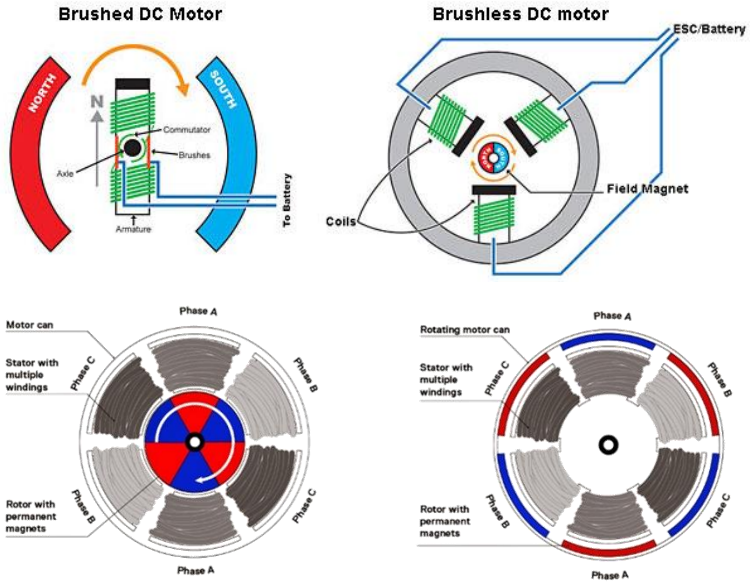

Figure 19 - On top brushed Vs brushless motors, below inrunner vs outrunner motors [40,41]

In a classic DC motor, the inner part is the rotor, which consists of a wound coil generating a rotating magnetic field, and the outer part is either an electromagnet or permanent magnet stator, which creates a fixed magnetic field. The electrical connection between the rotor and the external power supply are ensured by brushes. Hence, the rotation will continuously change the coil polarity, thus generating an oscillating current. This current is at the origin of the rotating magnetic field and the turning moment. The limitations of direct current (DC) motors are due to the need for brushes to press against the commutator that creates friction, sparks and electrical noise, especially as currents and speeds get higher. Also, the windings induce a high inertia to rotate and as they are placed in the centre of the motor, they have trouble getting rid of the heat due to the Joule effect.

In a brushless DC motor, often abbreviated as BLDC, the coils do not move, figure 19. Instead, the permanent magnets rotate and the armature remains static. This gets around the problem of how to transfer current to a moving armature. In order to do this, the brush-

system/commutator assembly is replaced by an electronic controller that performs the same power distribution found in a brushed DC motor.

When configured with the magnets on the outside, they are referred to as out-runner motors, otherwise they are called in-runner. The advantages of BLDC motors are numerous: very precise speed control, high efficiency, reliability, reduced noise, longer lifetime (no brush abrasion), no ionizing sparks. Additionally, they run much cooler than brushed motors which allows the use of higher currents and for this reason, their power to weight ratio is exceptionally high [40,41].

In the light of the above, the electric motor chosen to power the LEEUAV was a DC brushless out runner, since it needs to be compatible with the DC power supply (battery).

2.7 Propeller

A propeller comprises a rotating power-driven hub, around which several airfoil-shaped blades are mounted around. When the propeller is rotating, it accelerates incoming air particles creating a reaction force called thrust, providing propulsion of a vehicle through a fluid.

Although it sounds simple, the propeller design has to consider many variables in order to get high efficiency and reduce the power losses. The Blade Element Theory (BET) gives a detailed explanation of how it works and how it can be optimized for different operating conditions. In this theory, figure 20, the blade is assumed to be composed of numerous, infinitesimal strips with width 'dr' that are connected from hub to tip. The lift and drag are estimated at the strip using the 2-D airfoil characteristics of the section. Also, the local flow characteristics are accounted for in terms of inflow and angular velocities. The section lift and drag may be calculated and integrated over the blade span.

A propeller's efficiency η_{plr} is determined by the ratio between the propeller thrust T times the propeller axial speed v and the resistance moment M_{plr} times the rotational speed ω.

$$\eta = \frac{Propulsive\ Power\ Out}{SHaft\ Power\ In} = \frac{Tv}{M_{plr} * \omega} \tag{13}$$

Looking at the efficiency formula (13) it is easy to understand the variables that influence the global efficiency of the propeller, namely, the airfoil, chord and incidence angle. In order to achieve high levels of performance for a given axial speed, the propeller should have the best airfoil, chord and incidence angle that minimize the resistance torque and maximize the thrust. A good propeller designed for a specific flight, highly depends on the Reynolds number and its value cannot be generalized. However, a propeller efficiency above 70% could be considered excellent. Other important variables of the propellers such as the number of blades, diameter and advance ratio have to be considered too.

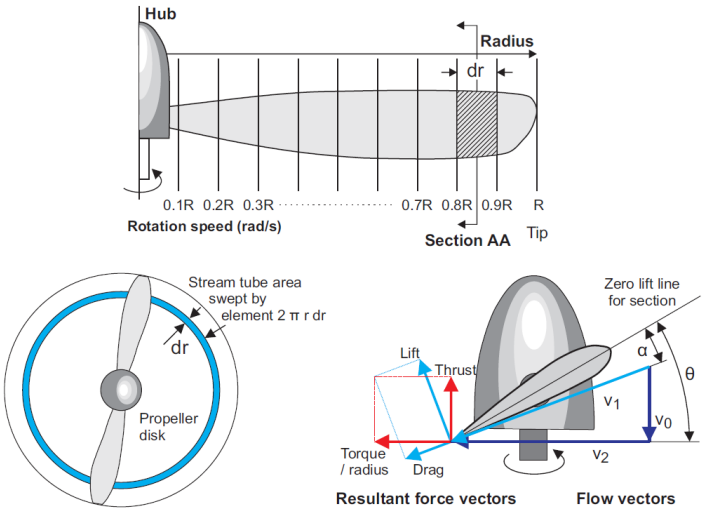

Figure 20 - Concept of the blade element theory [39]

Increasing the aspect ratio of the blades reduces drag but the amount of thrust produced depends on blade area, so using high-aspect blades can result in an excessive propeller diameter. A further balance is that using a smaller number of blades reduces interference effects between the blades, but to have sufficient blade area to transmit the available power within a set diameter means a compromise is needed. Increasing the number of blades also decreases the amount of work each blade is required to perform, limiting the local Mach number, a significant performance limit on propellers.

Although it seems difficult to optimize a propeller, there are some ways to simplify it, namely, the way a propeller attaches to the power source. It could be connected directly to the driveshaft or, especially on larger designs, through a reduction mechanism using a gearbox, allowing to reduce the propeller angular speed. There is an additional mechanism named variable-pitch propeller which permits the change the blade's pitch, improving the propulsive system performance of the aircraft across varying speeds. This mechanism can be set manually to a few set positions, or of the automatically-variable "constant-speed" type [39].

2.8 Solar Cell

A solar cell or photovoltaic cell is a device that converts solar energy into electricity by the photovoltaic effect. The applications are endless but they are usually used in systems that requires a long-duration source of energy, low maintenance requirements and where space and weight are not relevant. The majority of solar cells currently used are composed of various semiconducting materials as silicon, constituting one or more layers.

2.8.1 Working Principles

There are a several types of solar cells but the most commonly used are configured with a p-n junction cell and use silicon as a semiconducting material. Inside the cell there are two layers of a semiconducting material, one p-layer is bonded with boron (giving it a deficit of electrons) and the other, n-layer, with phosphorus (giving it an excess of electrons). The

different chemical electric charges of these two layers create a potential difference between them.

These types of cells, figure 21, when the sunlight strikes the solar cell surface, it is absorbed by the n-layer, which has an excess of electrons. In order to get stable, the excited electrons can either dissipate the energy as heat and return to its orbital or travel through the cell until it reaches the p-layer with a deficit of electrons. When this happens, an electric current is created and flows through the two layers to cancel the potential. The electricity can be captured by connecting the two different layers to two different electrodes and further to a converter or charger.

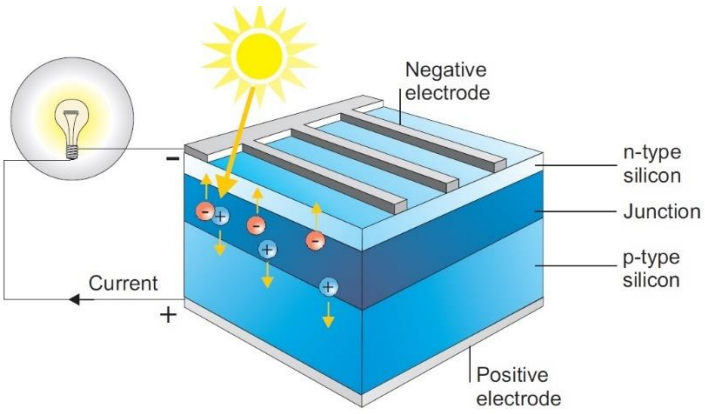

Figure 21 - Working principle of a solar cell [42]

To protect the solar panels cell from the outside environment, they are usually covered by layers of anti-reflex materials, which in turn increases the amount of energy absorbed by the solar panel [42].

2.8.2 Solar Irradiance

The solar aircraft flight endurance depends on the amount of energy that it is able to collect from the sun during the day. That amount of energy is influenced by the disposal of the panels in the aircraft, the efficiency of the solar cells and the solar irradiance which, in other words means, the amount of energy that comes from the sun.

The solar irradiance depends on the location in the world as well as the season of the year and the time of the day. A standard solar irradiation spectrum is shown in figure 22, and it represents the irradiance of the sun on earth at different altitudes of atmosphere. The reference AM0 (Air Mass 0) represents the irradiance at the top of the atmosphere corresponding to a total energy of 1353W/m^2. At sea level, it is referenced as AM1.5 and the total energy equals 1000 W/m^2.

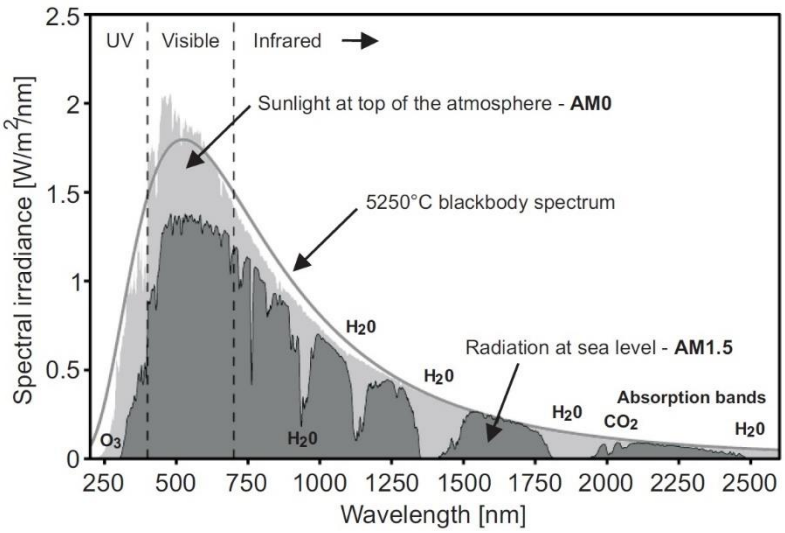

Figure 22 - Earth solar radiation spectrum [42]

Besides the direct irradiance, there are other types of irradiation like diffuse irradiance which is predominant on a cloudy day, and the reflected irradiance that depends on the reflectivity of the Earth's surface.

2.8.3 Types of Solar Cells

Since the discovery of the photovoltaic effect the world has witnessed several generations of photovoltaic cells. The solar cells can be sorted according to the type of material, fabrication process, substrate, etc. There is an exhaustive list of existing types of solar cells, but to simplify the list the solar cells can be categorized in four main groups, the Crystalline Silicon PV technology (c-Si), Thin-Film technology, Dye Sensitized Solar Cells and Polymer Solar Cells.

The silicon solar cells (c-Si) are the most widely used due to the abundance silicon material and low extraction cost. The silicon solar cells could be categorized in three different types, monocrystalline, polycrystalline and amorphous.

- Monocrystalline, in which absolutely pure semiconducting material is used providing a high level of efficiency but at a high cost.
- Polycrystalline, composed of crystal structures of varying sizes. The manufacturing process is more cost efficient but leads to less efficient solar cells.
- Amorphous, or thin-layer cell, where a silicon film is deposited on glass or another substrate material. The thickness of this layer is less than 1 μm, thus the production costs are very low, but the efficiency is poor as well.

There are however, several limitations to this generation technology such as the fragility of the silicon layers, the process involved in the manufacturing is difficult and labour intensive, which results in high costs.

In order to lower some of the production costs of the c-Si cells, a new technology of thinner cells permitted a reduction of the semi-conductive material used in each cell, as well as the simplification of the manufacturing process, resulting in cost reduction. However, the

Thin-Film technology has lower efficiency and these cells have a shorter life span than the c-Si cells.

The polymer solar cells made of organic material and the dye sensitized solar cells are very promising technologies because of their low manufacturing costs. However, these technologies suffer from unstable efficiency problems that must still be solved and are not yet viable for commercialization.

Many other types of solar cells can also be produced too, using the combination of the other materials belonging to different elements from the periodic table, like gallium, arsenide, copper, indium, etc. creating a compound solar cells which are usually more efficiency but more expensive.

2.8.4 Efficiency of the solar cells

Despite exiting a lot of types of solar cells, the maximum efficiency achieved to date is below 50%. This means that the solar cells just can at most capture half of the irradiance provided by the sun. According to the NREL's laboratory results, the most efficient solar cells are the ones which have a stack of individual single-junction cells in descending order of bandgap. The last 40 years of research efforts are summarized in the graphic of figure 23, below [43].

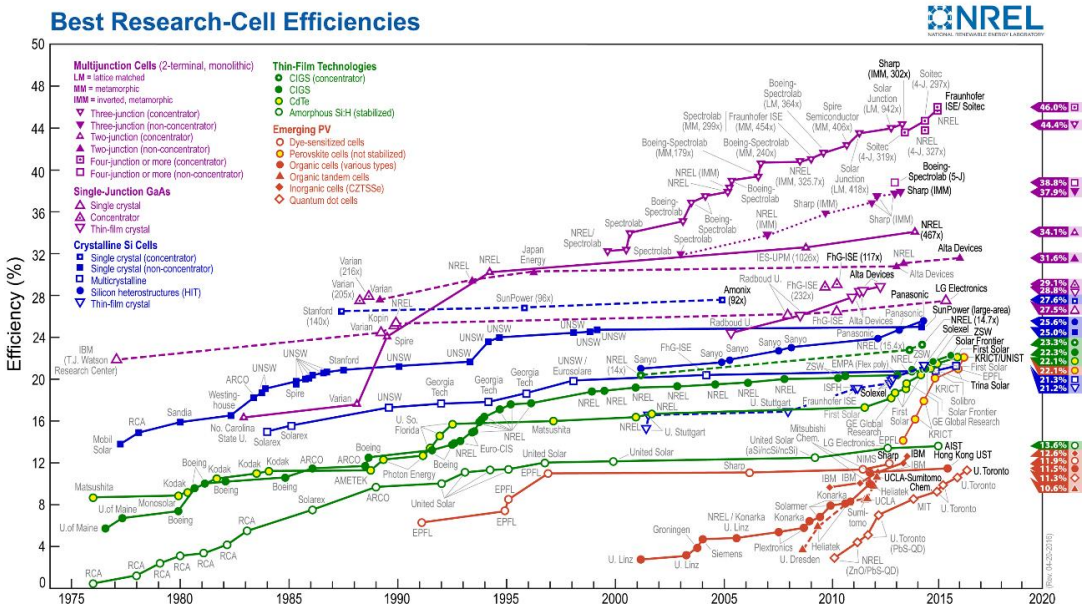

Figure 23 - Best research (NREL)- cell efficiencies [43]

2.8.5 Solar cell I-V characteristic curve

The current and power output of photovoltaic solar panels are approximately proportional to the sun's irradiance. At a given irradiance, the solar panel's output current and operating voltage are determined by the characteristics of the load. When the solar panels are directly connected to a battery, the battery's internal resistance will dictate the module's operating voltage.

To understand better how an output power of a cell works, there is a characteristic curve for the current to voltage of a solar cell, the typical I-V curve is depicted in figure 24.

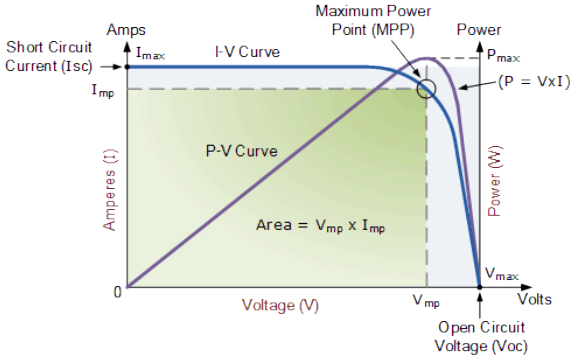

Figure 24 - Solar cell current to voltage (I-V) characteristic curve [44]

As is shown in figure 24, when the cell pads are not connected or when there is no load on the cells, no current is produced and the voltage equals V_{OC}, the open circuit voltage. When it is short circuited, the voltage is zero but the current equals I_{SC}. In between these two points, where in both cases the power retrieved is zero, there is a working point, called the maximum power point (MPP), where the power one can retrieve is the highest and equals $P_{max} = V_{MPP}I_{MPP}$ [44].

In order to extract the maximum power from the solar cells, they should be working at this (MPP) point and the ratio between P_{max} and the light intensity represents the efficiency of the solar cell. However, this I-V curve is not fixed and varies with temperature, number, arrangement of cells (series and parallel) and power load.

The current of a solar cell is proportional to its area and varies almost linearly with the light intensity (figure 25). The voltage has a small variation when the light intensity changes and is independent of the cell surface, but depends on the semiconductor material.

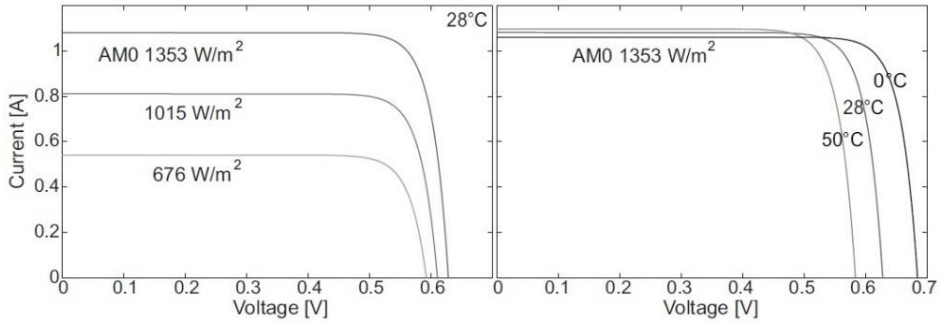

Figure 25 - Variation of the current to voltage curve of a solar cells with irradiance and temperature [33]

As referred before, the temperature affects the operation of the solar cells, when it increases the voltage decreases slightly, reducing the maximum output power provided by the cells. So, for the same irradiance conditions, lower temperatures provide more power [33].

In order to properly power up the solar charger it is necessary to arrange the solar cells taking into account their operating voltage and current. To increase the voltage, the solar cells must be assembly in series. On the other hand, to maintain the voltage but increase the current the solar cells have to be assembled in parallel.

2.9 Energy Storage

Despite the constant production of energy by the solar cells, a solar aircraft cannot fly using a direct connection between the solar panels and components. Not only for the reasons explained in section 2.9.3, but also because solar aircraft must have energy stored for when there is no solar irradiance or for redundancy effects.

Although the specific power of photovoltaic cells is very low when in comparison to the internal combustion engines, the use of batteries increases the overall energy density of the airplane and consequently its endurance. Moreover, the actual batteries have already proven to be very reliable by assuring an approximately constant voltage during their charge/discharge process as well as long life with hundreds of cycles with low energy loss.

2.9.1 Types of Batteries

There are many ways to store energy and thus many types of batteries. The different technology applied to the different energy storage methods is justified by the requirements of their specific applications. The main selection criteria of a battery or energy store method are the power density, response time, lifetime, efficiency, costs, discharge and charge rate among others. The most successful and commonly types of energy storage methods used are [46]:

- Chemical (hydrogen, biofuels, gas);
- Electrochemical (batteries, fuel cells);
- Electrical (capacitors);
- Mechanical (compressed air, flywheel);
- Thermal

For the specific application in a solar powered aircraft with a very low weight and high endurance requirements, the energy storage method specifications must ensure a high-energy density (Wh/kg), relatively high discharge rate (W/h) and a considerably long life time.

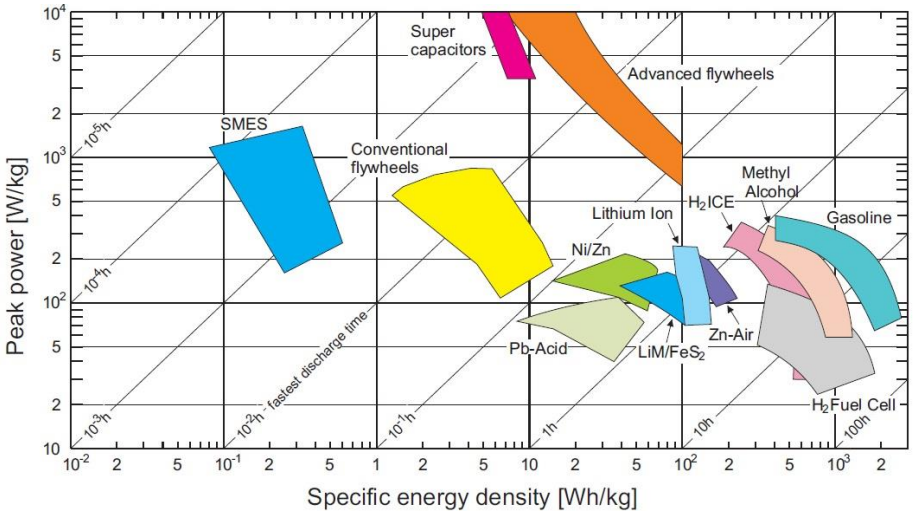

Figure 26 - The Ragone Plot - Peak power and specific energy density of various energy storage methods [39]

Figure 26 shows the specific energy of the most common types of energy storage methods, including the different types of electrochemical batteries. Analysing the figure 26, excluding the petroleum-derived liquids (once the propulsion system of LEEUAV is electric) it is possible to highlight the electrochemical batteries, fuel cells and flywheels, however the fuel cells are expensive and the energy stored in flywheels is not reversible, that is, they are not rechargeable during the flight.

By elimination, the electrochemical batteries are the most appropriate for an application in a solar UAV. Within the field of the electrochemical batteries there are a lot of combinations of elements and technologies currently used. However, this type of batteries has a common working principle, they convert chemical energy into electrical energy during a discharge process and the reverse when it is being charged through a chemical reaction between an anode and cathode. To store and provide energy, the cathode and an anode are made of two different metals which in turn are in contact with an electrolyte.

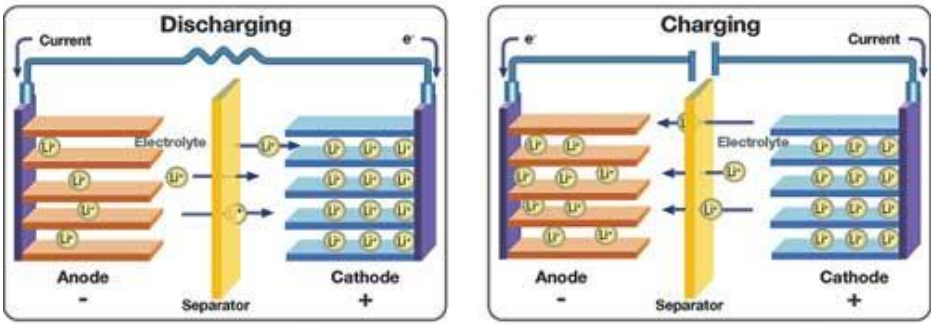

Figure 27 - Charge and discharge process of a lithium battery [47]

When the battery is charging there is an internal flow of ions through the electrolyte from the positive electrode (cathode) to the negative electrode (anode), until the maximum capacity of the battery is reached. On the other hand, when the cathode and anode are connected in a closed circuit the ions flow in the opposite direction and a current of electrons is released into the circuit.

The diversity of electrochemical batteries lies in the different possibilities of combining dissimilar materials for the cathode, anode and electrolyte. The most successful batteries currently under commercialization are lithium-ion (or lithium-ion polymer), nickel-cadmium (Ni-Cd) and nickel-metal-hydride (NiMH) [48].

Inside the field of electrochemical batteries and according to the figure 26, the lithium-ion have proved to be the batteries with the highest specific energy density, so they are used in LEEUAV aircraft.

2.9.2 Properties of the Batteries

Focusing on the polymer lithium-ion batteries, which are going to be used in the LEEUAV, some additional information must be perceived in order to operate them safely, namely, the

charging and discharge processes, the efficiency and external influences such as the temperature.

The lithium-ion batteries may have different physical forms, cylindrical, flat, prismatic, etc. but all of them are a group of one or more cells. Each cell has a nominal voltage of 3.7V that can reach 3.3V when are completely discharged or 4.2V when are fully charged. Parallel assemblies of Li-ion cells will increase the battery capacity (mAh) and series assemblies will increase the output voltage of the battery.

The charging process of lithium-ion batteries is quite simple, but has to be done very carefully because of safety reasons. During a first phase, a constant current charges the battery while the voltage increases as depicted in figure 28. Once 4.2V is reached, the second phase starts during which the voltage is kept constant, while the current accepted by the cell slowly decreases. When this current is below 5% of the maximum current, the battery is charged.

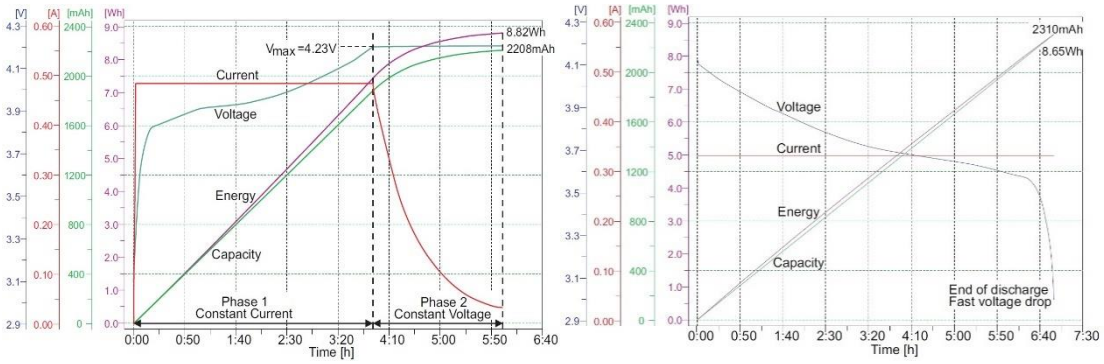

Figure 28- Charge (right) and discharge (left) process of a lithium-ion battery [48]

Another important characteristic is the charge/discharge rate, which is the minimum recommended time that the battery takes to get fully charged/discharged. The charge/discharge rate is measured by the maximum current that a battery is able to accept/provide in a space of time and usually are represented by C. For example, a battery with a capacity of 2200mAh and 1C of discharge rate, means, the battery is able to provide at its nominal voltage 2.2A of electric current. If the charge/discharge rate is exceeded the battery temperature will rise which for a long period of time may burn or explode. Some batteries have an internal electronic board which is responsible for safely charging and discharging the battery cells.

The discharge process of a Li-ion battery is similar to the charge process (figure 28), under a constant current discharge, the voltage slightly decreases from the 4.2V to 3.3V but when it reaches lower voltages (under 3V), the voltage drops very fast and the battery will probably no longer stand its nominal capacity.

These batteries have some particular properties that makes them the most used nowadays, especially, their high efficiency, no-memory effect, lifetime of charge/discharge cycles, low self-discharge rate, low cost and mainly the specific energy currently reaching values of 500Wh/kg (Li-S).

2.9.3 Solar Panel Charge Controller (SCC)

To transfer the energy collected from the solar cells to the batteries a proper is required so as to ensure that the current and voltage provided to the battery are adequate and will stop charging when it is fully charged, thus avoiding over-charging and other problems.

Other facts that justify the need of a SCC is the unstable current and voltage of the solar panels in a solar aircraft flight. At low temperatures, the solar panel's output voltage increases and with a higher irradiance, the output current will be higher. This current and voltage oscillations can damage the battery if there is no any charger or regulator between them.

2.9.4 Maximum Power Point Tracker

As described in section 2.8.5 the solar cells have a working point in which their power output is maximized. Like the I-V curves, the MPP is not a fixed point and to work on this point a maximum power point tracker (MPPT) is required. The MPPT is a fully electronic system, similar to a DC/DC converter with variable and adjustable gain between the input (solar panels) and the output voltage (battery). It contains electronics sensors that monitor both the current and the voltage on each side. This allows the determination of how the gain has to be changed to ensure that the solar modules provide to the batteries the maximum amount of power.

Chapter 3

3 Aircraft Description

3.1 Introduction

In this chapter, although the project and the design of the LEEUAV airplane does not form part of this thesis, its specifications are addressed for a better understanding and perception of what it really is.

Besides the technical specifications, the materials used, a short review of the construction process as well as a detailed diagram describing all the components for each system of the aircraft are also addressed in this section.

3.2 UAV Final Design and Specifications

The final stages of the multidisciplinary preliminary design of the LEEUAV prototype, have resulted in a built-up monoplane aircraft with high wing configuration, without wing supports and a large aspect ratio, without wing sweep or dihedral. The wing is constituted by three panels, one at the centre with constant chord and two tapered panels at the outward tips. The outward panels of the wing have 4.5 degrees of negative twist and an endplate to prevent wing tip stall during the tight turns of the aircraft.

The LEEUAV has a conventional tail configuration, with the horizontal stabilizer distanced from the vertical, to facilitate the spin recovery. The rudder and elevator are made of balsa covered by a thin layer of heat shrink film. The propulsive system configuration is a pusher and has a single electric motor attached to the propeller that is located at the front of the aircraft.

Despite not having a landing gear for take-off, the LEEUAV uses a small ground bogey with wheels to facilitate land manoeuvres.

From previous works [31,33,34] the final design and main specifications of the LEEUAV are presented in table 2 and the three drawing views are below in figure 29.

Table 2 - LEEUAV final design specifications (without solar panels)

Dimensions	Wingspan [m]	4.500	**Weights**	Empty mass [kg]	3.890
	Length [m]	2.370		MTOM* [kg]	4.900
	Height [m]	0.360		Payload* [kg]	1.000
	Mean chord [m]	0.330		Structure mass [kg]	1.590
	Wing root chord [m]	0.350	**Performance**	Take-off distance* [m]	8.100
	Wing tip chord [m]	0.250		Endurance* [h]	8
	Wing area [m^2]	1.518		Maximum speed* [m/s]	21.10
	Aspect Ratio [AR]	13.50		Stall speed* [m/s]	6.100

* estimated from theoretical calculations

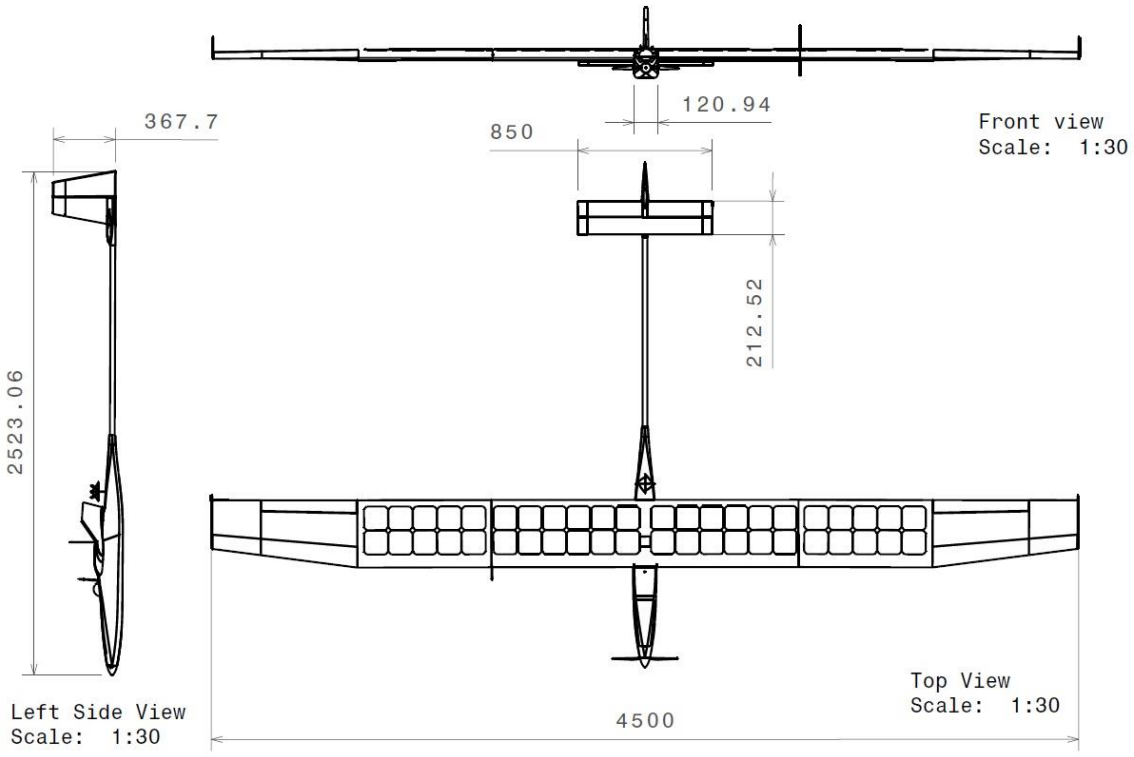

Figure 29 - 3D Drawing views of LEEUAV

In annex A a table is attached containing the full LEEUAV aircraft specifications, before and after all systems integration and structures modifications.

3.3 Materials

As a long endurance platform, this aircraft requires a structure as lightweight as possible. In order to achieve the theoretical calculations, the majority of the present materials are composite fabrics and balsa wood. The entire fuselage is made of carbon fibre, including the tail boom and the electronic covers. On the other hand, the wings are supported by a main carbon fibre spar connected to a wing box which contains a low density extruded polystyrene foam, covered with a thin shell of carbon fibre. To maintain the airfoil shape along the wing, including the central and outward tapered panels, the wing has 36 ribs of balsa, 10 ribs of plywood reinforcement and some additional stringers to support the aileron loads during the flight. All of these wing structural components are covered with a thin layer of heat shrink film.

Similar to the wings, the horizontal and vertical stabilizer as well as the rudder and elevator are made of balsa covered with the same thin layer of heat shrink film.

In order to prevent wear of the bottom of the aircraft fuselage, a layer of fiberglass was applied over the carbon fibre.

3.4 Fuselage, Wings and Tail Construction

To obtain an entire carbon fibre fuselage in a single part, two moulds were designed with a computer aided design (CAD) software and then built using a 3-axis CNC router. After the moulds were completed, the lamination process was started and using the vacuum-assisted

method, two halves of the fuselage were obtained. Afterwards these fuselage halves were bonded with a specific carbon fibre ribbon. The wing box lamination process was different as it would have been difficult to hand-layup them in moulds. So, first a dual side print of each twist box was made in polystyrene foam, using a 3-Axis CNC router, then it was hand-laid up with carbon fibre and epoxy. The carbon fibre tail boom was purchased. To manufacture the wing and control surfaces balsa ribs, a two-axis laser cutting machine was used, after the CAD design.

After an initial flight test of the LEEUAV, several problems were observed in relation to the wing behaviour. First, loss of roll control of the ailerons occurred at lower speeds together with a tip stall tendency while turning. Second, the spiral mode was unstable. The former effects could be corrected by modifying the wing tip in order to have adequate washout so as to reduce local lift coefficients. The latter effect could be corrected by applying dihedral to the outer panels of the wing. Since this second modification would be difficult to implement, wing tips were added instead, to minimize the instability although it did not correct it.

In order to take advantage of the existing wing structure, the wing box of the outward panel was removed and a new one was designed. The new wing box is made of the same materials of the previous one, extruded polystyrene covered with thin layer of carbon fibre, including the ribs and a solid balsa trailing edge. This modification process was part of this thesis work and it is explained in detail in chapter 4.

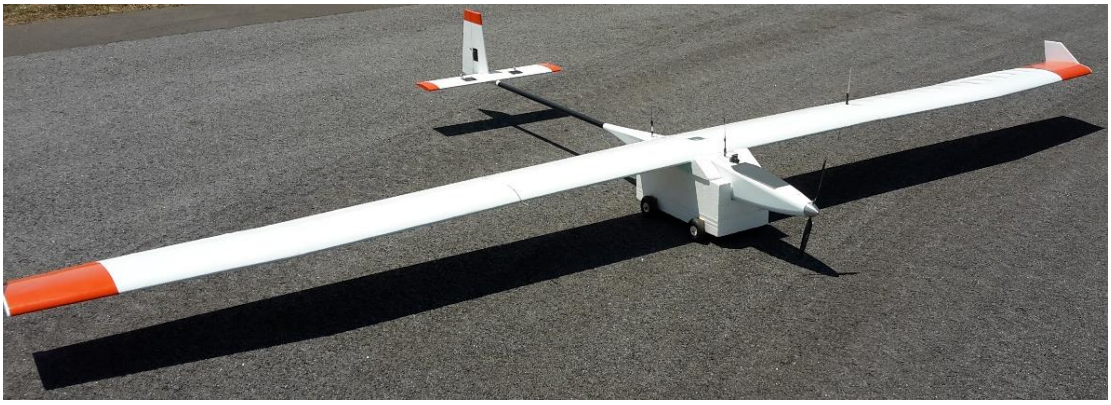

Figure 30 - Photo of the LEEUAV during flight test campaign

To attach the tail to the fuselage, there are two connection points, the first is the tail boom connection to the fuselage. This connection is held by a single screw and the horizontal alignment of the tail is achieved by a notch in the tail boom that fits into a plywood structure inside the airframe. The second is the connection between the vertical and horizontal stabilizers as well as the elevator and rudder control surfaces to the carbon fibre tail boom. This connection is made through a balsa structure and it also has a holding bolt. The configuration of these structures was designed considering the possibility of removing them for transportation. The same philosophy was taken into account for the wings, where other similar bolts attach the wing to the airframe.

3.5 Systems of Solar LEEUAV

The LEEUAV is an integrated unmanned aerial system (UAS) which can be subdivided into multiple subsystems according to their functionality. From a macroscopic viewpoint, these subsystems may be grouped in two main categories:

- Ground control station (GCS): It is a land control centre where the aircraft is controlled and monitored during its flight. All the flight information about aircraft attitude, on-board sensors and video stream is directed to the GCS equipment;
- Aircraft: It is a flying device which carries all the components for the desired mission, including all sensors for data recording and antennas for data streaming to the GCS. It also has an on-board FPV system to allow the manual flight control.

In figures 31 and 32 the systems of the LEEUAV and GCS are respectively detailed:

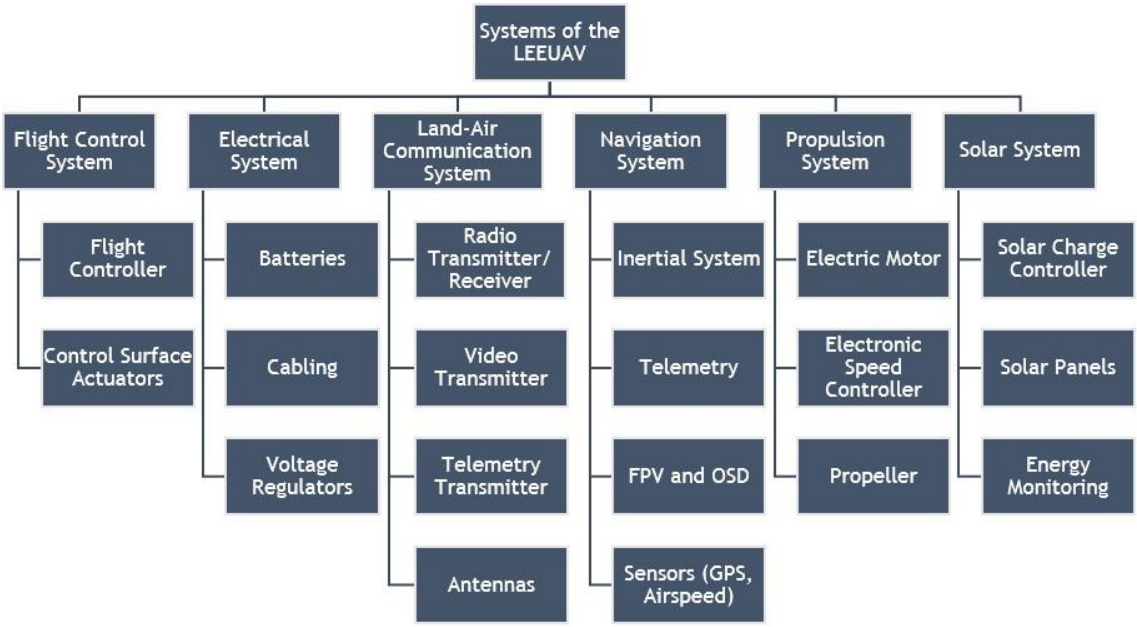

Figure 31 - Systems of the LEEUAV

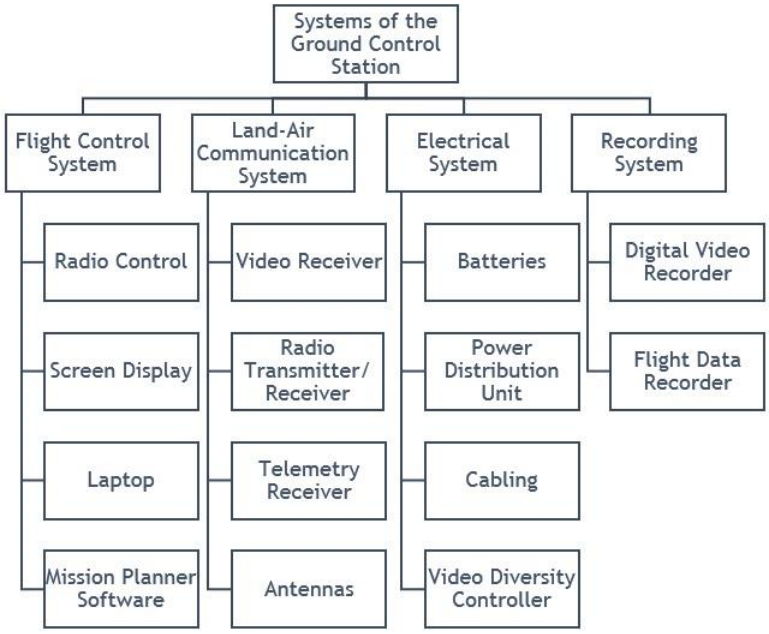

Figure 32 - Systems of the ground control station

Despite their differences, both the systems of the LEEUAV and the GCS are physically and electronically closely related, mainly the control, navigation and communication systems.

As core part of this work all systems, operation modes/functionalities, components and their respective connections are explained in detail in chapter 5.

Intentionally left blank

Chapter 4

4 Wing Tip Modification

4.1 Introduction

This chapter is the result of the practical segment of the LEEUAV wing tip modification, so the main goal is to explain the reason of this modification, the possibilities of doing it and the justification for the methods adopted.

4.2 Wing Tip Modification Goals and Corrective Actions

During the initial flight tests performed with the previous version of the LEEUAV, it demonstrated a wing tip stall tendency while turning. In a wing tip stall situation, the air does not flow through the wing tip which makes the ailerons unable to change the roll of the aircraft.

This could result in an unstable spiral mode which in turn makes the aircraft uncontrollable and possibly crash. So, the main goal of this modification is to change the wing tip in order to prevent this flight behaviour.

From an engineering perspective, in the wing tip region, two main phenomena can occur, the wing tip stall and the wing tip vortices. The first occurs when the aircraft is flying at low airspeeds and worsens with tight turns and larger wingspans. It is caused by a much lower airspeed flow through the inner curving wing tip, when compared to the opposite wing. The wing tip vortices are small tornados formed by the difference between the pressure on the upper surface and the lower surface of an airplane wing. High pressure on the lower surface creates a natural airflow that makes its way to the wing tip and curls upward around it. When flow around the wing tips streams out behind the airplane, a vortex is formed [49].

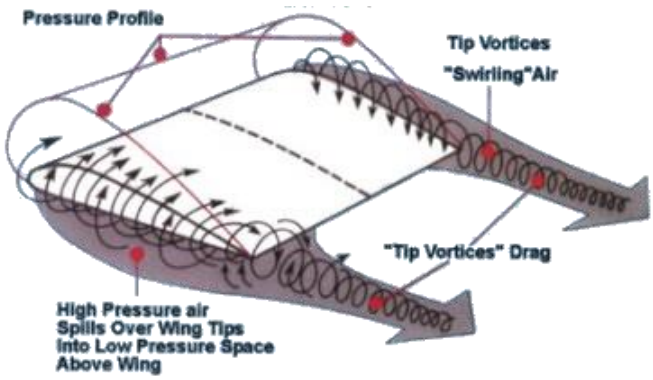

Figure 33 - Wing tip vortices formation [49]

These vortices represent a loss of energy by increasing the total drag of the airplane and which in long flights could be very harmful. So, for an 8-hour flight of a solar UAV this wing tip influence was taken into account.

To correct the wing tip stall there are some main modification possibilities: increase the dihedral angle of the wing/wing tip, change the wing airfoil, or apply a negative twist (washout) at the wing tip.

The dihedral angle increases the stability in roll axis through the dihedral effect, which is the amount of roll moment produced per degree of sideslip. When the aircraft is disturbed from an upright position such as a wing tip stall situation, it will sideslip toward the down-going wing, increasing airflow along the length of the wing from tip to root. The dihedral effect increases the angle of attack to this lateral flow, generating additional lift so as to restore the aircraft to a level attitude.

However, this modification requires to cut the spar and re-join both parts at the position the wing taper starts, which in turn will increase the total wing weight. Changing the current airfoil to a more suitable one, involves a complex modification of the existing wing and requires a detailed parametric study to amend it.

Applying a structural washout effect through a slight negative twist on the wing tip, will reduce the angle of incidence from root to the tip (decreasing the lift coefficient C_L), and therefore cause a lower angle of attack at the tips than at the roots, avoiding wing tip stall and approximating the ideal elliptical distribution of lift along the wing, for the same airspeed flow.

Regarding the wing tip vortex formation, the easiest way to solve the problem is to apply wing tip devices. There are a lot of wing tip devices and its shape and appliance depends on each type of aircraft. Since it is not make part of this work, the wing tip device used was a simple square endplate with an aerodynamic shape preventing the mixture of the lower and upper wing airflow.

Considering the options available and keeping the practical procedure as simple as possible to solve the wing tip stall, an adequate washout at the wing tip was carried out. The amount of twist that should be applied has to be carefully determined, once a low twist cannot totally prevent the wing tip stall and an excessive twist will increase the drag and makes the airplane unstable. So, to calculate the precisely amount of twist required, a parametric design optimization work was carried out by Nuno Silva [50], using the Vortex Lattice Method and a prescribed wing chords and span, with a twist distribution equal to zero from the root to the start of the wing taper and varying linearly from this point outwards, an optimization procedure was performed to minimize wing drag. The tip twist was found to be -4.5 degrees.

4.3 Possibilities for Practical Procedures

Taking into account the existing wing, the washout modification can be done by different ways. One of them is a total reconstruction of the wing tip, cutting the outer panels and connect new ones with the desired twist. In order to sustain the flight loads and transmit the moments to the wing central panel, this method requires the re-joining of the main carbon fibre spar in both parts at the position where the wing taper starts. Another initial option is to take advantage of the existing wing and substitute only the wing box with another one with the desired twist (figure 34), keeping the carbon fibre spar and the balsa ribs of the wing. This

second option seems easier and less complex since part of the wing does not need to be rebuilt. This was the chosen option.

Figure 34 - Photo of the wing tip with the wing box removed

For the modification option considered there are different practical procedures and materials that can be used in the new wing box. For the particular case of the LEEUAV wing two suitable options for the new wing box were considered.

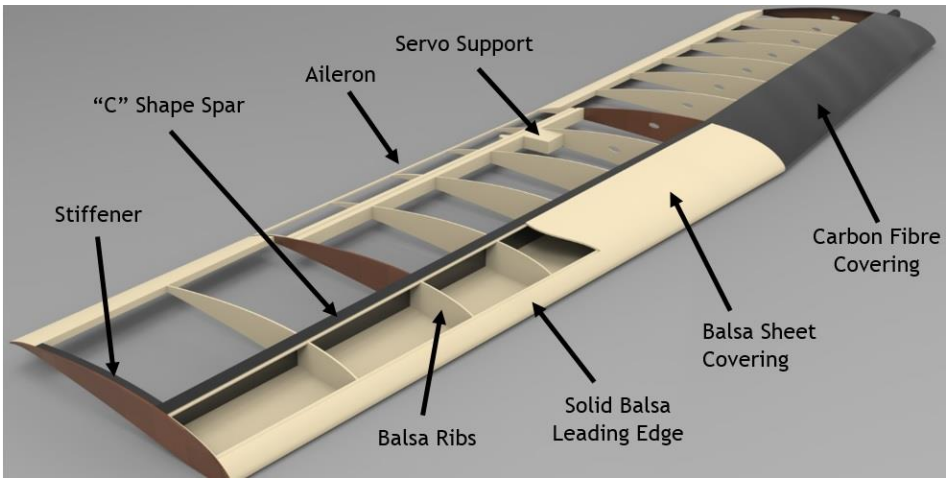

Figure 35 - CATIA rendering of a wing tip modification (Method 1)

The first option considers a wing box made of balsa with several balsa ribs connecting the existent carbon fibre spar to the solid balsa leading edge and covered with a thin layer of balsa sheet (figure 35). The second option comprises the same materials of the previous wing box, i.e. a wing box made of expanded polystyrene core covered with the carbon fibre layer ensuring the desired twist (figure 36). Despite the higher level of complexity of this second option, it was decided to adopt it, seeing that it would support the same loads with a lower weight.

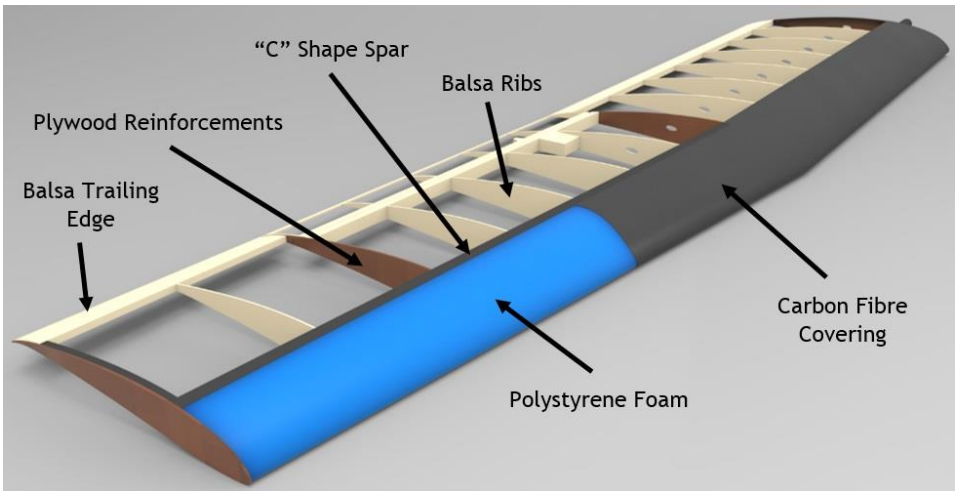

Figure 36 - CATIA rendering of a wing tip modification (Method 2)

4.4 Final Wing Tip Modification

Considering the modification method adopted, the expanded polystyrene core was created with the desired twist using CATIA V5 software. Once designed, it was exported and "fabricated" using a 3-Axis CNC router with the dual-side "print" for both tips of the wing (figure 37).

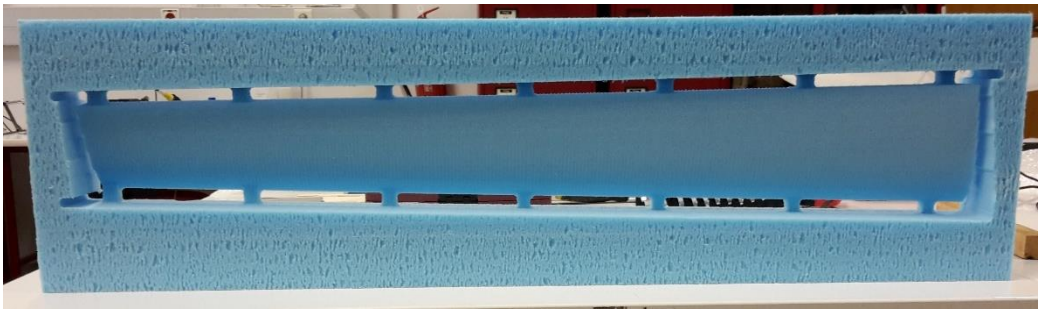

Figure 37 - Photo of dual-side print result of the new wing box polystyrene core

The next step was to remove the old wing boxes from the outer panels of the wing tips, saving the existent carbon fibre spar (figure 34). The new polystyrene foam wing boxes were then cautiously placed and bonded to the carbon fibre spar with epoxy resin.

Still regarding the 3-Axis CNC router programming, two counter moulds for each wing tip were made in order to press the carbon fibre against the polystyrene wing box during the curing ensuring the correct twist.

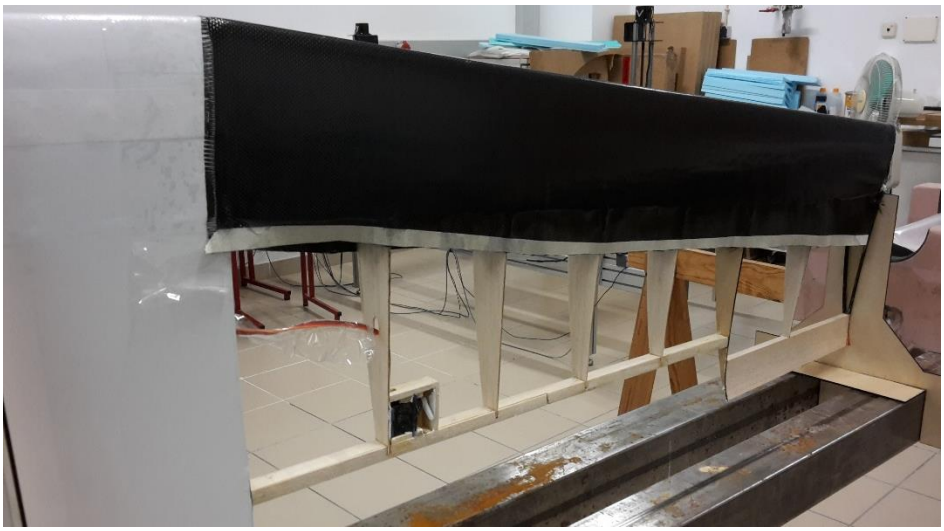

Figure 38 - Lamination of the new wing box

In order to keep the right twist and maintain the wing tip stable during the lamination process, a 2mm thick plywood support structure was designed in CATIA and cut using cut a laser cutting machine figures 38 and 39.

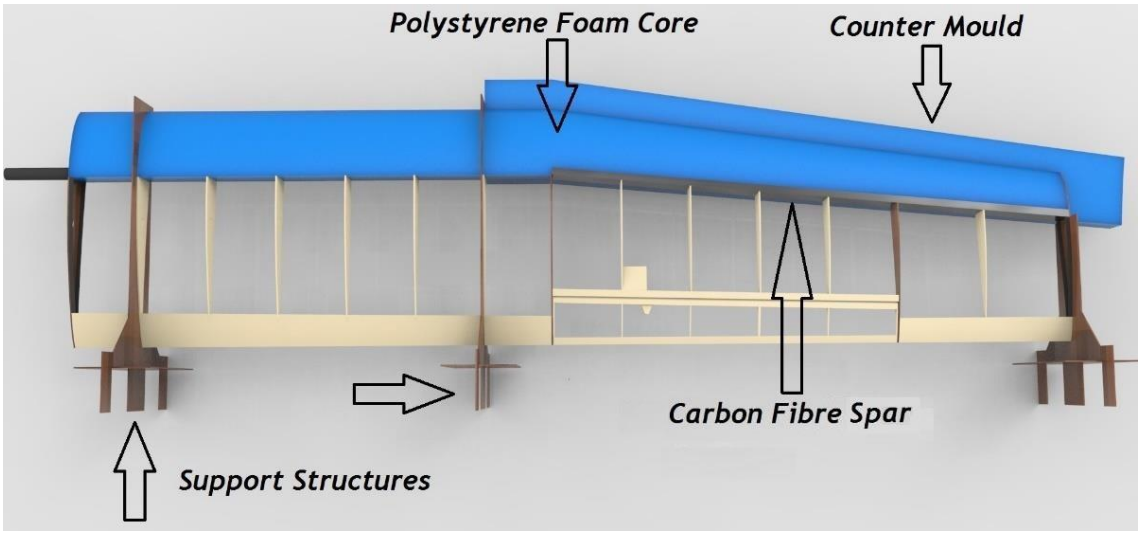

Figure 39 - CAD design of wing tip modification method

After the polystyrene core has been bonded, the lamination process was started by preparing all the required tools including the cutting of the carbon fibre and plastic film. After that, a first layer of epoxy resin was applied onto the polystyrene core and a 0.3mm carbon fibre fabric was also bonded with epoxy resin. The lamination process ended with the application of the plastic film between the carbon fibre and counter-moulds.

After the lamination of both wing tips, the splinters were cut and a layer of heat shrink film was applied covering all internal components of the wing, including the antennas, the airspeed sensor and the ailerons servos, resulting in a smooth and aerodynamic surface.

Table 3 - Weight variation of the wing tips modification

Wing tip	Weight before modification [N]	Weight after modification [N]
Left	5.389	5.543 (+2.86%)
Right	5.326	5.445 (+2.23%)
Wing without systems	16.529	17.274 (+4.51%)
Wing with systems	17.256	18.001 (+4.32%)

Table 3 refers to the weight variation of the wing tip outer panels modification. It is possible to see that total wing weight slightly increased by 0.745N with the wing tip modification. This can be justified by the overlapping of the fibres, epoxy glue absorption by the polystyrene foam, the different quantity of epoxy applied and the repaired parts during the lamination process.

Other important information that can be extracted from table 3 is the weight difference between the wing tips, this information permitted us to choose on which side of the wing the airspeed sensor was to be installed in order to balance the wing.

According to the airspeed sensor mass (12.7g), the best configuration which better centre the wing C.G. is to place the airspeed sensor on the right wing.

Chapter 5

5 UAV Systems Integration

5.1 Introduction

After a brief explanation (section 3.5) of all LEEUAV systems, in this chapter the functionalities, the requirements of the components of each system are clarified and explained. The final assembly of all the LEEUAV components, including connectors, fixation methods, layout, positioning and solar panels integration method are also addressed.

In order to clearly understand the final assembly of electrical, control, navigation and solar systems, a final assembly diagram is presented in section 5.4. At the end of this chapter the LEEUAV is fully equipped with all systems integrated and ready to fly.

5.2 LEEUAV Systems Integration

5.2.1 Flight Control System

Control Surfaces and Actuators

The LEEUAV's attitude during flight is controlled by five control surfaces, i.e. the two ailerons, two elevators and one rudder, actuated by servomotors or just servos.

There are many servos available at the model aircraft world of different brands, specifications and qualities. For this specific project, servos have to be reliable and oversized in order to not fail during long flights. To check the servomotor's reliability, it is necessary to load the servo for short periods of time, monitoring its current consumption and temperature. If during the test the temperature and current are approximately constant the servo will be usable on the LEEUAV.

Another important specification of the servos is the torque and the response time. The torque is the strength that the servo has to deflect the control surface. This required torque depends on the control surface area, control surface and servo deflections as well as flight speed [51].

$$T = 5.95 * 10^{-6} \frac{c^2 v^2 L sin(S_1) tan(S_1)}{sin(S_2)} \quad (14)$$

Table 4 - Required torque for each control surface servomotor

Control Surface	Control surface chord (c) [cm]	Control surface span (L) [cm]	Aircraft Speed (v) [m/s]	Max surface deflection (S_1,S_2) [°]	Torque (T) [Nm]
Aileron	6.7	50	15	45°	0.0108
Elevator	10.6	42.0	15	45°	0.2295
Rudder	11.0	36.8	15	45°	0.2217

According to Chuch Gadd [51], in table 4 the required torques for each control surface servomotor are calculated. The torque values presented are for the maximum designed LEEUAV airspeed (15m/s) and surface deflections of 45 degrees where the demanded torque is maximum.

The servomotors acquired for LEEUAV integration were the "Corona 939MG Metal Gear Servo 0.2452Nm/12.5g/0.14sec" for ailerons and elevators and a "Hitec HS-5125 MG 1.2749Nm/24g/0.17sec" servo for the rudder. The rudder servo was oversized in order to increase the reliability level.

Autonomous Flight Controller

To actuate the servos at the precise angles there are two options, they can be manually controlled by the pilot on the ground via radio transmitter or automatically by an advanced autopilot flight controller on board. Both options require a connection between the servos and the flight controller device which in this case will be the Pixhawk from 3D Robotics.

Despite the existence of other types of autopilot for radio controlled aircraft, Pixhawk is the most used and recommended due to its features, additional optional hardware, open firmware, advanced configurations and manufacturing quality. The Pixhawk hardware is a lightweight (38g), low-power consumption device of small dimensions (81.5x50x15.5mm). The internal system has an advanced 32bits ARM processor and several sensors, namely a gyroscope, accelerometer/magnetometer and barometer and a lot of connectivity options for additional sensors. Another important characteristic of this autopilot is its integrated backup system for in-flight recovery and redundant power supply inputs for better in-flight safety.

The setup options for this device are endless, so to simplify its application, in this work, only the chosen options are addressed.

Other important components that compose the Pixhawk system are the buzzer and switch. Buzzer is a simple speaker alarm programmable to advise the pilot of the state of the Pixhawk if the battery voltage is low or some problem has occurred. The switch is a simple button to arm/disarm the flight controller. Both are fixed inside the fuselage with a plywood support structure and velcro, respectively.

Even when LEEUAV is flying autonomously it is always necessary to monitor the aircraft, mainly when it is at long distances, i.e., flying out of line of sight. For these situations, a telemetry and video stream system inside the unmanned aircraft are required to simulate a "human presence". In spite of being part of navigation and communication systems, the telemetry data comes from the autonomous flight controller, which in turns reads the sensors. In sections 5.2.2 and 5.2.3 more information about the FPV and telemetry systems is presented.

Flight Control System Integration

The flight control system includes Pixhawk flight controller, 5 servomotors, wiring, control surfaces connections and mechanisms. Starting with servos, they were fixed with bolts

and epoxy glue in their respective pre-designed support structures on the wing, horizontal and vertical stabilizer. Subsequently the control arms and push-pull rods were securely bolted to connect the control surface to the servo.

The tail servo cables were pulled through the inside of the tail boom and aileron servos cables inside the wing structure, both up to the airframe Pixhawk position. Inside the LEEUAV airframe a thin plywood platform was created (figure 40) close to the aircraft C.G. to hold the Pixhawk device and align it with the three airplane axes. This platform ensures that all the accelerations, angular speeds and movements measured by Pixhawk are correct.

Once all servo cables were inside the airframe, they were connected to the 1st,2 nd,4 rd,5th and 6th main out ports on the Pixhawk (figure 41).

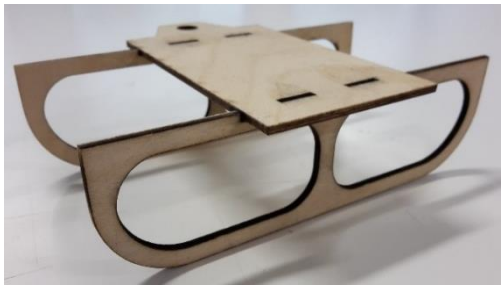

Figure 40- Flight controller support structure

In order to power the flight controller internal circuit and sensors, the flight controller was connected to its own power module. This power module from 3D Robotics is a simple stepdown circuit which adjusts the battery voltage to the correct Pixhawk operating voltage. This power module also has the functionality of measuring the current and voltage of the battery.

The Pixhawk's servo rail also need a separate power supply of 5V, so the two output JR cables from the UBEC to the Pixhawk rail were connected, namely, on the 1st and 8th ports of auxiliary out and main out, respectively. The Pixhawk would now use the power from these ports to power any external component.

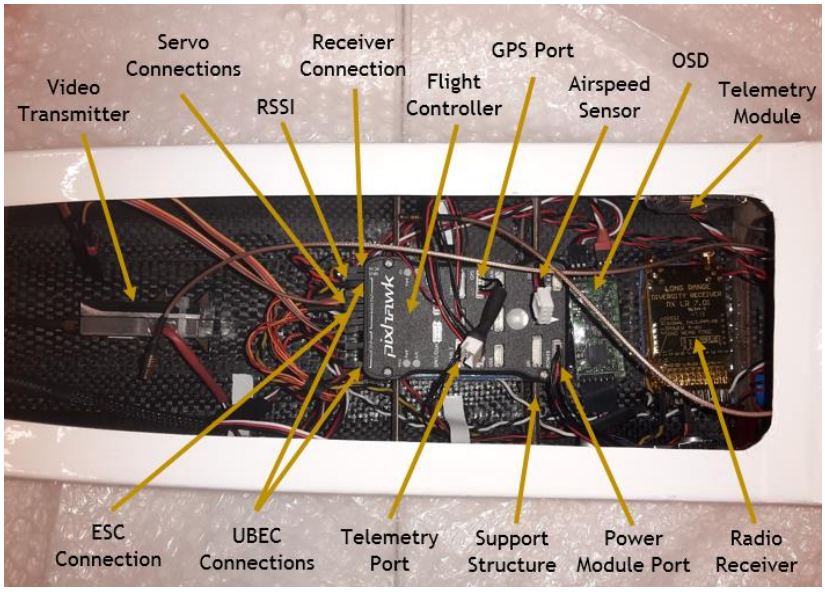

Figure 41 - Photo of the LEEUAV flight controller connections

5.2.2 Navigation System

GPS Sensor

The navigation system of an aircraft can be characterized in two main categories: the systems that use external references for guidance (GPS, GLONASS, etc.) and systems that do not require external references, inertial navigation systems (INS).

The Global Navigation Satellite System (GNSS), is a space-based navigation system that provides location and time information in all weather conditions, anywhere near the Earth surface using the triangulation method where at least three satellites are required to detect and locate a satellite signal receiver on Earth. There are some satellite navigation systems currently available, such as GPS (USA), GLONASS (Russian), GALILEO (Europe), BeiDou-2 (Chinese), etc. However, all of them use the same working principle.

Despite the great utility of the advanced technology used in satellite navigations systems, they are not very accurate and the accuracy worsens in bad weather conditions, which in aviation area could be disastrous. To enhance the accuracy of these systems it is usual to use additional inertial systems whose function is to aid the satellite based navigation. The inertial system uses a computer, motion sensors (accelerometers) and rotation sensors (gyroscopes) to continuously calculate the position, orientation, and velocity (direction and speed of movement) of a moving object, via dead reckoning, without the need of external references.

The LEEUAV inertial system belongs to the flight controller which already has the required sensors for the inertial navigation. For flight planning purposes and navigation procedures a GPS module from Drotek was added and connected to the Pixhawk as well. The "Ublox NEO-M8N" GPS used is capable of working with multiple GNSS systems, which means that it can receive the signals from GPS, GLONASS, BeiDou, Galileo and other positioning systems. A low-profile patch antenna providing a thin and flat surface at low weight, a dedicated rechargeable battery for faster start-up, EMI shielding to reduce the electromagnetic field, SBAS, D-GPS augmentation systems and USB micro connector for adjustment and configurations are some of the features of this GPS.

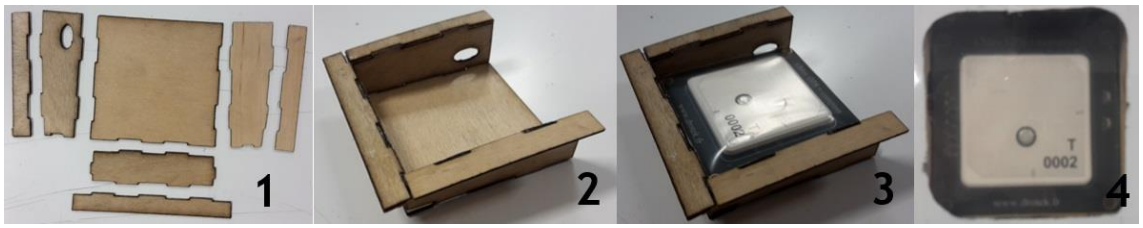

Figure 42 - GPS support structure

This GPS has an integrated digital compass "HMC5983 Magnetometer" module, which provides heading information through a digital interface.

Regarding the GPS module placement, this device was positioned in its own plywood platform (figure 42) on the upper surface of the wing, far from carbon fibre in order to avoid interferences and signal losses. The GPS and compass cables were passed through the wing, up to the airframe Pixhawk position and connected to the Pixhawk GPS port.

Airspeed Sensor

Still in the navigation system components, another needful element is a digital airspeed sensor. The chosen airspeed sensor (from 3DR) is constituted by a 100mm pitot tube connected to a small sensor circuit board through two silicon tubes for static and total pressure readings. This airspeed sensor has a resolution of 0.84Pa and it is capable of reading airspeeds up to 100m/s. Another interesting feature is its internal temperature sensor which allows the calculation of the true air speed (TAS) from indicated airspeed (IAS) using a static pressure sensor of Pixhawk. The airspeed sensor calculates the IAS through the difference between the static and total pressure acquired by the pitot tube and it subsequently calculates the air density based on its internal temperature readings and Pixhawk's static pressure readings. Using the indicated airspeed and the local air density it calculates the TAS. The installation of this sensor required careful attention since its silicon tubes and pitot tube cannot be obstructed or perforated otherwise it will give wrong airspeed readings.

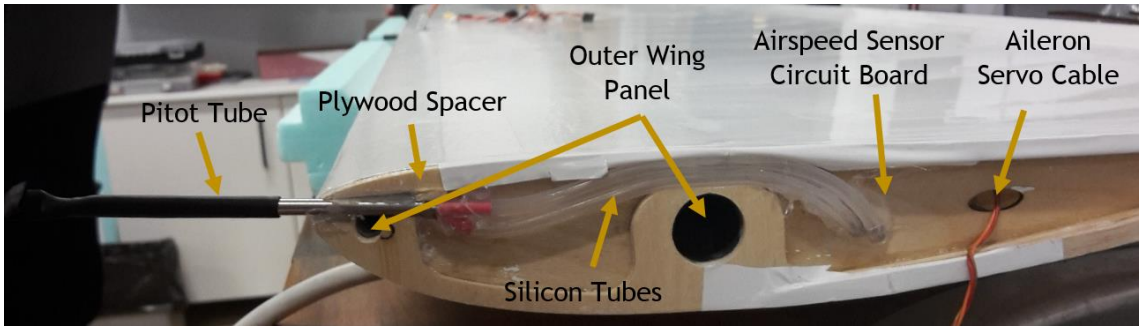

Figure 43 - Airspeed sensor installation and support structure

To avoid the influence of the propeller's flow in the airspeed sensor readings it was decided to place the pitot tube at the leading edge of the wing where the airflow is almost clean, without disturbances.

Taking into account the importance and reliability of the flight data collected by this sensor and in order to fit the pitot tube and respective silicon tubes, a 4mm plywood spacer was created between the central panel of the wing and the right outward panel (figure 43). The digital airspeed sensor cables were placed inside the wing structure up to the fuselage.

There are a lot of sensors, such as temperature sensors (for monitoring the internal and external air conditions), rpm sensors (to measure rotational speed of the propeller) and many other sensors for redundancy effects could be added to the Pixhawk peripherals. However, for the LEEUAV mission goals, these would increase the flying weight and power consumption, consequently decrease the flight endurance. So, to maitain the low theoretical weight and achieve the proposed endurance, these extras were not considered.

Telemetry

Telemetry is an automated communication process by which measurements and other data are collected at remote or inaccessible points and transmitted to a receiving equipment

for monitoring. In this case the telemetry consists of collecting, transmitting and receiving the on-board sensors information and display it on the GCS.

The telemetry information acquired by the on-board sensors, including airspeed, relative and absolute altitude, distance from launch, position, aircraft attitude, flight mode, battery voltage and current, are redundantly transmitted to GCS on FPV system.

More information about the streamed telemetry data can be found in sections 5.2.3 and 5.3, land-air communication system and ground control station, respectively.

First Person View and On Screen Display

Despite the very wide interface of the Mission Planner software, it is difficult and unsafe to control an out of line of sight aircraft using just the instruments data provided by Mission Planner (MP). To solve this problem additional hardware had to be included, namely, the first-person-view (FPV) system. This feature allows the pilot to operate the aircraft without seeing it. To stream the video image, the FPV system requires an on-board camera and an on-board dedicated video transmitter module.

In ground control station, a screen display connected to a video receiver module shows the view from the aircraft during the flight.

To control an aircraft just with video image could be difficult and unsafe due to the spatial disorientation in bad weather or low visibility conditions. To solve this problem a second telemetry information stream was superposed in FPV video through an on-board electronic circuit board, the on-screen-display (OSD). This device stands between the video camera and video transmitter, collecting the sensor information from the flight controller and superimposing it in FPV video.

This configuration allows to monitoring of the aircraft status, namely, the horizontal and vertical speed, the attitude, remaining battery capacity, radio signal strength, home altitude, airspeed and other information, while operating (figure 47).

The OSD chosen to integrate the LEEUAV was the “AlceOSD 0v3” the justification is in line with the open-source firmware and versatility of this device, namely the graphical interface of the information displayed on video image. The LEEUAV video camera is a “RunCam 600TVL” with a 2.8mm lens of 86° view angle, infra-red (IR) sensitive option, combined with a very low mass (12g) and dimension (28x28x22mm).

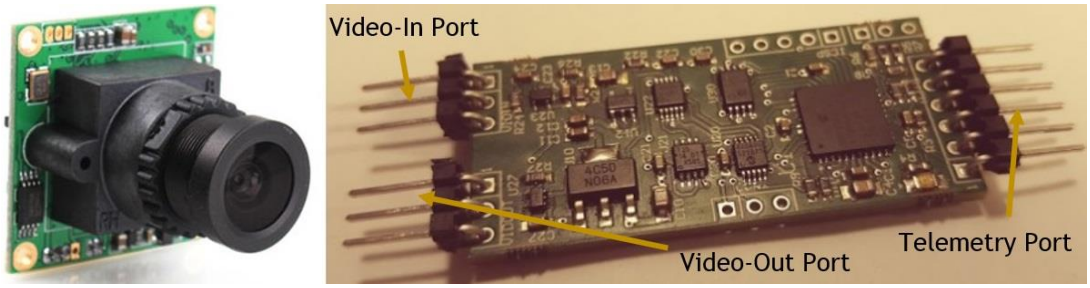

Figure 44 - On left the "RunCam 600TVL" and on right the OSD "AlceOSD 0v3"

5.2.3 Land-Air Communication System

To control the aircraft from ground station, a communication system that allows to transmit/receive flight data to/from the aircraft, respectively is required. The input signals on the ground control station are modulated and sent by a transmitter to the aircraft. In the aircraft a receiver acquires this signal, and once acquired, the information is demodulated and processed by the receiver and then controls the components of the aircraft.

The wireless streaming method of the information between the ground station and the aircraft, through the air, is made by electromagnetic waves and this method was carefully chosen in order to avoid interferences and ensure an adequate range for LEEUAV's mission. There are several types of wireless information streaming, such as Bluetooth, Wi-Fi, FM/AM radio, infrared, etc. Although they belong to the same electromagnetic spectrum, they have different characteristics, namely, frequency, speed, range, wavelength, propagation and bandwidth.

The LEEUAV mission requires three independent communication protocols, for flight control inputs at long distances, for feed-back information from on-board sensors (telemetry) and for video streaming (FPV). Furthermore, an omnidirectional propagation of all of these signals is required, once the airplane goes out of line of sight.

The three independent communication protocols mentioned must have different operating frequencies between them, to avoid interferences.

The commonly used frequencies for radio controlled systems are, like the name itself indicates, the radio waves (3kHz to 300GHz). The radio waves have a lot of interesting characteristics, such as the non-interference with electronic circuits, the low energy transported does not penetrate the human skin and they have a huge wavelength (long transmission range) making them the most appropriate for this application.

However, nowadays there are a lot of radio signals under use as a normal radio or TV broadcasting. In order to operate an RC system at the same time as these broadcasting systems, an interval of the radio frequencies spectrum, which can be used for RC airplane purposes, was established (by law), to "facilitate" the choice of the currently commercialized RC systems for the LEEUAV.

One last notion that has to be explained is the channels of a radio transmission. These channels are just small variations of the operating frequency, so that they can control different components of the aircraft such as servos, ESC, landing gear, etc. For the LEEUAV operation at least a 4Ch transmission for independent control of ailerons, rudder, elevator servos and ESC is required. However, 7Ch were used to control the flight modes, OSD information and dual rates.

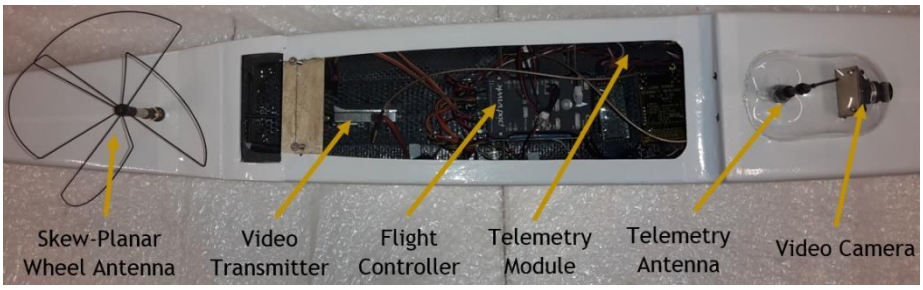

Figure 45 - Arrangement of the land-air communication system components

Radio Receiver

The on-board equipment of the communication system can be sub-divided into two types, reception and transmission equipment, the reception of the input signals is merely guaranteed by the 12Ch receiver (Scherrer RX700LR V7).

The choice of this on-board receiver was based on its exceptional features, namely the low operating frequency of 433MHz and dual diversity antenna system which allows the co-existence of other on-board transmitters operating at different frequencies without interferences. Another important feature of this device is the selectable option between PPM/PWM signals since the input signals acceptable by Pixhawk are only PPM, otherwise a PPM encoder would have been necessary. The radio signal strength indicator (RSSI) feature allows the measurement and display of the signal strength that aircraft is receiving in real time.

Video Transmitter

For video streaming (FPV) a higher radio wave frequency was required in order to have a better image quality, however a bigger frequency has a lower range, so the radio frequency of the FPV system has to balance these two requirements. The interferences with television channels operating frequencies is another parameter that has to be taken into account, which in Portugal is around the 900MHz. So, considering the availability of the FPV equipment on the market, the operating frequency of the FPV system chosen was 1.3GHz.

An analogical video transmitter connected to a Skew-Planar Wheel radial antenna was used, not only for video image streaming but also for microphone audio streaming.

Telemetry Transceiver Module

As referred before, the telemetry information acquired by on-board sensors and Pixhawk is doubly transmitted by an on-board telemetry transceiver module connected to a linear vertical antenna with a dedicated service of 2.4GHz frequency. A RM024 from Laird Technologies transceiver module was used.

Wiring and Connections

The 8th port of the on-board receiver was connected to one of the Pixhawk's auxiliary ports and its purpose was to power the receiver (5V). On 12th port of the receiver was soldered the RSSI cable and then connected to Pixhawk's SBUS port. To transmit the encoded PPM signals

from the receiver to the flight controller there is a connection between 11th port of the receiver and the RC port on Pixhawk. This connection carries all the input signals to control the aircraft, encoding multiple channels through a single cable by PPM signals.

Still connected to the receiver are two dipole antennas, which are located in the left and right wing respectively at an angle of 90°, with a specific disposition according to the manufacturer's manual.

Regarding the physical connections of the FPV system, which includes the telemetry, OSD circuit board, FPV transmitter and the video antenna, first the telemetry port 2 from Pixhawk was connected to the OSD circuit board. Once done, to overlay this telemetry information on the video image, the OSD video input port was connected to the camera and the OSD video output port to the video transmitter. In turn, the video transmitter was connected to the Skew-Planar Wheel radial antenna which is located at the rear part of the airframe, far from other antennas to avoid interferences.

Like video transmitter, the telemetry transceiver module is located inside the airframe and its input port was connected to the telemetry port 1 of the Pixhawk. The remaining output port of the telemetry module was, of course, connected to the linear 2.4GHz antenna which is located at the front of the airframe, behind the camera bubble (figure 45).

5.2.4 Propulsion System

After the flight control, communication and navigation systems, the fourth but no less important, is the propulsion system. In the LEEUAV the propulsion system is electric, so the topics covered in this section are the battery, ESC, electric motor and propeller.

Considering cruise, the most significant phase of the flight, the propulsion system was designed for this phase. However, the power requirements for other flight phases such as take-off and climbing cannot be ignored. Due to the large wingspan, the take-off is done with a bogey, so the propulsion system has to ensure the sufficient power for the rotation of the aircraft. On the other hand, in the climbing phase the aircraft must have enough power to guarantee a satisfactory rate of climb to reach the cruise altitude and comply with the project requirements.

Other important consideration is the reliability of all propulsion system components since for the long 8-hour flight a reliable system (battery, ESC and motor) which does not heat up or fail during continuous power consumption is required.

Electric Motor and Electronic Speed Controller (ESC)

In Luís Cândido's work [31] a suitable propulsion system for the LEEUAV, which considers the take-off, climb and cruise requirements, was briefly described. This propulsion system includes an electric motor (Hyperion ZS 3025-10) (figure 46) with a maximum power output of 1150W controlled by a Phoenix Edge ESC with 75A of continuous current.

Despite the 1150W of the electric motor output power, this value is far from being reachable with the current LEEUAV propulsion system configuration. The maximum power

installed depends on the battery voltage and propeller. The higher propeller pitch or the diameter, the higher current consumed. So, the maximum power installed it is the input voltage (battery) times the measured current for a given propeller. Considering the biggest propeller tested (16x8 in) the maximum installed power was 643W.

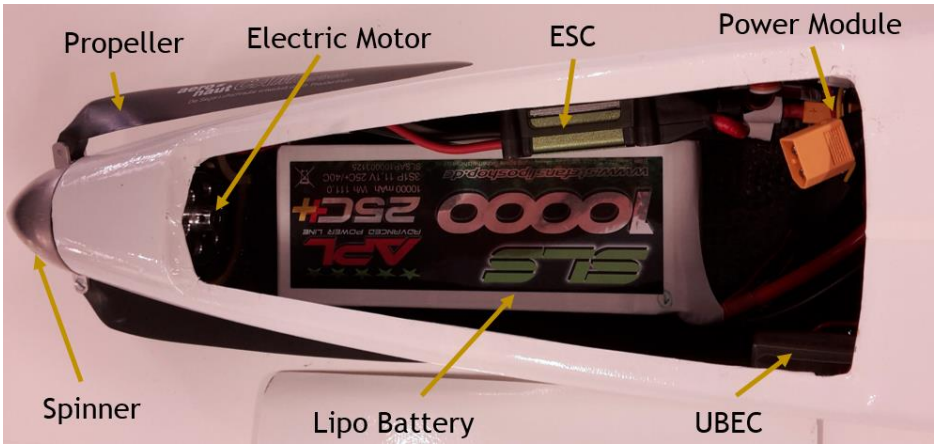

Figure 46 - Propulsive system of LEEUAV

The majority of the ESCs available on the market have an internal function which consists of braking the electric motor when the throttle is at zero setting by shorting two of the terminals electronically. This function allows less drag, since the propeller is forced to stop spinning when thrust is not required and thus does not withdraw kinetic energy from the aircraft. Another reason for the use of the dynamic brake lies in the fact that the propeller blades are retractable and they must be stopped in order to be retracted without damaging the fuselage.

Propeller

To produce thrust the electric motor has to be connected to a propeller. However to get high levels of efficiency the choice of the propeller has to be carefully studied. As described above in section 2.7 there are many types of propellers that may varied airfoil, shape, twist and variable/non-variable pitch. Variable pitch propellers are more suitable if the flight conditions often change, since adapting the pitch can ensure a highest efficiency at each speed of each flight phase. This functionality can be used automatically with an in-flight thrust measuring device. However, additional mechanisms are required to control the propeller, which means more weight. In the case of the LEEUAVm, more than 90% of the flight time is carried out at constant speed in cruise, so the propeller can be selected for that condition. To select an adequate propeller, a comparative study of various propellers had previously been carried out at UBI [31] to assess the total power consumption for a typical flight. Then, considering the existing propellers in Structures and Vibrations Laboratory and after a numerical analysis performed by Professor Pedro Gamboa, a fixed pitch folding blades propeller from Aeronaut was chosen. This propeller is 16 inches in diameter and 8 inches of pitch.

Fixation Methods

The electric motor was fixed with 4 bolts inside the airframe carbon fibre reinforced nose (firewall) using thread-locking fluid. Outside the fuselage and attached to the motor shaft is a mechanism for propeller folding and spinner fixation. Inside the airframe, the battery, PM and ESC were secured with velcro into the fuselage.

Despite the LEEUAV not having any internal refrigeration, the critical components, i.e. the components which may become hot (ESC, motor and battery), are securely fixed away from each other as well as from main on-board equipment. Due to the oversized components and low power requirements no component heating related problems are expected during the LEEUAV cruise flight.

Wiring and Connections

Starting from the battery, there are two electrical cables (+ and -) that connect to the PM through an XT60 connector. In turn, the PM output cables connect the battery to the ESC. The ESC has three other input cables to connect with the flight controller, so that, Pixhawk can control the current provided to the electric motor. The remaining three output cables of ESC are obviously for connecting the electric motor.

5.2.5 Electrical System

The electrical system is responsible to provide electric energy at correct voltage to all on-board electronic components. For that, there are a set of cabling connections and different components to regulate and distribute the adequate power for all consumable components. The propulsion system is by far the one that requires more power. During cruise, the average value of the energy used by the electric motor is 84.3% and the flight controller, servos, video camera, transmitters/receivers and other modules consumes the remaining 15.7% energy.

In table 5 below is the acceptable voltage range and the maximum operating power consumption for each on-board electronic power consumer. The power source for each component is also identified in Table 5.

Table 5 - Voltage range and operational power consumption of all on-board components

Component	Voltage Range	Power Consumption	Power Source
Flight controller*	5.37 V	12.080 W	Power module
Servo	4.8 - 6V	0.960-1.440 W (x5)	UBEC
Video camera	5 - 17 V	0.600 W	Lipo battery
Video transmitter	10.5 - 13 V	6.500 W	Step-down converter
Radio receiver	5 V	0.670 W	UBEC
UBEC	6 – 12.6 V	<0.690 W	Lipo battery
Step-up/down converter	3.8 – 32 V	<0.100 W	Lipo battery
ESC	6.4 - 33.6V	<0.200 W	Lipo battery

*GPS, airspeed sensor, telemetry module, buzzer and switch power requirements are included.

From practical tests, it was observed that the average power consumption with all systems operating (except the propulsive system) was 0.98A at 12V corresponding to a total of 11.75 W.

Battery

A battery is required not only to power up the propulsion system and on-board equipment, but also to store the surplus of energy produced by the solar panels. The battery specifications, namely, the voltage and rate of discharge, are chosen by the propulsion system. In this case a 11.1V (3S) and at least a 36A discharge rate battery is required. Generally, the capacity of a battery is proportional to the battery weight, however there are different battery producers with different battery specifications and prices.

Taking into account the LEEUAV propulsion system design, mission requirements and considering the existing batteries from Structures and Vibrations Lab. at UBI, there were two suitable options to becomes part of the LEEUAV electrical system, a 10000mAh (3SP1) or 18300mAh (3SP1) battery.

With a single 10000mAh battery, the first option is the lightest one, although it has a lower endurance. Using the 18300mAh battery pack it will almost double the on-board available energy with a slightly increase in weight, since this pack has a bigger specific energy. However, during the flight tests it was found that the 18300mAh pack does not comply with the manufacturing specifications, i.e., the battery was found to have a much lower discharge rate and capacity (11000mAh), huge internal resistance (41.79Ω for 10A continuous discharge) when compared to the 10000mAh battery (6.98Ω for 10A continuous discharge). So, it became useless for LEEUAV application.

Universal Battery Elimination Circuit (UBEC)

UBEC is an electronic circuit that converts the high voltage (12.6 V) of the battery pack to a consistent and safe 5 or 6 volts (selectable) for the desired components. In LEEUAV, the 5V components are the 5 servos and the radio receiver. Considering the power requirements and leaving some extra margin for other future applications, the Turnigy 15A UBEC was chosen.

Step-Up/Down Converter

Similar to UBEC, a step-up/down converter is a device that converts DC-to-DC power stepping up or down the voltage (while stepping down or up the current, respectively) from its input (battery) to its output components, in this case the video transmitter and video camera.

Power Module

In order to properly power the flight controller it is necessary to use a power module (PM). This PM is a dedicated device that has three important functions:

- Provide a stable 5.37V and 2.25A power supply for Pixhawk operation, reducing the chances of a burn-out;

- Monitor the battery's voltage and current and triggering a return-to-launch when the voltage becomes low or the total power consumed during the flight approaches the battery's capacity;
- Accurately compensate the interference on the compass from other components based on PM readings.

Wiring and connections

Starting from the battery, this was first connected to the power module in order to provide a stable power supply for the operation of the flight controller and also allow the monitoring of the battery voltage during the flight. After that, two JST connectors for UBEC and step-up/down converter were directly soldered onto the power module output XT60 connector. The Turnigy UBEC has two 5V output cables connected at the ends of Pixhawk servo rail, as referred before in section 5.2.1, powering the servos and radio receiver.

The other JST cable takes the electric energy from the battery to the step-up/down converter, which in turn provides for video transmitter and video camera a stable 12V.

All the additional components and sensors connected to the Pixhawk are powered by the Pixhawk internal circuit itself, getting its energy from Pixhawk PM.

5.2.6 Solar System

The solar system of LEEUAV is composed of 4 modules each one with 2 sets of 10 and 12 photovoltaic cells respectively covering 53.3% of LEEUAV wing area with 0.792m^2. The reason for these solar cell modules is that the wings may be disassemble for transportation. The solar cells used on this project were the C60 solar cells from Sunpower. The maximum efficiency of these cells is 22.5%, so it means they are capable producing a maximum of 4.3W (per cell) of electric power with 1000W/m^2 of solar irradiance.

Despite the existence of many solar chargers, a Genasun GV-10 for Li-ion batteries was chosen. The justification is based on its low weight, high electrical conversion efficiency, compatibility with C60 solar cells and 3S Li-ion batteries used in LEEUAV. Other exceptional and decisive features of this SCC are the integrated ultrahigh speed MPPT controller, low power consumption and compatibility with total solar panel output voltage/current range.

So, the components that integrate the solar energy system are 44 solar cells arranged in four panels sets with a nominal voltage of 25.6V and 5.93A of maximum current (depending on the irradiance), a solar charger controller with MPPT function and a 100A current sensor to control the amount of energy produced by the panels during flight.

Wiring and Connections

In order to have an adequate voltage and current at the input port of the SCC and knowing the single C60 solar cell nominal voltage (0.58V), the solar cells were firstly arranged in series between (A–B) and (C-D) panels and secondly between (B-C) panels (figure 47). Between the centre panels and outer panels there are JST connections and between centre panels (B-C)

there are 3.5mm bullets and a XT30 total output connector. For better understanding, there is an electric wiring diagram in annex B.

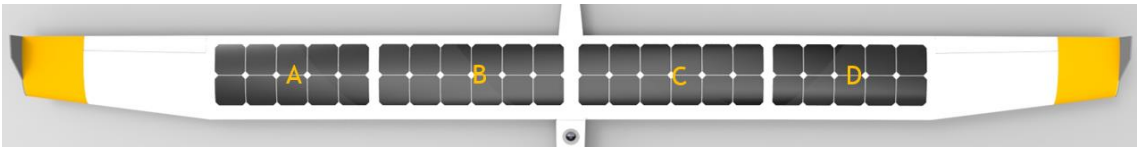

Figure 47 - Top view of LEEUAV wing with solar panels

As soon as the panel's electrical connections were completed, the output cable from solar panels was connected to the SCC through a XT30 connector directly soldered onto Genasun GV-10 power input slots. After that, the output slot of the SCC was connected to the current sensor and to the battery. This current sensor was also connected to flight controller ADC 3.3V port.

5.2.7 Integration onto the Wing

There are several possibilities for solar panels integration onto the wing, however considering the existing wing there are some restrictions, such as airfoil shape, wing internal and external structures, ailerons, GPS and antennas positions. Taking into account the existing wing and to avoid modifying the wing structure, the easiest way to fix the solar panels modules is on the upper surface of the wing. To fix them a very strong double-sided adhesive tape was applied over the heat shrink film of the wing and a transparent adhesive tape to smooth the edges of the solar panels, reducing the drag and the airfoil leading edge step.

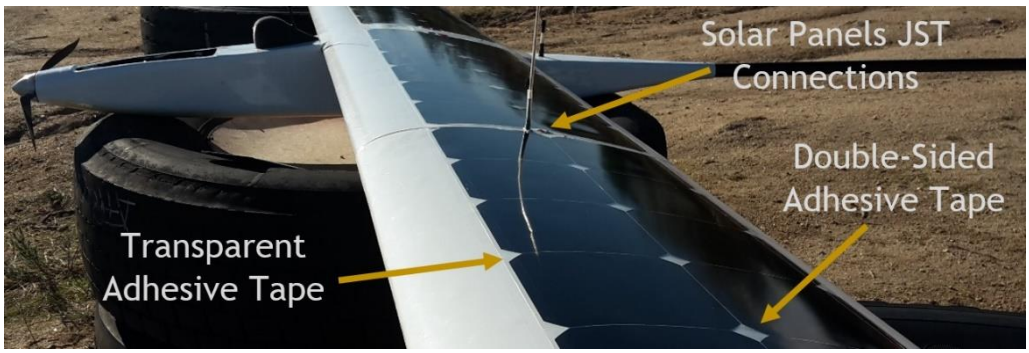

Figure 48 - LEEUAV solar panels fixation method

Despite of the low thickness of the solar panels, their position on the wing influences the airfoil efficiency during flight. So, based on the analysis performed in the work of Luís Freitas [35], the best position for placing the solar cells on the upper surface of the LEEUAV's wing, is between 21% and 23% of the airfoil's chord. The performance coefficient most affected by the presence of the solar cells is the drag coefficient, and between the best positions, none of them exhibit best performance for all the lift coefficient range. For the lift coefficient range tested, the position at 23%, delivers best performance for most of the lift coefficient range. But, the position at 21% presents the best performance for the mid design lift coefficient, the cruise lift coefficient. The associated losses are of around 5% of the lift-to-drag ratio relative to the clean airfoil performance.

There were other alternatives for the solar cells integration, such as the integration on other parts of the aircraft (fuselage, stabilizers and wing tips) or a different wing integration method. The reasons why the solar cells were not placed on other parts of the airplane are that there would be a higher risk of breaking, the C.G. position, the wiring and the available space to place them.

Regarding the solar panels placement on the wing, the ideal fixation method would be flush with the wing's upper surface so that the airfoil contour would stay smooth without any discontinuity on the profile but this would require the creation of a new wing with a special notch of the same thickness of the solar panels where the solar panels would be placed.

5.3 Ground Control Station

5.3.1 Flight Control System

Radio Control

Considering the LEEUAV flight control system, an 8-channel radio would be enough to handle all the functionalities of this aircraft. However, a 16Ch radio controller Royal SX from Multiplex was used since it had already been acquired by the Structures and Vibrations Lab.

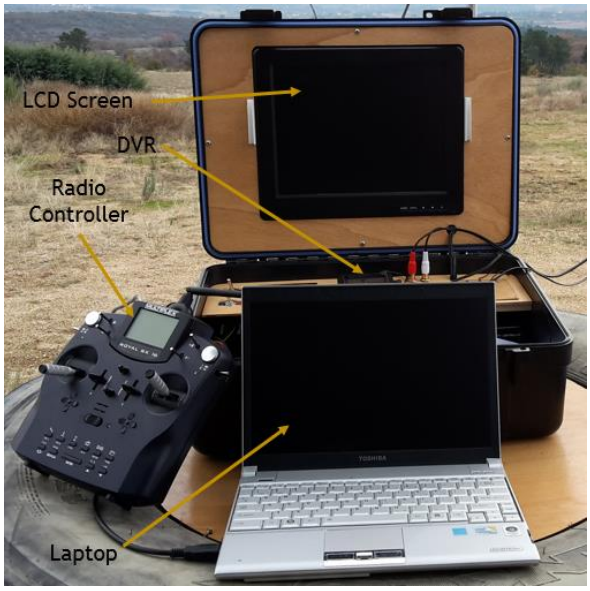

Figure 49 - Ground control station

This radio control has a lot of interesting characteristics such as different template modes and comprehensive adjustments for fixed wing aircraft, four memory slots for trim and exponential settings for each aircraft, timers, small LCD screen where up to fifteen parameters of telemetry information can additionally be displayed.

Screen Display

In order to display the video image acquired by the LEEUAV on-board video camera in real time a high brightness 12.1" LCD monitor was used, enabling good visualization even when sunlight falling directly onto it. Another very important feature of this monitor is the non-

bluescreen function, i.e., if the video signal received is low, the screen does not turn off and displays the received image, with much noise associated of course.

N°	Description	N°	Description	N°	Description
1	Battery Percentage	7	Coordinates	13	Radio Signal Strength
2	Battery Voltage	8	Number of Satellites	14	Artificial Horizon
3	Current Consumption	9	Compass	15	Home Heading
4	Airspeed	10	Vertical Speed	16	Home Distance
5	RADAR	11	Barometric Altitude	17	Relative Altitude
6	Flight Mode	12	Wind Speed	18	Throttle

Figure 50 - Video image received on GCS during LEEUAV flight

Figure 50 shows a screenshot of the video interface displayed on the GCS. No. 1 shows the battery percentage based on the stored energy in the battery at the beginning of the flight and the used energy during the flight. No. 2 and 3 refers to the battery's voltage and real-time current consumption, respectively. No. 4 is the airspeed in m/s (with a decimal place) read by the airspeed sensor. No. 5 is the radar which shows the relative position of the aircraft to the runway/airstrip. No. 8 shows the number of locked GPS satellites. The compass sensor gives the heading of the aircraft (No. 9). No. 11 shows the absolute altitude (sea level). In the No. 12, the wind speed and direction are displayed. In the artificial horizon it is possible to see the pitch and bank angles (from gyroscopes) and in the numbers 15, 16 and 17 are the heading, distance and altitude to home, i.e., the relative altitude to the launch site, respectively.

Laptop

To control the LEEUAV flight controller and monitor the flight data collected by the sensors in real time, a small laptop Toshiba Portege model R600 with long life battery was used to handle the Mission Planner software from which the majority of the commands and flight controller configurations can be inputted.

Mission Planner Software

To operate, monitor and record all the flight information of an unmanned aircraft using an open source flight controller like Pixhawk, a software with a graphical interface (GUI) which continually displays the flight data read by the on-board sensors is recommended. The software used in this work was the Mission Planner, created by Michael Oborne, which is a configuration utility or a dynamic control supplement for an autonomous vehicle, with which is possible to programm missions, log and analyse telemetry data, enabling a ground-control set up for in-flight performance optimization [52].

Figure 51 - Mission planner software (flight data screen) [52]

Mission Planner software is able to setup, configure and load a flight plan for an autonomous flight and at the same time record all the flight data for further analysis, including all flight controller parameters, altitude, ground speed, airspeed, waypoint distance, vertical speed, bank angle, heading, artificial horizon, receiver and telemetry signal strength, GPS status, flight mode, etc.

Figure 51 shows the typical GUI of the MP, in upper left hand corner it contains a head up display (HUD) with the most important information of the flight status including an artificial horizon background, on the right, a map with the flight path and actual position of the aircraft and on the left under the HUD a numerical display of some important parameters of the aircraft, such as altitude, speed, waypoint distance, etc.

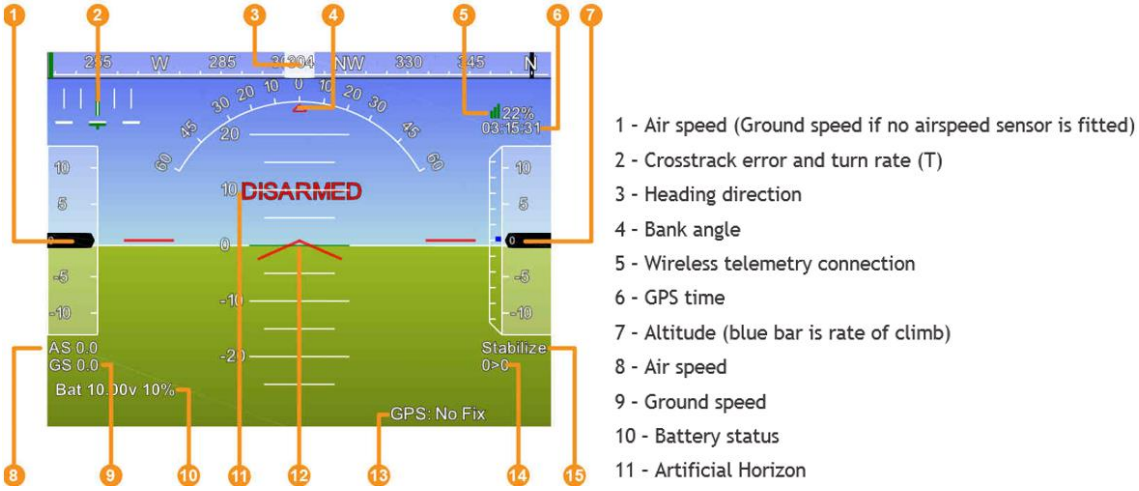

Figure 52 - Artificial horizon of MP software interface [52]

In figure 52 a detailed view of the MP artificial horizon is displayed, where all the required parameters to control the aircraft are present.

5.3.2 Land-Air Communication System

Radio transmitter

In order to establish a connection between the radio transmitter and the aircraft it is necessary to connect (by cable) an UHF module (figure 53) capable of operating at the same frequency of the on-board receiver (433MHz). So, a compatible Tx700 PRO Long Range station was applied, with three output power levels of 0.5, 1 and 2W to secure the range and signal desired. At maximum output power level, this module can communicate with the aircraft at a distance up to 100km.

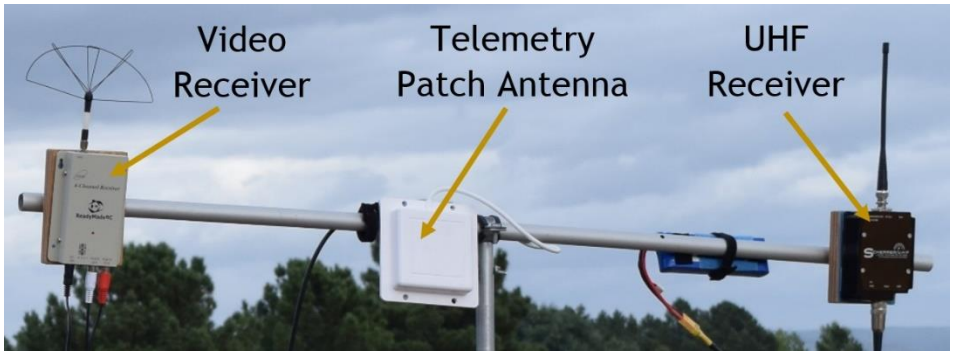

Figure 53 - Ground control station antennas tripod

Video, Telemetry Receivers and Antennas

In order to receive the video signal from the LEEUAV two analogical video receivers at a frequency of 1.3GHz were used simultaneously. One of the receivers was connected to a helical antenna of 11dBi which operates at a frequency range of 910-1680MHz with a receiving angle of 60°. This antenna is ideal when the aircraft is away from the reception point. However, this short receiving angle makes this antenna impractical for closer distances.

For a good reception of the video signal over short distances, a Skew Planar Wheel omnidirectional antenna was used, which operates at frequencies between 1200-1360MHz. The pattern of radiation of this antenna (radiates in all directions), does not require any adjustment in place, but its range is smaller than the helical antenna mentioned above.

Regarding the telemetry receiver, a simple transceiver similar to the one installed on LEEUAV was used and connected to a 2.4GHz patch antenna.

5.3.3 Electrical System

The construction of the GCS used during the LEEUAV flight tests was not part of this work. Nevertheless, to understand its operation, its components and features are explained here.

Video Diversity Controller (VDC)

This (Oracle) video diversity controller is a device whose function is to compare the two input signals from video receivers and decide which one has better video quality. Once done, the VDC pass this signal to its output. This allows the use of two different video receivers coupled with different antennas. Where, in a certain condition, an antenna may have better performance than the other, and the VDC will choose the better one to show on LCD screen.

Power Distribution Unit (PDU)

This function of this component (EzPowerBox from Immersion) is to distribute the power and video signal received from the different video receivers on GCS. In terms of power distribution, this unit has four regulated outputs that are connected to the inputs of other GCS components. In turn, this unit has two inputs to which are connected two 3S LiPo batteries, thus making the power system redundant.

Batteries and Wiring

Despite the physical simplicity of the GCS, it has to be portable, easy to assemble and reliable in order to ensure its operability during the long solar flights. Thus, the transmission/reception modules and components of the GCS have to be correctly powered by suitable batteries so that they do not fully discharge until the aircraft lands.

Considering the power consumption of each module the batteries used in GCS was two 3SP1 8000mAh LiPo batteries to power the PDU and one 3SP1 5000mAh battery to power the radio transmitter, thus allowing at least 10h of continuous operation.

With regard to wiring, the two 3S LiPo batteries are connected to the PDU inputs, then the PDU spreads the batteries energy for its four PDU outputs ports, which are connected the two video receivers, the VDC and the LCD screen.

The received video signals are injected into the VDC that selects automatically the signal that has better quality to subsequently pass it to the LCD Screen.

The radio controller “Royal SX” has its own dedicated nickel metal hybrid battery and it is directly connected by cable to the radio transmitter.

Lastly, the telemetry transceiver and its antenna are simply connected and powered by USB cable from the laptop.

5.3.4 Recording System

In order to analyse the flight data collected by the flight controller sensors and video camera in lab environment a recording system was necessary.

There are two ways to record telemetry flight data by data-flash logs using an on-board data flash memory in the flight controller and telemetry logs (tlogs) recorded by the Mission Planner in GCS via MAVLink. The main difference between these two logs is in the receiving time, the data-flash logs are only available after landing but the tlogs are available during the flight time. For this case, it will only be used the data-flash logs for further LEEUAV performance analysis in MATLAB, since there is no need to analyse the information during flight.

On the other hand, for video image recording a digital video recorder (DVR) was used, which is a small device connected to the LCD screen and records all the flight video as well as OSD information to an SD card.

5.4 Final Assembly Diagram

For a better understanding, in figure 54 is a side view of the physical positioning of each LEEUAV internal component.

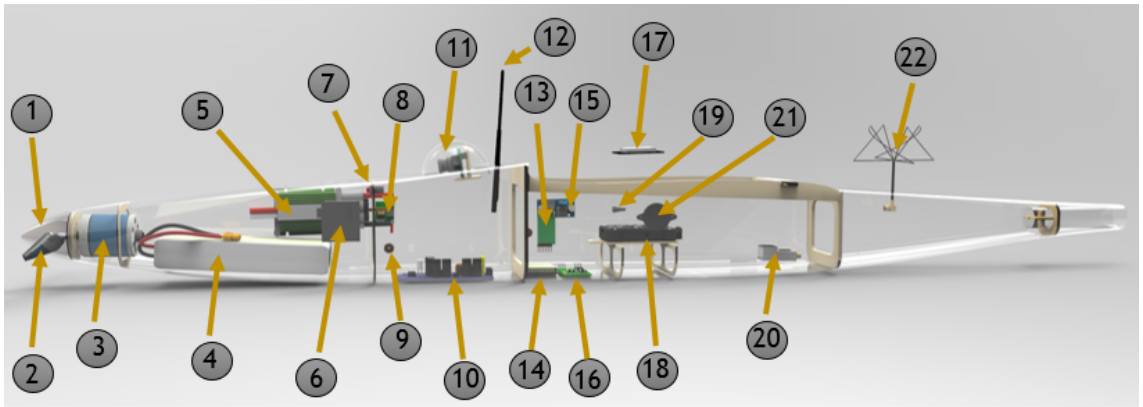

Nº	Description	Nº	Description	Nº	Description
1	Spinner	9	Ferrite	17	GPS
2	Propeller	10	Solar Charge Controller	18	Flight Controller
3	Motor	11	Video Camera	19	Microphone
4	Battery	12	Telemetry Antenna	20	Video Transmitter
5	ESC	13	Telemetry Transceiver	21	Buzzer
6	UBEC	14	Radio Receiver	22	Video Antenna
7	Switch	15	Step up/down Converter		
8	Power Module	16	On screen Display		

Figure 54 - LEEUAV on-board components positioning

Considering the importance of a well-balanced aircraft for a stable flight, the justification for the positioning of the components depicted in figure 54, takes into account the interference factors, components cooling and effects in C.G. of the aircraft.

In order to facilitate the comprehension of all the wiring and connections of LEEUAV systems, there is an electric wiring diagram in Annex B.

5.5 System Integration Test

System Integration Testing (SIT) is a critical phase of the aircraft project, which took place in a lab environment following individual component and subsystem testing. The importance of this tests lies to the impossibility of thoroughly testing all the systems of the aircraft before flight, and in some cases this is the first and only time that all of the components and subsystems are tried out in the intended operational configuration.

During the LEEUAV systems integration, everything, from the perfect alignment and fixation of the systems components, to the welded connections and joints inside the electronic components were verified and tested.

Chapter 6

6 Aircraft Mission and Flight Testing

6.1 Introduction

After the final assembly and integration of all LEEUAV's systems and components the aircraft was tested. A total of 9 experimental flights were carried out summing more than 10.4 hours in the air. The flights took place at Castelo Branco aerodrome and in Terlamonte (Covilhã) in Portugal, each one with different purposes. This chapter not only aims to validate the concept, but also, estimate the aerodynamic efficiency of LEEUAV through the analysis of the recorded flight data.

This section also covers the methodology and the planning of the flight tests, including a brainstorming of mission objectives, briefing and de-briefing of the flight tests, emergency, safety procedures and ground tests before flight.

6.2 Solar UAV Mission and Objectives

Although the main objective of the LEEUAV project is the achievement of the continuous 8-hour flight, there are other goals which need to be approved in order to validate the airworthiness concept of the unmanned solar UAV. In order to validate the airworthiness concept, finding and fixing design problems, the aircraft should pass several tests including tests before, in and after flight, TBF, TIF and TAF, respectively.

The base objectives/requirements of the project are:

- Take-off in a very short distance (8 m) or Launched by hand (3 m);
- Climb to 1000 m above ground level for a cruise altitude, in 10 minutes;
- Sustainable-flight of 8 hours at equinox with a flight cruise speed (>7 m/s);
- Descent from cruise altitude to ground level without power in 29 minutes;
- Landing in the field.

6.3 Solar UAV Mission Simulation

6.3.1 Typical Mission Profile

There are many types of mission profiles, some more complex than others. However, all of them include a take-off, climb, cruise, descent and landing phases. For the case of the LEEUAV the mission profile adopted to perform the tests is depicted in figure 55. During the cruise flight phase the majority of the flight tests were performed.

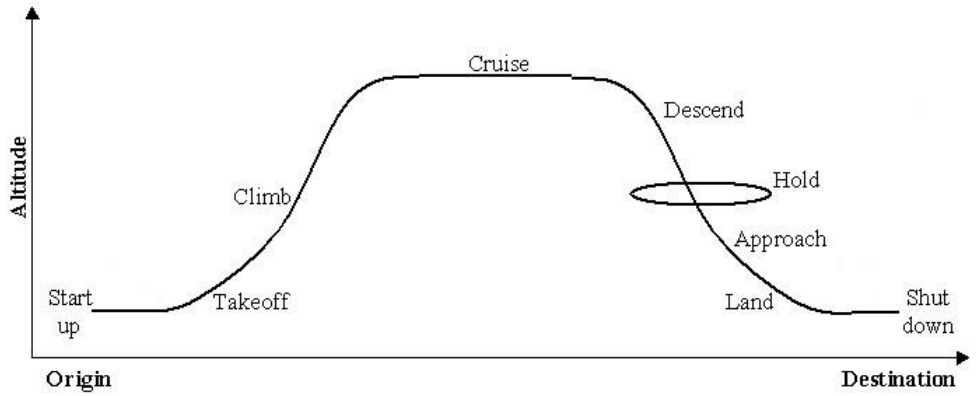

Figure 55 – LEEUAV and general aviation mission profile [53]

Start-up: Is the initial phase of the flight, it is preceded by ground tests, including C.G. positioning, control surfaces tests, battery capacity check, flight plan preparation, etc. In this phase, all systems of UAV are powered up and the aircraft is ready for take-off.

It is also in this stage that any damage in the aircraft should be detected and communications interferences or issues have to be removed or fixed. Other important tests such as range tests, engine tests, weather conditions checks, communications tests and take-off bogey tests should be performed too.

Take-off: Take-off is a critical phase of flight in which an aircraft is usually "pushed to its limits", where the engines are running at full power until the airflow through the wings is such that it creates enough lift to overcome the aircraft weight and start flying.

The take-off runway length required varies according to the air density, aircraft weight and aircraft configuration. High-lift aircraft, such as LEEUAV, require a very short runway length, therefore, it is not expectable that the take-off performance be significantly affected by the air density, field elevation and air temperature.

Climb: After leaves the ground the aircraft starts to climb to a higher altitude until the lifting force and weight are in balance. The lift force can be changed by varying the angle of attack of the wings or increasing the flight speed. When the aircraft reaches the cruise or a predetermined altitude the climb phase ends.

Cruise: Cruise is typically the flight level where the flight is most aerodynamically efficient and it is commonly used by commercial airliners to save fuel and increase the profit margins.

Between minimum and maximum speed of an aircraft, for each flight level, there is an ideal flight speed where the required power to fly is minimum and thus the flight endurance is maximized (figure 16).

Considering that in cruise phase, L=W (constant altitude) and T=D (constant airspeed), the required power to fly is equal to the drag force times cruise velocity, so that:

$$P_{req} = DV = \frac{1}{2}\rho V^3 S C_D \tag{15}$$

The available power for an electric powered airplane is given by:

$$P_A = \eta_{prop} P_{shaft} \delta \quad (16)$$

The available power depends on the propulsive efficiency of the propeller, the shaft power (which depends of the battery, ESC and electric motor efficiencies) and of course the throttle setting.

Descent: This is the phase where aircraft decrease altitude from the cruise flight level to the airfield approach. In the descent phase, depending on the rate of descent and pitch angle, the aircraft usually does not use the motor, since that the horizontal component of the weight times the gravity force that are acting in the direction of the flight, increase the aircraft speed.

Hold: Despite not always being used, the hold phase is important just for energy or fuel considerations. When there is a traffic congestion at the airport or other problems on-board the aircraft, this phase is used.

Approach: The approach phase is when the aircraft is prepared for landing, which includes the speed reduction, runway heading alignment and a low rate of descent.

Land: Following the approach phase, the landing is the final phase of the flight, when the airplane must be perfectly aligned with the runway, flying at low speeds and with a low rate of descent in order to touch the ground smoothly without damaging the on-board equipment. After touch the ground the aircraft decreases its speed until a complete stop.

Shut-down: After landing, the aircraft systems must be turned off, if applicable, the aircraft parts are disassembled and the flight data information retrieved and saved.

6.3.2 Airworthiness and Emergency Situations

Airworthiness

Airworthiness is the measurement of an aircraft's suitability for safe flight and it consists of a set of evaluating procedures which aim to certify the airworthiness of an aircraft. For commercial airplanes is initially conferred by a certificate of airworthiness from a national aviation authority of each country, and is maintained by performing the required maintenance actions throughout the life of the aircraft until it is withdrawn from service.

For the LEEUAV (UAS category) an extensive documentation to prove the flight airworthiness it is not required since it will not be sold for commercial use. However, in this work, this evaluating process was tailored to suit the complexity and requirements of the LEEUAV systems concerning the ground control station, aircraft and the surrounding airspace.

In addition to the previous work done on the LEEUAV some new configurations and structures have been upgraded, such as carbon fibre fuselage and wing tip washout. Therefore, this “new version” of the LEEUAV had never been studied or tested before and the flight test procedures had to be based on a risk management program where the flight envelope and the airspace are restricted.

So, the flights tests were therefore conducted in restricted airspace over unpopulated areas and later extended as system matures, and demonstrates via accumulated flight hours and testing, that the appropriate level of airworthiness had been attained.

In order to plan correctly the tests for this category of aircraft, three main lines of thinking, were considered in relation to risk reduction, [38]:

- Test Hazard Analysis (before flight);
- Test Specific Emergency Procedures (before and during the flight);
- Safety Check List (before flight).

Emergency Situations

Despite all the pre-flight and in-flight checks, it is always possible that something might go wrong. Whenever there is an unpredictable situation, there are two categories where it can be inserted, the first category is where the in-flight issues affect the secondary structures of the aircraft and do not require a forced landing. On the other hand, when an unexpected failure affect a primary safety structure of an aircraft it will lead to an emergency situation and the aircraft is forced to land.

In order to avoid these situations an initial brainstorming of the technical and theoretical aircraft specifications had to be studied by the pilot and flight assistants.

6.3.3 Weather Conditions

The weather conditions are crucial for the flight of any aircraft, from historic data the larger aircraft are in general more resistant to in-flight loads such as wind gusts and fast manoeuvres. So, all aircraft have weather restrictions for their flights, namely as maximum wind permitted, temperatures, runway conditions, etc. For the LEEUAV, the weather condition restrictions forbidding the flight are defined in table 6.

Table 6 - Weather restrictions for LEEUAV flight

Weather condition	Minimum	Maximum	Motive
Temperature [ºC]	0	40	Battery and solar panels efficiency
Field Wind [km/h]	-	15	Structural integrity of the LEEUAV
Irradiance [W/m^2]	- *	-	Requirement for HALE flight
Precipitation [mm]	-	0	Operating electronic systems
Hours of Sun	8	-	Requirement for HALE flight

* The inexistence of solar irradiation does not prevent the LEEUAV flight, though the endurance is affected.

6.3.4 Take-off and Landing Field

Although the LEEUAV does not require a long runway, this section aims to answer the questions: Is this airfield adequate to fly this model (size, runway, bordering, trees, full-scale air traffic, people, etc.)? and This airfield has enough surrounding airspace for HALE flights?

Considering the alternatives available for this study, the nearest airfield which met these requirements are the Castelo Branco aerodrome and Terlamonte airstrip. The Castelo Branco aerodrome has a 1460m asphalt runway and a large wide area, far from urban centres and obstacles, which makes it ideal for LEEUAV testing. The Terlamonte airstrip is a much smaller gravel runway with 60m of length but satisfactory safe airspace to fly this aircraft.

6.3.5 Safety Procedures

To ensure the safety of the nearby airspace and to safeguard the high investment in the materials and components involved in this project, it was necessary to consider some safety procedures in order to have a safe flight and reduce the risk of incidents and accidents:

- Check the weather conditions before flight;
- Fly in open spaces and in line of sight whenever possible, away of urban spaces;
- Avoid fly over the ground control station and in the sun's direction;
- Fly far from ground objects such trees, pylons, posts, power lines, etc.;
- Perform all pre-flight and in-flight checks.

6.4 Ground Tests before Flight

Even knowing all the safety procedures and possible emergency situations that may occur during the flight, before flight it is necessary to ensure that the aircraft is ready for flight, in order to minimize the flight hazards. All the pre-flight checks performed before each flight are described in this section.

6.4.1 Stability and Structural Tests

After the aircraft assembly or after any structural modification it is mandatory to rectify the C.G. position of the aircraft to ensure a stable flight. The C.G. position is determined by the displacement of all components and structures of an aircraft. In the design stage of the airplane, the location of all these on-board equipment is engineered since this is crucial to the airplane's flight characteristics.

A correctly balanced aircraft equals a stable flight, therefore a safer flight since the pilot required attention for longitudinal pitching corrections is lower.

Centre of Gravity Positioning

Regarding the longitudinal static stability, which is defined as the tendency of a body to return to its equilibrium position after a suffered disturbance, such as wind gust. If the C.G. is located ahead of the neutral point., which corresponds to the point where all the aerodynamic forces are applied, usually located at ¼ of wing chord, the airplane becomes more stable. However, if the C.G. location is too far forward, it is difficult for the pilot to increase the pitch of the aircraft during the flight or to land.

If the C.G. is closer the neutral point, the moment arm between them diminishes, reducing the inherent stability of the airplane and providing more manoeuvrability. On the other hand, if the C.G. is behind the neutral point the aircraft will be longitudinally unstable and in an extreme far position could take the airplane into stall situations. After this brief explanation, the C.G. position for LEEUAV should be slightly ahead of the neutral point, more exactly, at 21% of the wing chord.

In practice the C.G. positioning has to be hand configured and this can easily be done by changing the position of some heavy weight components inside the fuselage, such as the battery.

To ensure that the C.G. position was located at the desired point, the "fingertip" method (figure 56) was adopted using only two supports (fingers) applied at 21% of wing chord (left and right, respectively) sustaining the fully assembled aircraft in air and searching for a small pitch-down movement.

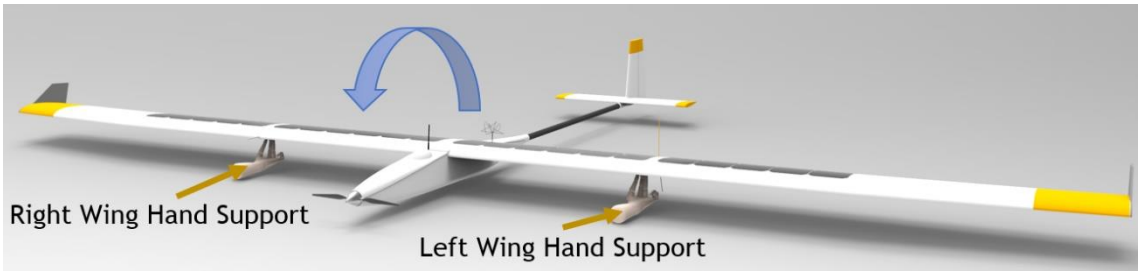

Figure 56 - Fingertip method for C.G. positioning

Although it is not as important as the longitudinal stability, the lateral stability can make the pilot's life difficult if one side of the airplane is heavier than the other. However, during the wing tip modification (section 4.4) it was ensured that the aircraft wings have approximately the same weight.

Still within the stability and structural adjustments, before flight it is essential to confirm if all the on-board components and systems are firmly fixed in their correct positions so that they do not change the C.G. position during the flight.

6.4.2 Propulsion and Control Systems Tests

To ensure that the aircraft is ready to fly it is mandatory to check the operability of the propulsion system and the control surfaces actuators.

In general, the propulsion system is tested by pushing the engine or electric motor to its maximum power, but for the specific case of a HALE platform it is necessary to ensure that the propulsion system can stand the entire flight without failing. To test the reliability of the propulsion system, a previous laboratory work was done to test the battery, the ESC and the electric motor during long periods of time, monitoring the temperature and power evolution.

To check the engine-related problems such as the tightness of the propeller nut, the fixture of the spinner, the operability of the electric motor and the propeller vibrations, several tests were done.

Regarding the control system, it was essential to adjust some parameters of the servomotors, namely the neutral positon, dual rates and exponentials. The neutral position of the servos is important to guarantee the airplane flies with a minimum drag as possible. All servos came with a pre-assigned neutral position from their manufactures and should be fixed in the aircraft according to that position. But it is possible to change this position in order to perfectly align the control surfaces with the fixed surfaces by trimming the aircraft through the RC transmitter. An initial trimming was made on the ground by observation, but the required neutral position of the control surfaces, i.e., the position where the aircraft flies in a straight line, was not exactly the "eye-trim position". Therefore, to get the exact trim of the aircraft an auto-tune flight was made.

In MP software, within the initial setup section to calibrate the radio transmitter, it was mandatory to select the transmitter mode and the limits/range of the control sticks.

The dual rates and exponentials of a servo allow to change the response of the plane to the stick movements by changing the maximum deflection of the servo and thus the control surface (dual rates) or through varying the deflection speed in relation to the stick position (exponential).

Still within the control system, several tests and verifications were performed:

- Ensure all servos, control surfaces linkages and hinges are secure;
- Servo linkages and control surfaces are able to move freely and are not hooking on anything;
- Electronic servo connections and cables are securely fixed and are not frayed;
- Control surfaces are moving in the correct direction according to the transmitter inputs.

6.4.3 Solar Panels Tests

The solar UAV requires additional tests related to the solar panels. So, before flight it is essential to ensure that the solar cells are well fixed onto the wing and the cable connections between panels are properly attached. Depending on the time of take-off, the sun irradiation varies and thus the flight endurance is greatly affected. However, based on the time of take-off and day's solar irradiance it is possible to conclude about the expected flight endurance for that day.

6.4.4 Communication and Navigation Systems Tests

Concerning, the telemetry and FPV systems, the tests are quite simple, only the range, working temperature, interferences and cable connections have to be checked. Regarding the range test, two tests were performed one at an approximately distance of 2.5km in a straight line between two points with an altitude difference of 487m and a second test, where the GCS stayed at 801m and the LEEUAV at 1288m of absolute altitude. All the communications systems were proven to be reliable without a significant level of interference.

Another important consideration taken into account was the stability and position of the antenna's tripod in the GCS, since its signal is affected by some reflective materials such as the carbon fibre. The RC transmitter, the laptop and FPV screen of the GCS should have enough energy stored in their batteries to withstand the entire flight.

Regarding the Navigation systems tests, GPS and flight controller need to be calibrated before the flight. So, for the GPS calibration the airplane must remain stopped on the ground while it searches for enough satellite connections (locking). To arm the flight controller it is necessary to immobilize the aircraft on ground for 5 seconds, so as to set the Pixhawk internal sensors.

6.5 Flight Controller Programing and Flight Data Retrieval

Flight Controller Programing

The LEEUAV flights were done in two ways, manually for the take-off, land and flight tests, and autonomously for the long flights. Before inserting a flight plan into the autonomous flight controller, a firmware and a several parameters were loaded and configurated. Firstly, the flight controller was connected to the computer to load the firmware for fixed wing aircraft, through the MP interface. The next phase was to insert all the desired limits of the aircraft, such as minimum and maximum rate of climb, throttle setting, airspeed, altitude, pitch, yaw and roll angles and rates. Other parameters as cruise speed, altitude, RTL altitude, loiter radius and flight modes were also configured.

Regarding the flight modes used on LEEUAV:

- FBWA: FBWA is a flight mode where the flight controller partially controls the aircraft, i.e., it is a stabilizing mode that allows to fly the aircraft manually, but it self-levels the roll and pitch axis (rates and angles);
- Auto: In auto mode, the aircraft follows a pre-programmed mission script stored in the flight controller memory which is made up of navigation commands (waypoints) and action commands;
- Loiter: Loiter mode automatically attempts to maintain the current location and altitude, flying in circular flight paths with a pre-set airspeed and radius;
- RTL: RTL is a fail-safe flight mode and it is used when the aircraft losses the GCS signal or when there is an emergency. This flight mode simply brings back the aircraft to its launch position or to a pre-set position;
- Manual: This mode is the one used for take-off and landing or whenever the pilot wants to fly the aircraft manually.

Regarding mission planning, it starts by setting the home or launch location for RTL purposes, otherwise it will assume the home location as the power up location.

Concerning the mission planning, the flight path is defined by a set of waypoints. These waypoints are added by clicking on the map or by inserting the latitude and longitude

coordinates. Airspeed, altitude and other flight parameters can also be defined for each waypoint.

Moreover, the route can be set or changed at any moment of the flight via an encrypted set of commands transmitted from the MP interface to the Pixhawk in the aircraft.

After finishing the flight plan, it needs to be sent to the flight controller, what can be done by USB cable or via telemetry.

Flight Data Retrieval

During the flight, autonomous or manual, the Pixhawk records, with a pre-set frequency, more than 100 flight parameters, at each millisecond, in a log file inside its micro SD card.

The information contained in a Pixhawk log is vast, requiring an after-flight screening for particular analysis. The log flight data retrieval is shown by a log browser window in MP software where all the numerical recorded flight data is presented in a tabled and graphical format.

Despite the focus of this work being on the flight data required for performance analysis, in each flight other recorded parameters were also analysed, such as ESC and motor current, aircraft vibrations, compass interferences, GPS glitches, among others.

6.6 Flight Testing

6.6.1 First Flight Test

After all ground tests and pre-flight safety checks were performed, to validate and evaluate the LEEUAV's airworthiness several non-solar version flights tests were carried out.

This first flight was very important and one of the most critical, since it was the first time that the integrity and stability of the aircraft was tested. The ability for circuit manoeuvres (pitch, roll, and yaw) was the second goal. The control surfaces trim, the balance of the aircraft (C.G. position) and how the airplane is affected by wind gusts were also examined in this flight.

6.6.2 Flight Tests for Concept Validation

There are numerous flight tests that are suitable to be performed in order to validate the different aspects and characteristics of the LEEUAV. The most important tests to validate the aircraft comprises the integrity, balance, trimming, manoeuvres, systems operability, flight performance, autonomous flight, take-off and landing qualities and of course the main goal of this work, the maximum endurance.

To facilitate the comprehension of the tests performed, table 7 shows some of the flight test conditions and goals in their respective order.

Table 7 - Flight tests specifications and goals

Test No.	Airspeed [m/s]	Height [m]	Flight Pattern	Initial TOW [N]	Flight Time [min]	Goals
A-1	7<20	<151	Visual	40.221	10	Integrity, trimming, balance, circuit manoeuvres, wind gust effects and take-off/landing qualities
A-2	8<16	<221	FPV	46.107	40	Auto-tune and Systems Operability
A-3	6<15	<359	FPV	46.107	100	Autonomous flight
A-4 **A-5**	6<26 6<20	<504 <718	FPV	46.107 54.129	159 137	Flight Performance (Aerodynamics)
A-6	6<16	<355	FPV	54.129	121	Flight Performance (Power)
A-7	6<15	<718	FPV	54.129	188	Range and Endurance

6.6.3 Flight Test for Performance Analysis

Despite the numerous flight performance areas suitable to be evaluated and due to the reduced time available, it was decided to conduct the study to obtain the most important performance indicators of an aircraft, the aerodynamics coefficients and required power for level flight.

So, this section aims to determine the practical lift-to-drag ratio or aerodynamic efficiency (L/D) of the LEEUAV based on the retrieved flight data from the on-board sensors. For this, there are three suitable different practical methods [54,55] to obtain the L/D ratio:

- Speed-Power Method;
- Prop-Feathered Sinks or Glide Polars Method;
- Mechanical Energy Method.

The Speed Power Method is based on the fact that for level and unaccelerated flight, thrust equals drag (section 2.2). Therefore, determining the thrust at a given flight speed, it is possible to determine the corresponding drag at that given speed. The problems fall in the area of determining the installed power and propeller efficiency for different flight conditions, which not only requires specialized on-board sensors such as load cell and RPM sensor or torque meters, but also leads to high experimental errors values. Thrust can also be measured indirectly by knowing the propeller characteristic curves (Ct vs J or Cp vs J and eta vs J) and the current flight speed, motor speed and air density. However, the manufacturers do not always provide this information.

The Prop-Feathered Sinks Method comprises an airplane in a steady-state glide flight. In this particular condition the only forces remaining to vectorially balance the weight are the lift and the drag.

$$L = W_T \cos\gamma \tag{17}$$

$$D = W_T \sin\gamma \tag{18}$$

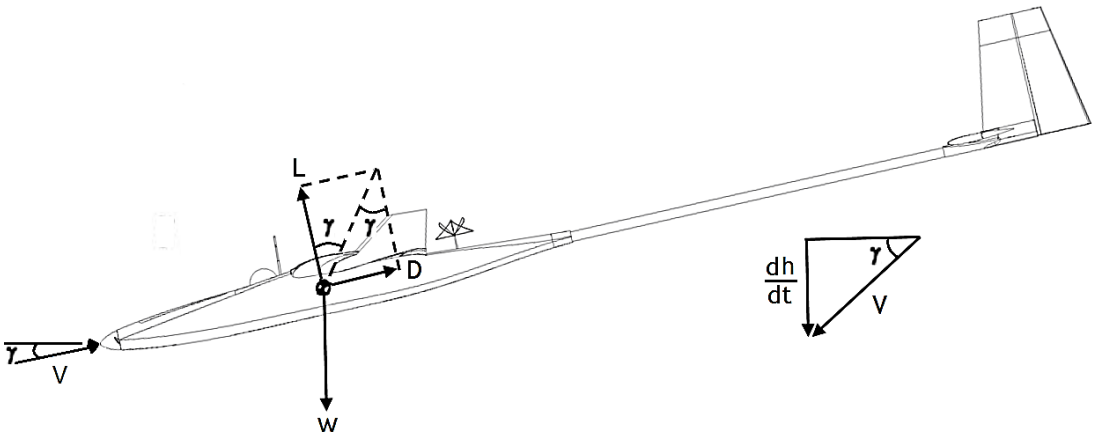

Figure 57 - Aircraft acting forces in steady-state glide flight

To determine the glide angle (γ) it is necessary to know the rate-of-descent dh/dt and the true airspeed V_T. The strengths of this method are in the fact that it does not require the determination of the power or the propeller efficiency, on the other hand, it does not consider the lateral wind. In regards to the lateral wind, a decomposition of true airspeed vector in its components (u, v, w) is required and it depends on the angle of attack (α) and sideslip angle (β), which further requires an Alpha-Beta sensor probe.

The method applied in the L/D calculation, was the Mechanical Energy Method due to the reasons listed above, which prevented the use of any of the other methods.

Considering the same steady-state flight condition of the second method, where the only forces acting in the airplane are the Lift, Drag and Weight and taken into to account that the aircraft is a dissipative mechanical system, the main energy variations are Potential, Kinetic and Dissipative.

$$E_{pot} = mgh \tag{18}$$

$$E_{kin} = \frac{1}{2}mv^2 \tag{19}$$

$$E_{Dis} = \int Dv\,dt \tag{20}$$

Taken into account that power is a variation of energy along time, in this specific case of an aircraft, the flight powers are demonstrated by the formulas 21, 22 and 23:

$$P_{potencial} = \frac{d}{dt}(E_{pot}) = \frac{d}{dt}(mgh) = mg\frac{d(h)}{dt} = mgRC \quad (21)$$

$$P_{kinetic} = \frac{d}{dt}(E_{kin}) = \frac{d}{dt}\left(\frac{1}{2}m{v_G}^2\right) = \frac{1}{2}m2v_G\dot{v_G} = mv_Ga_G \quad (22)$$

$$P_{Dissipative} = \frac{d}{dt}(E_{Dis}) = \frac{d}{dt}(Dv_{Air}dt) = Dv_{Air} \quad (23)$$

When there is no other force acting in the aircraft, the sum of the of the powers above is zero, and the drag force can be calculated for a given airspeed.

$$P_{potencial} + P_{kinetic} - P_{Dissipative} = 0 \quad (24)$$

$$mgRC + mv_Ga_G - Dv_{Air} = 0 \quad (25)$$

$$D = \frac{mgRC + mv_Ga_G}{v_{Air}} \quad (26)$$

Where: D is the drag force, m is the aircraft mass, g is gravitational force, v_G is the ground speed, a_G is the longitudinal acceleration and v_{Air} the airspeed.

For the Mechanical Energy Method to be applied the LEEUAV has to fly in a pre-determined pattern without using motor (gliding). To correctly determine the LEEUAV drag force and taking into consideration the theoretical safe airspeed range of the LEEUAV (6-25m/s) [31], several gliding flights with different airspeeds were performed. The flight mission pattern consists of climbing to a pre-determined altitude (300-500m), apply a suitable trim to achieve the desired airspeed and set the throttle level to zero, gliding the aircraft during a period of time no less than 60 seconds. The process was repeated at least 3 times for each gliding speed in order to minimize the sensors errors and wind disturbances.

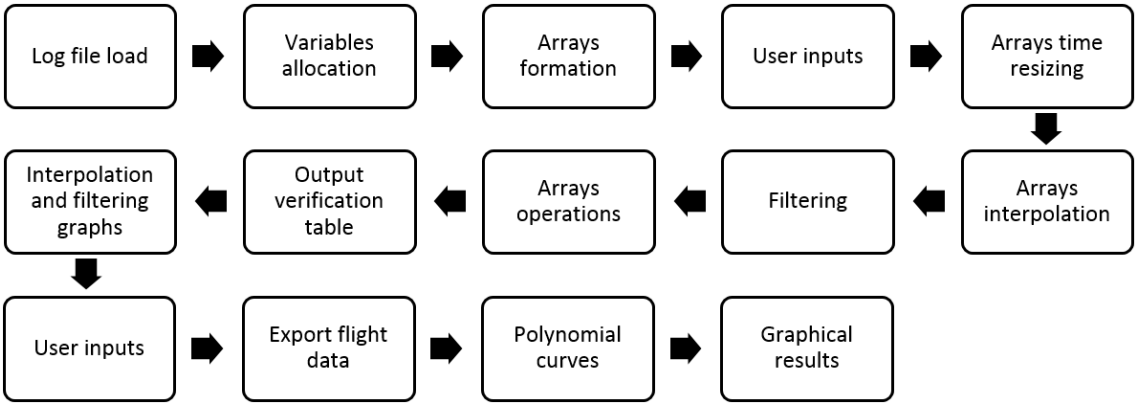

Figure 58 - MATLAB algorithm diagram

Figure 58 shows a simple diagram concerning the MATLAB algorithm logic, so as to better understand the code also addressed in the Annex C.

Intentionally left blank

Chapter 7

7 Results

7.1 Introduction

At the end of this chapter the majority of the LEEUAV flying capabilities and design problems were identified and described. The analysis of the relevant flight data downloaded from on-board flight controller during the LEEUAV flight tests permitted to understand and determine its flight performance. A deeper analysis of the flight difficulties and hazards can also be found in this section in order to sustain and enhance future versions of this aircraft.

7.2 Flight Tests Results/Analysis

7.2.1 Flight A-1 (Integrity, Balance and Circuit Manoeuvres)

The first flight took place in Castelo Branco aerodrome on 18th July of 2016 and LEEUAV's flight performance was qualitatively in line with the predictions and requirements of the project. The integrity of the low-speed LEEUAV's flight was in accordance with the requirements. All the fixations and fittings, including wing bolts for wing-fuselage attachment, tail boom fixation bolt and groove, tail support, wing outer panels - central panels connections and motor support prove to be adequate and reliable so as to ensure a safe and good flight. First the trimming was adjusted on ground by visual alignment of the control surfaces with the fixed surfaces and then, during a straight level flight.

Regarding balance, during the pre-flight tests, 465g of small weights were applied near the nose of the fuselage ensuring a C.G. position between 20-22% of the wing chord. Unfortunately, this is not the desired solution, since it is carrying more weight and thus reducing the available payload.

Despite the LEEUAV good results in regard to the integrity, the manoeuvrability was not so good. Due to the large aspect ratio of the wing and the small area of the ailerons, the roll movement was very limited specially at low speeds, something that had already been detected in previous flight tests of the current wing. However, there is a significant improvement of the negative twist upgrade at the wing tips. Both pitch and yaw movements were considered suitable for this type of aircraft.

At the end of the flight a malfunction was detected on the ESC which forced the landing of the aircraft. After some analysis, it was concluded that ESC had overheated during that hot summer day flight and the solution adopted was to replace the ESC with a better one.

7.2.2 Flight A-2 (Auto-tune and Systems Operability)

At the same place, on 28th July, the second flight test, intended to test more flight manoeuvre capabilities and systems operations, was not successful. A severe hazard related with the aircraft assembly was detected when the aircraft was already flying. Since the

structural integrity of LEEUAV was in doubt, the landing was forced. In turn, this emergency landing caused nose crash of the LEEUAV resulting in damage in the wings and tail structures as well.

After repairing the broken structures of the LEEUAV, the A-2 flight (on 9th November) began with an auto-tune flight. As soon as the flight controller was configured, systems operability tests were started.

This second part of the A-2 flight allowed the checking of the operability of the systems, namely the control, FPV and telemetry systems. This high relevance flight, allowed the detection of some unexpected configuration aspects through some flight hazards such as spatial disorientation and inconsistent telemetry data display.

Table 9 provides the information of some of the unexpected hazards during all flight tests. As soon as all the systems and components prove to be operational, the remain flight tests were conducted on the LEEUAV.

7.2.3 Flight A-3 (Autonomous Flight)

With the auto-tuning completed, the LEEUAV was ready to perform an autonomous flight. In Terlamonte on 12th November, a pre-set 45min flight plan, established by several waypoints with different altitudes, positions as well as airspeed variations was loaded on the Pixhawk. This flight was also an opportunity to check and correct some pre-defined parameters such as loiter radius, minimum and maximum flight speeds, maximum pitch, roll and yaw angles, maximum line of sight distance, RTL behaviour and climb/descent rates.

Figure 59 - LEEUAV during A-3 flight test

Analysing the results, the loiter radius should not be smaller than 200m; the flight envelope speeds must in the range of [7,20]m/s; the maximum pitch, roll and yaw angles were well predefined, and their values were [-20º,+20º], [-35º,+35º] and [-20º,+20º] respectively; the maximum line of sight distance is 800m in a clear weather day; the RTL parameters should be 200m for the radius and 8m/s of airspeed; the climb/descent rates are limited by the throttle setting which cannot exceed the 60A of current defined by the motor producer and the maximum aircraft speed 20m/s regarding the descent rate.

7.2.4 Flight A-4 and A-5 (Flight Performance – Aerodynamics)

On 11th, 12th and 17th of November the aerodynamic tests of the non-solar version of the LEEUAV were performed. Despite the calm weather, different days have different weather

conditions, so these flights help to minimize the sensor errors (temperature/wind). Regarding the sample size, figure 60 shows the total acceptable values of each 0.5m/s airspeed interval of points analysed. For the non-solar version, the airspeed confidence intervals are [6.5,7], [8.5,10], [11,11.5] and [12,15] where it is possible to ensure more accurate results for the graphs of figures 60, 61, 62, 63 and 64. The airspeed range of more confidence is by far the [8.5,10] in which there is a mean value of 1750 points per 0.5m/s airspeed interval.

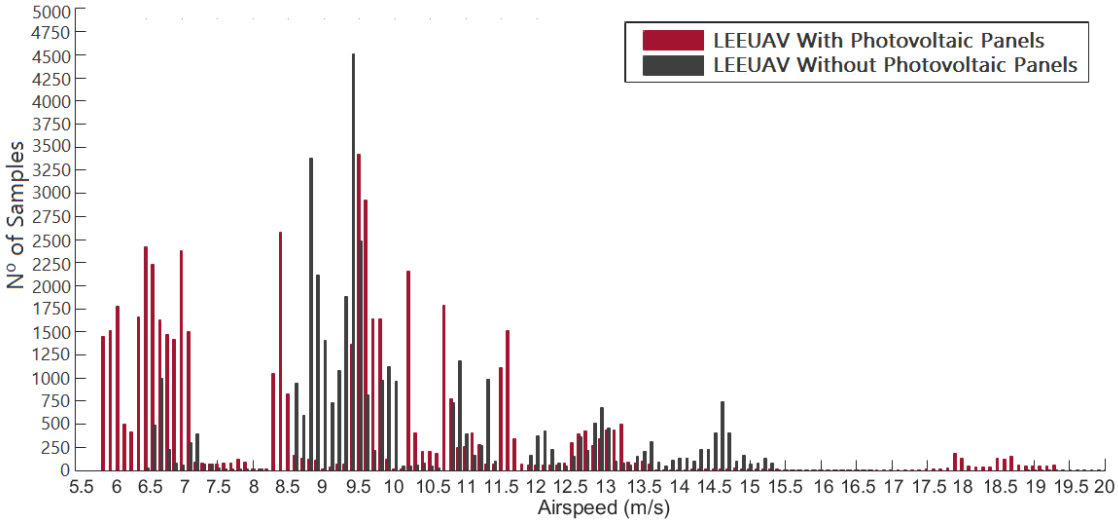

Figure 60 - Number of acceptable points per airspeed value

On the other hand, on 24th of November the 3-hour LEEUAV flight (with photovoltaic panels) resulted in 22 acceptable gildings, where the greater confidence intervals are [6,7], [8.5,9], [9.5,10] and [10.5,13]. The most reliable airspeed interval is [6,7] (mean value of 1500 points), so more accuracy in the results is expected for these airspeeds.

In MATLAB, after loading each log file and resizing the arrays to the time intervals of each glide, applying equation 26 it was possible to relate the drag value for each 0.1m/s airspeed interval, resulting in the graphs of figures 61 and 60, for LEEUAV without and with photovoltaic panels, respectively.

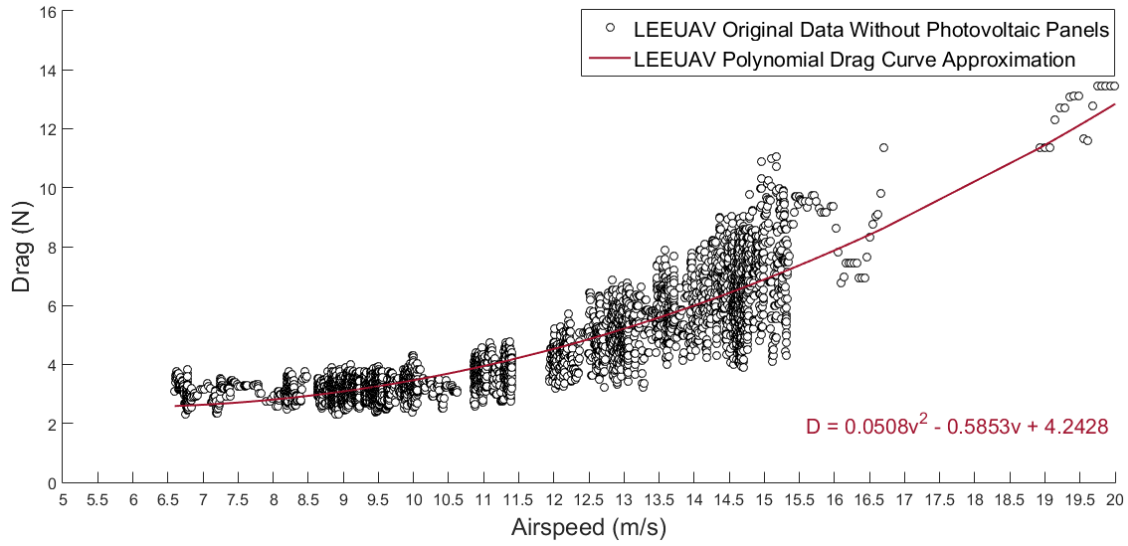

Figure 61 - Drag vs Airspeed (LEEUAV without photovoltaic panels)

Considering all the points analysed, it is possible to see the increasing dispersion of the values for higher airspeeds (figure 61). This fact can be explained by sensors errors, namely, the GPS and airspeed sensors.

The smallest value of drag is 2.59N and occurs at the minimum tested airspeed of 6.60m/s for the LEEUAV without photovoltaic panels. Conversely, for LEEUAV with photovoltaic panels the average drag value increases 0.95N, confirming the expectations, the minimum drag value is 3.54N for an airspeed of 6.88m/s.

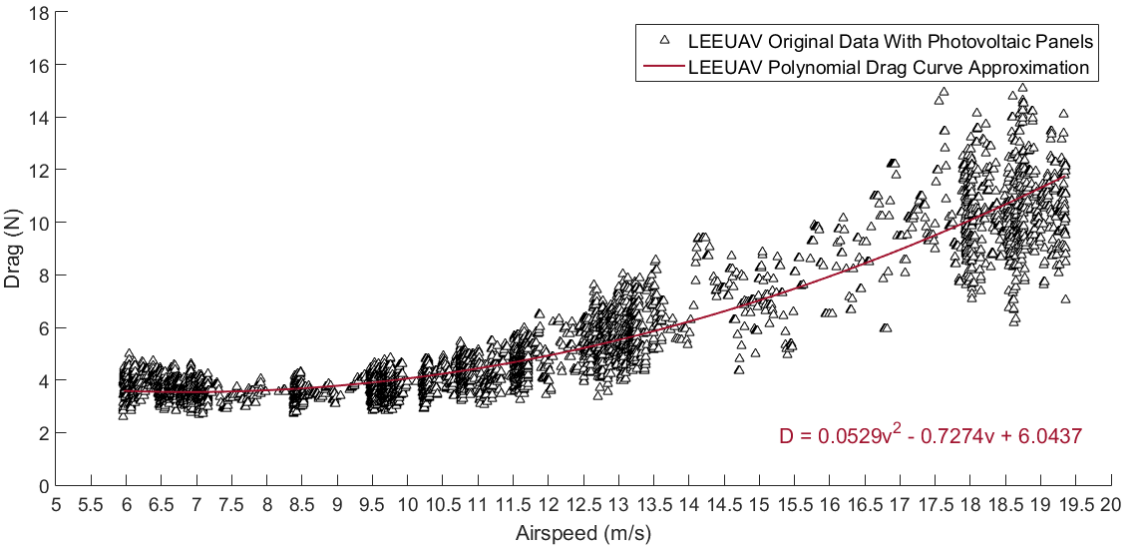

Figure 62 - Drag vs Airspeed (LEEUAV with photovoltaic panels)

With the drag values for each airspeed, using equation 5, it was possible to determine the correspondent drag coefficients (C_D) values. In order to obtain the drag polar for this aircraft, it is necessary to calculate the lift coefficient (C_L) for each tested airspeed. So, used equation 4 (L=W) was used, but with a pitch (γ) correction. Despite being small, this correction aims to account for the weight contribution on the horizontal axis of the aircraft which in turn affects the airspeed. The air density (ρ) values used to calculate the aerodynamic coefficients

have considered the day temperature and static air pressure recorded by the flight controller, during the flight time.

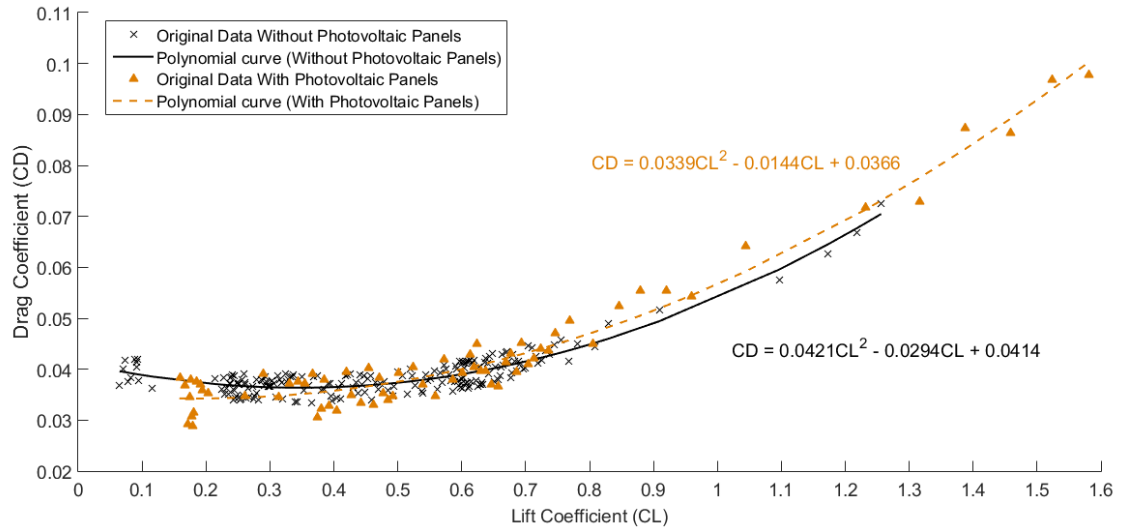

Figure 63 - LEEUAV with and without photovoltaic panels drag polar

The second-degree polynomial approximation curves for each polar of the figure 63 enabled the determination of the values of the lift and drag coefficients for tested airspeeds. In turn, it was possible to obtain the lift-to-drag ratio (C_L/C_D) and the endurance-airspeed ($C_L{}^{3/2}/C_D$) curves.

The lift-to-drag ratio curve enables to find the airspeed for best range from an aerodynamic point of view, i.e., without considering the propulsive system.

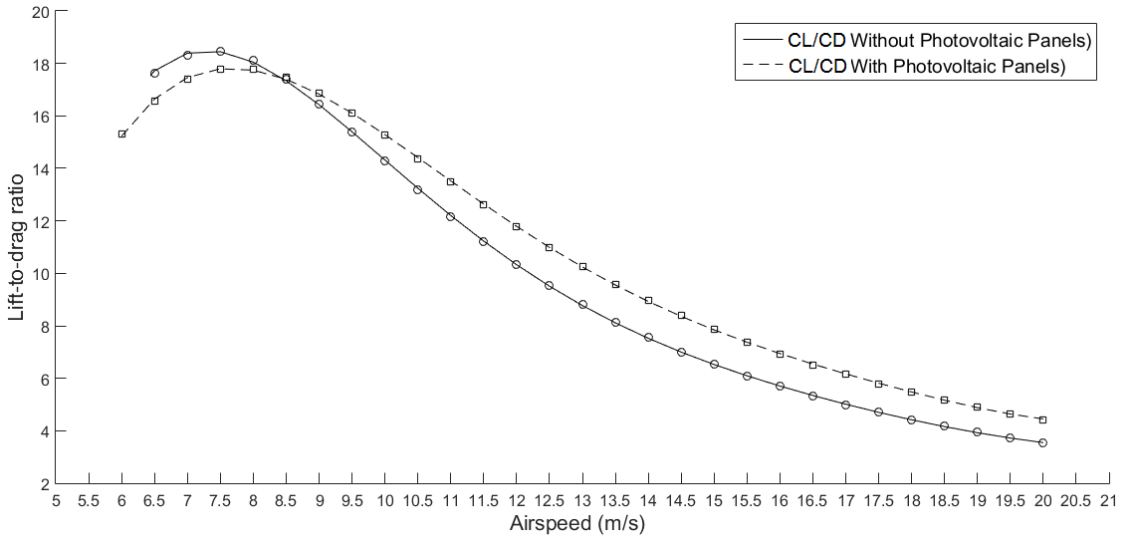

Figure 64 - Lift-to-drag ratio of LEEUAV (with and without photovoltaic panels)

Figure 64 shows the (C_L/C_D) curve for LEEUAV with and without photovoltaic panels respectively. As expected, there was a reduction in the L/D curve after the panels had been applied. This was due to the step created on the upper surface caused by the solar cells fixation on the wing and the additional drag caused by the photovoltaic panels wiring connections and soldering points.

The disadvantage of placing solar cells on the upper surface of an airplane wing is that, because the solar cells have a finite thickness, is that, they create a localized thickening or an offset in the airfoil, with a forward facing step (FFS) at the beginning of the solar cell array and a backward facing step (BFS) at its end. These steps cause separation of the flow: in the FFS flow, two regions of separation occur, one upstream and one downstream, and in the BFS flow, one separated region develops downstream of the step. The first flow separation, upstream the FFS, does not generate a significant amount of turbulence, but in the separation after the sharp corner of the FFS, it results in a significant increase of turbulence. Flow separation after the BFS also generates high turbulence levels, yet lower than those generated after the FFS [35].

Without photovoltaic panels, the LEEUAV's maximum aerodynamic efficiency is 18.45 and occurs at 7.4m/s. After applying the photovoltaic cells, the aerodynamic efficiency decreases by 1.02 to a value of 17.43 and it is achieved at 7.8m/s.

Another important fact is the shift of the lift-to-drag ratio curve which increments the best gliding range airspeed from 7.4 to 7.8m/s. This 0.4m/s shift is related with the increased weight (+0.720kg) of the aircraft after applying the photovoltaic system.

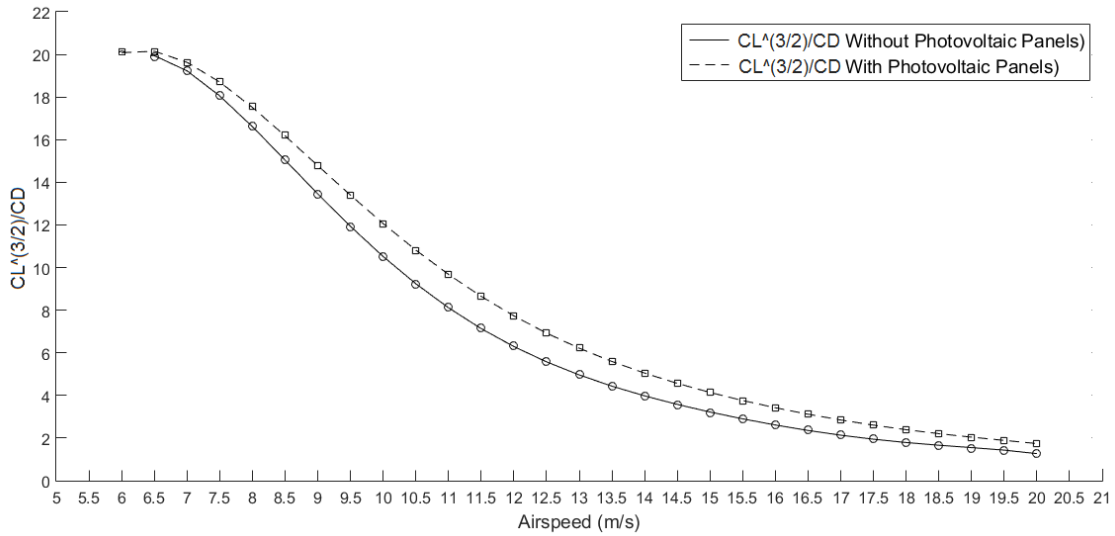

Figure 65 - $C_L^{(3/2)}/C_D$ vs Airspeed of LEEUAV (with and without photovoltaic panels)

As depicted in figure 65, the best airspeed which maximizes non-powered flight endurance occurs on the minimum tested airspeed, near the stall and for both of the LEEUAV versions (with and without solar panels). For LEEUAV without photovoltaic panels the best endurance airspeed is 6.60m/s and for the solar version it is 5.99m/s. Although the airspeeds below 6.5m/s of the non-solar version were not tested, the best endurance airspeed is clearly under this value. It would however be dangerous to test it.

7.2.5 Flight A-6 (Flight Performance - Power)

In the previous section, the performance of the LEEUAV was analysed only from an aerodynamic point of view, i.e., without considering the propulsive system. This section aims to analyse the LEEUAV propulsive system efficiency using the on-board power meter sensors.

The PM is situated between the battery and PDB, it calculates the amount of electric power that the aircraft is consuming, by measuring current and voltage.

When the throttle is set to zero it is possible to know the electric energy required for systems operation. As described in section 5.2.2 it has the average value of 11.75W.

In order to plot the electrical power required for each airspeed, an A-6 autonomous flight was carried out. This flight was composed by a 300m radius circular flight path, varying the flight speed from 7 to 15m/s with an increment of 0.5m/s. To reduce wind disturbances, for each analysed airspeed, two complete loiter circles were flown, with an average time of 2.86 minutes each.

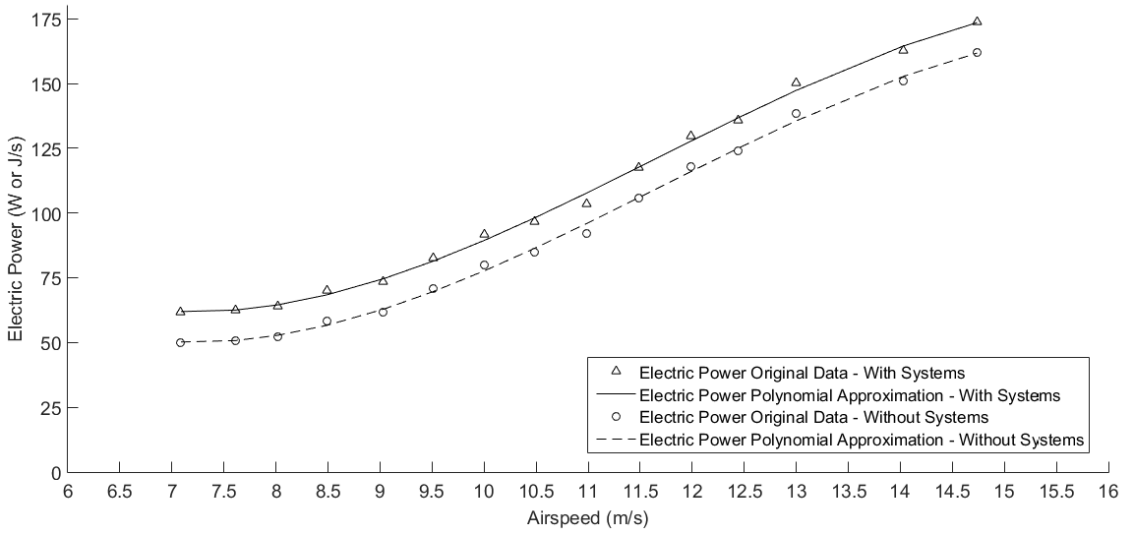

Figure 66 - Electric Power vs Airspeed (with and without systems)

Figure 66 reflects the plotting the electric power curve for LEEUAV with photovoltaic panels. Each point is a median value of the electrical power consumed for each airspeed tested. The lowest power consumption has the value of 61.65W and occurs in the lowest airspeed of 7.09m/s tested, this being the best airspeed for maximum endurance. Removing the systems contribution, the minimum electrical power required for the same airspeed is 49.90W. The significant increase of the required electrical power for airspeeds above 8.5m/s is noteworthy.

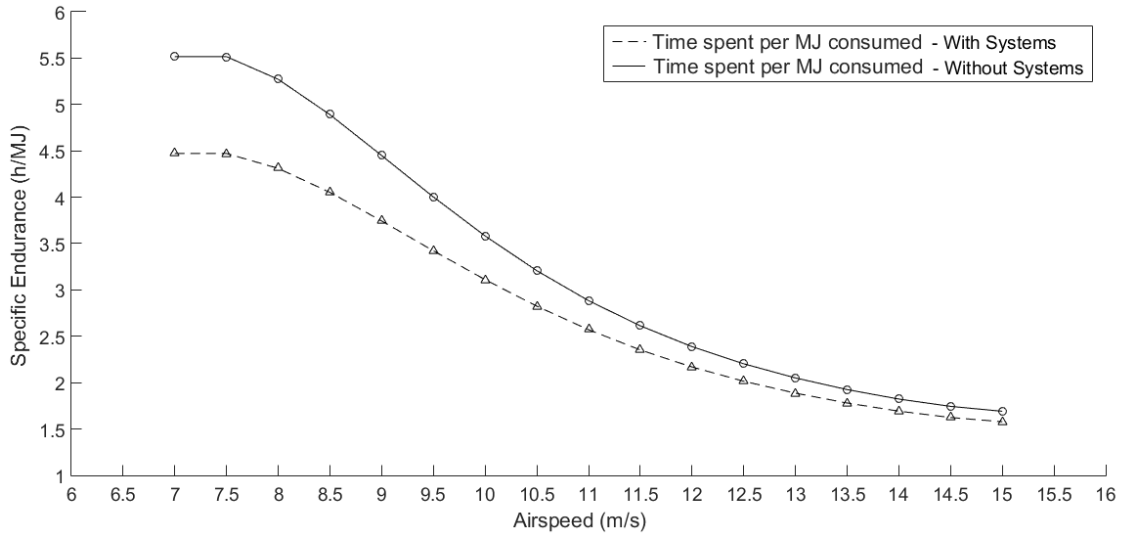

Figure 67 - Specific Endurance vs Airspeed

The conversion of the electrical energy consumed from joules per second (J/s) to joules per hour (J/h), enables the determination of the number of hours the LEEUAV can fly per MJ consumed. According to figure 67, the airspeed that maximizes the flight time per MJ consumed is 7m/s. Another important characteristic to be highlight is the decreased distance between the two curves along the airspeed. This fact is explained by the increasing difference between the power used by the propulsive system and the power of the systems with the increasing airspeed. If there were no systems on-board, at the lowest airspeed, the LEEUAV would be able to fly one more hour for the same MJ of energy.

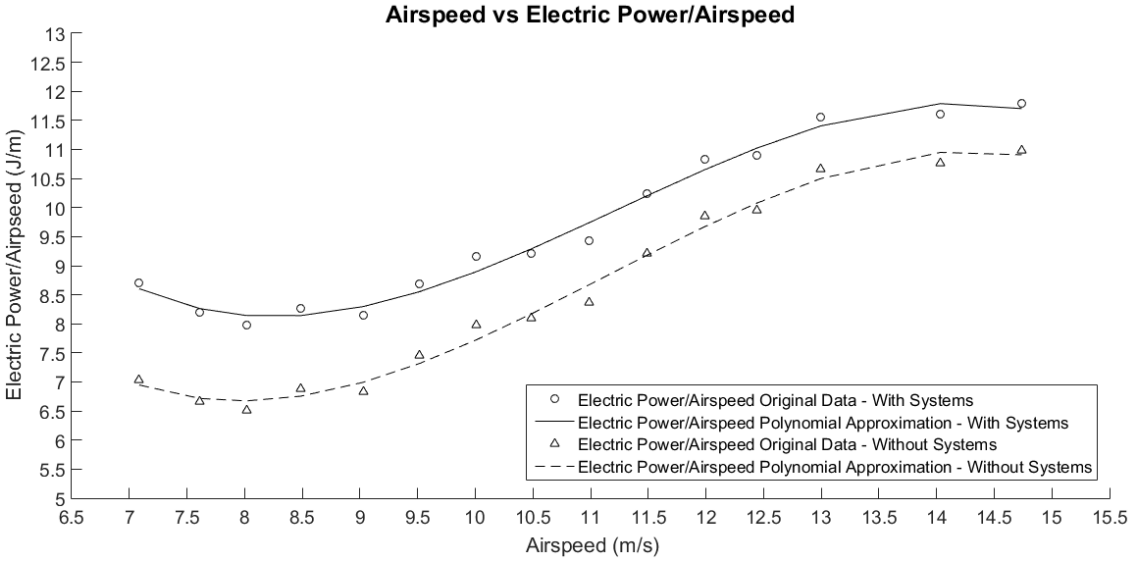

Figure 68 - Electric Power/Airspeed vs Airspeed

The plot shown in figure 68 was obtained by dividing the electrical power by the correspondent airspeed value, where the electrical power/airspeed has a minimum value which

corresponds to the maximum range airspeed. This airspeed has a value of 8.02m/s which in turn corresponds to 7.98 Joules per meter travelled.

Similar to the specific endurance graph, converting the electric power/airspeed (J/m) to specific range (km/MJ) it is possible to see how much distance is travelled for each MJ of energy consumed. In this case, LEEUAV is able to travel up to 150km/MJ at 8m/s.

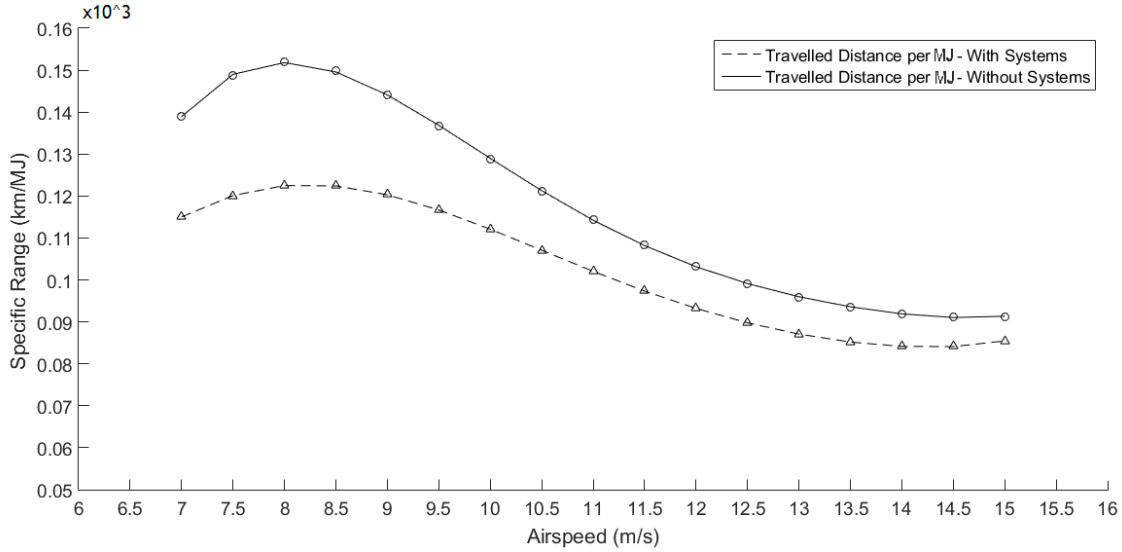

Figure 69 –Specific Range vs Airspeed

It is also relevant to compare the required power (P_{req}), from the aerodynamic point of view, with the required electric power (P_e), from propulsive system point of view.

Figure 70 shows the plotting of the electrical power (without systems) and the required power from the drag force times the airspeed (equation 23) for the solar powered UAV.

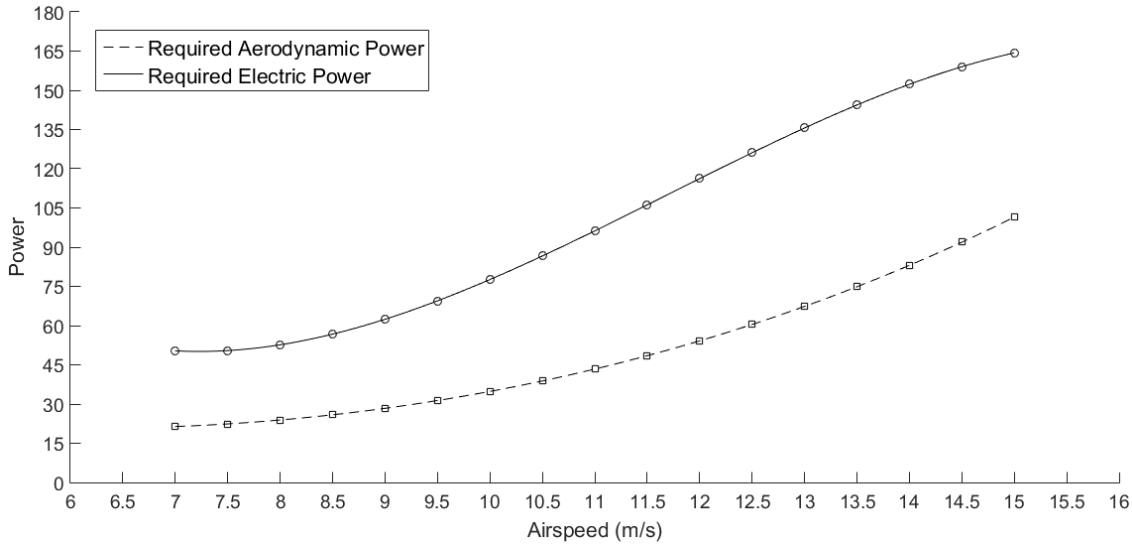

Figure 70 - Electric and Required Power vs Airspeed

The P_{req} curve shows the required power to fly in a cruise condition, where thrust equals the LEEUAV drag force. The P_e is the electrical power withdrawn from the battery to the

propulsive system and it is always higher than the required power, which is in accordance with the results shown in figure 70.

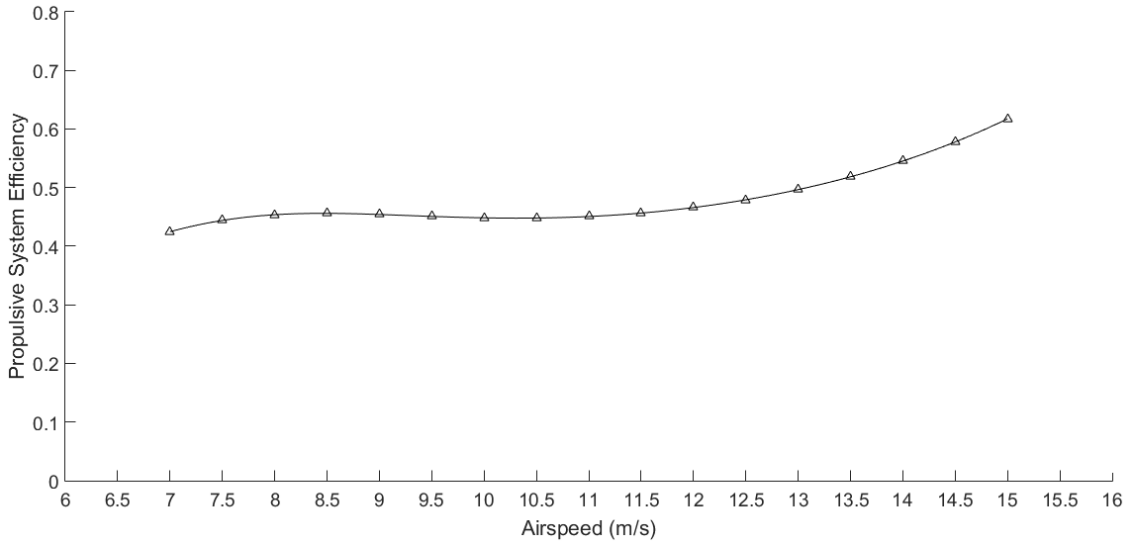

Figure 71 - Propulsive System Efficiency vs Airspeed

The propulsive system efficiency ($\eta_{ESC}\eta_{motor}\eta_{prop}$) can also be extracted by dividing the (P_{req}) by (P_e) and plotting the P_{req}/P_e vs Airspeed (figure 71). This efficiency comprises all the propulsive system components, namely, power module, ESC, electric motor and propeller. So, figure 71 shows the global efficiency of the propulsive system which for cruise speed is near 45%, getting higher for higher airspeeds.

The efficiency increasing at the end of the curve (for higher speeds) is unusual, but it is due to the negative curvature of the electric power curve (figure 69) at these speeds. This may be caused by measurement errors (sensors) or averages during the data handling.

7.2.6 Comparison of Experimental Results and Theoretical Estimates

In order to evaluate the agreement between the theoretical and practical results a comparison of the main aerodynamic and propulsive system indicators was made.

The graphical comparison depicted in figures 72, 73, 74 and 75 below considered the average value of the air density measured during the flight tests (1.12kg/m^3) and an aircraft weight of 54N, regarding the theoretical results. The presented theoretical results also consider the drag caused by external accessories such as antennas, control arms, camera's canopy, etc. and solar panels influence.

Starting with the aerodynamic efficiency indicators, figure 72 refers to the drag and required power curves comparison. The first aspect that stands out is the superior real values of the required power and drag curves when compared to the theoretical results. Considering the cruise speed, there is a difference of 0.44N between the drag curves and of 3.47W between

the required power curves. This difference is in the order of magnitude of the estimated experimental errors and it increases for higher speeds.

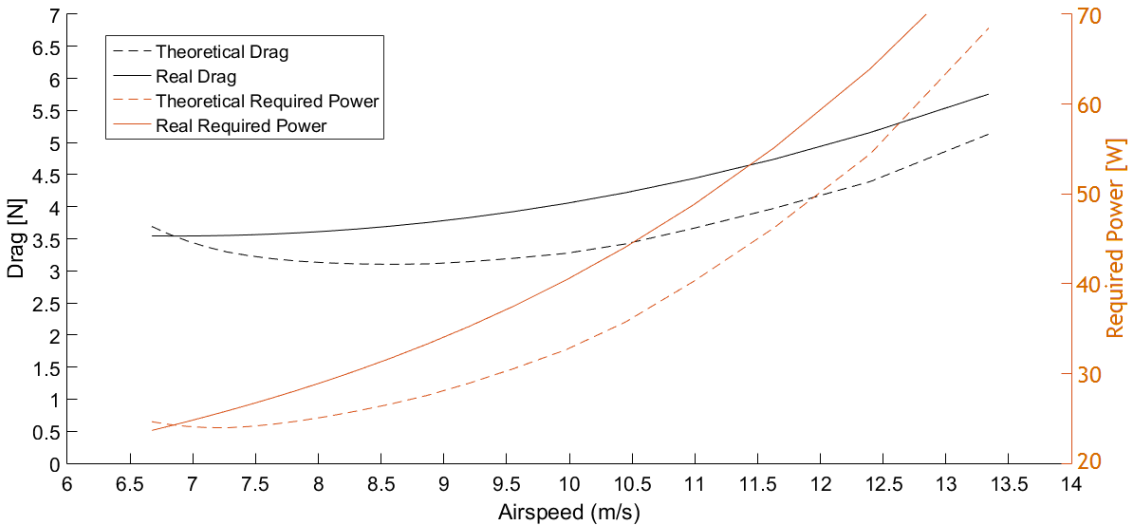

Figure 72 - Drag and Required Power vs Airspeed (real and theoretical results)

With respect to the aerodynamic efficiency (L/D), the results are somewhat in agreement with the theoretical marks for the cruise speed (7.8m/s). For lower speeds the real values of the aerodynamic efficiency demonstrated to be more optimist, this fact could be justified by the measured error related with the instability of the flight near the stall speeds. Regarding the $C_L^{3/2}/C_D$ curve, the results are similar to the C_L/C_D curve, where an increasing discrepancy (figure 73) for low speeds occurs.

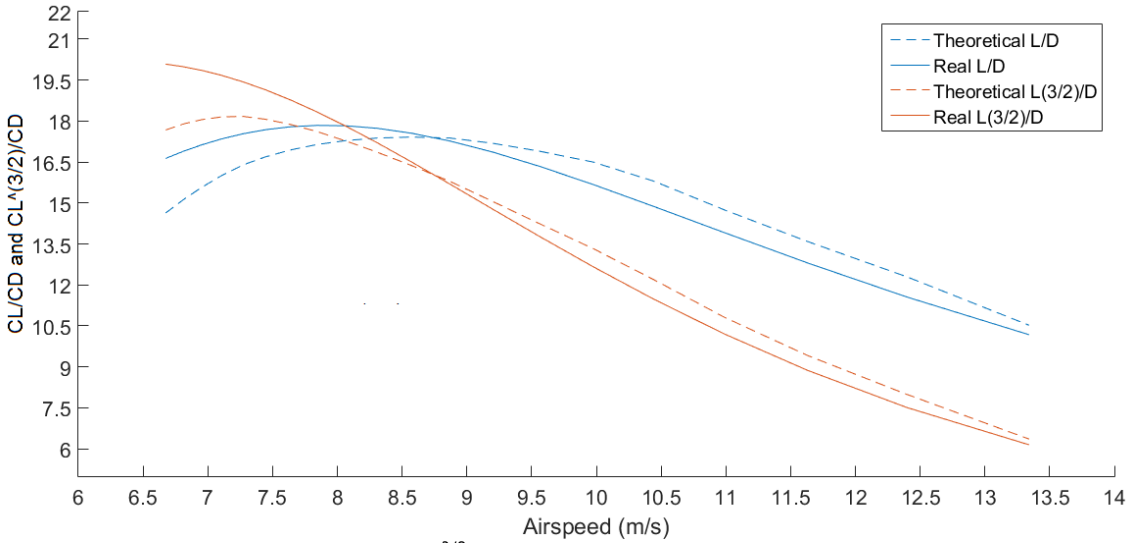

Figure 73 - C_L/C_D and $C_L^{3/2}/C_D$ vs Airspeed (real and theoretical results)

The propulsive system results depicted in figure 74, only consider the power used by the electric motor (without on-board systems). The results also contemplate the influence of the solar panels and the drag of the external accessories. Both the theoretical estimations for the specific range and endurance were obtained bearing in mind the same conditions referred above and a 120Wh battery (without external energy of the solar panels).

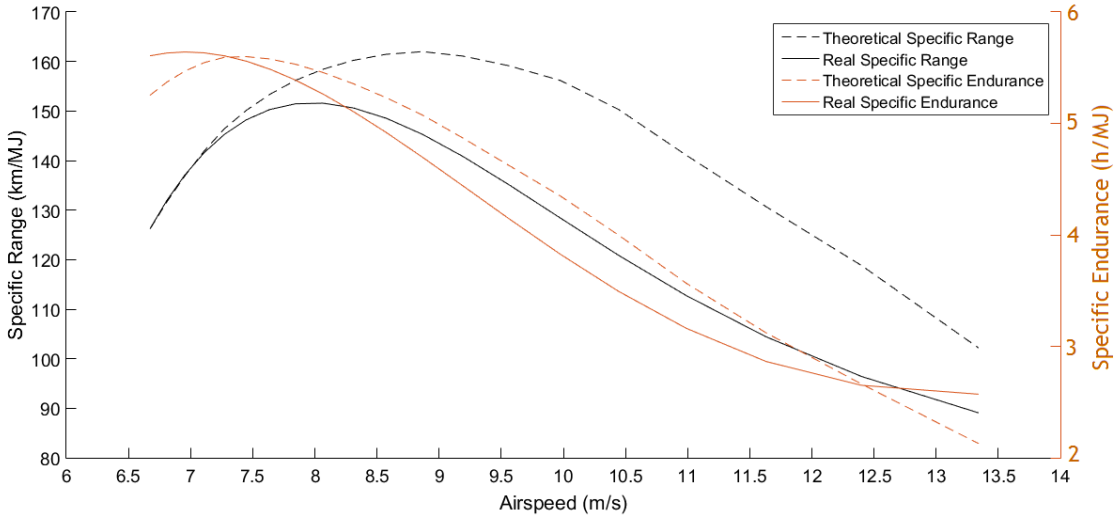

Figure 74 - Specific Range and Specific Endurance vs Airspeed (real and theoretical results)

The specific range results depicted in figure 74 are, in a certain way, disappointing. For speeds above the cruise speed there is a huge discrepancy between the theoretical and real results, this fact is probably related with the decrease of the propulsive system efficiency for high speeds. Considering a 10m/s flight speed, for the same amount of energy, the aircraft should be able to fly more 27,76km. Similar to the specific range results, the specific endurance is also lower than expected for high speeds, where with the same amount of energy the LEEUAV flies 31,34 minutes less than the theoretical results (at 10m/s).

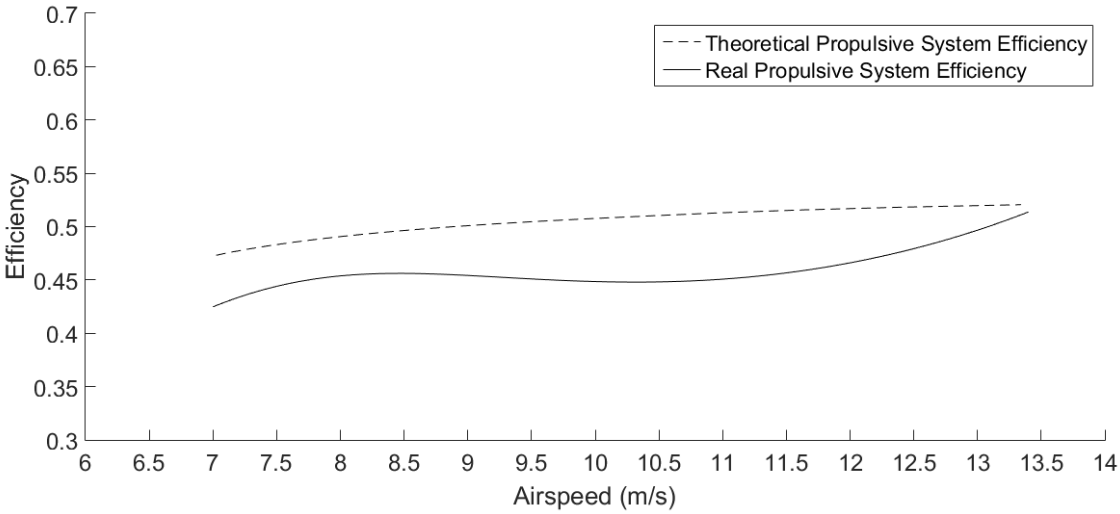

Figure 75 - Propulsive System Efficiency vs Airspeed (real and theoretical results)

The difference between the specific range and endurance curves of the figure 74 is a consequence of the poor propulsive system efficiency for high speeds. It is possible to highlight the difference between the theoretical and real measured propulsive system efficiencies (figure 75). This fact is related with the ESC-motor-propeller efficiencies. However, a deeper study of this system, considering other components (motor, propeller), would be desirable.

7.3 Continuous 3h Solar Flight

As soon as all flight tests were completed, on 24th of November 2016, the A-7 flight endurance test was performed with a surprising 3.13 hours of flight time. It took place at Terlamonte airstrip in Covilhã at an average relative altitude (AGL) of 327m. It was an autonomous flight (except take-off, landing and some tests).

The LEEUAV was launched at 11h16m, in a clear day, where the daily irradiance was already considerable and the weather conditions were calm (5km/h of wind). With a fully charged 10000mAh battery it flew continuously for 3 hours and 8 minutes, landing at 14h24m with 52% of remaining battery. An earlier take-off for the same weather conditions the LEEUAV would flew approximately 6 hours (winter). During the afternoon, the half square meter of solar cells provided enough energy to power the motor and at the same time charge the battery, however the lower solar irradiance during this winter days did not allow for better endurance results. Table 8 lists some of the A-7 flight characteristics.

Table 8 - LEEUAV A-7 flight characteristics

Flight Characteristic	Value
Total flight travelled distance [m]	96265
Total flight time [min]	188
Min/Med/Max flight airspeeds [m/s]	6/8/15
Min/Med/Max flight altitude [m]	0/327/718
Bat/Solar/Total energy used [mAh]	4824/14077/18901

Based on the aerodynamic and power results achieved it was possible to estimate the LEEUAV's theoretical endurance at the equinox. In order to know the amount of solar irradiation at each hour of the day, a simulation of the local solar irradiation (Castelo Branco) was performed. Using formula 30 for the aphelion [59], the solar constant obtained was 1332W/m^2, meaning the average value of the extra-terrestrial amount of solar irradiance. Taken into account that the aircraft does not fly outside the Earth's atmosphere, the influence of the zenith angle, the local latitude and the solar declination were considered. Using formulas 28, 29 and 30 and considering that 20% of the solar irradiance is reflected, absorbed and defunded by the atmosphere, the local solar irradiance model was found [59].

$$I_n = 1 + 0.033\, cos\left(\frac{360N}{365}\right) \tag{27}$$

$$I_z = I_n\, cos(Z_h) \tag{28}$$

$$cos\,(Z_h) = sen(\varphi)\, sen(\delta) + cos(\varphi)\, cos(\delta)\, cos(h) \tag{29}$$

$$\delta = 23.45\, sen\left[\left(\frac{360}{365}\right)(N - 80)\right] \tag{30}$$

Variables: φ is the latitude, δ is the solar declination, N is the day of the year, h is the hour of the day, I_n is the solar constant and I_z is the local solar irradiation [59].

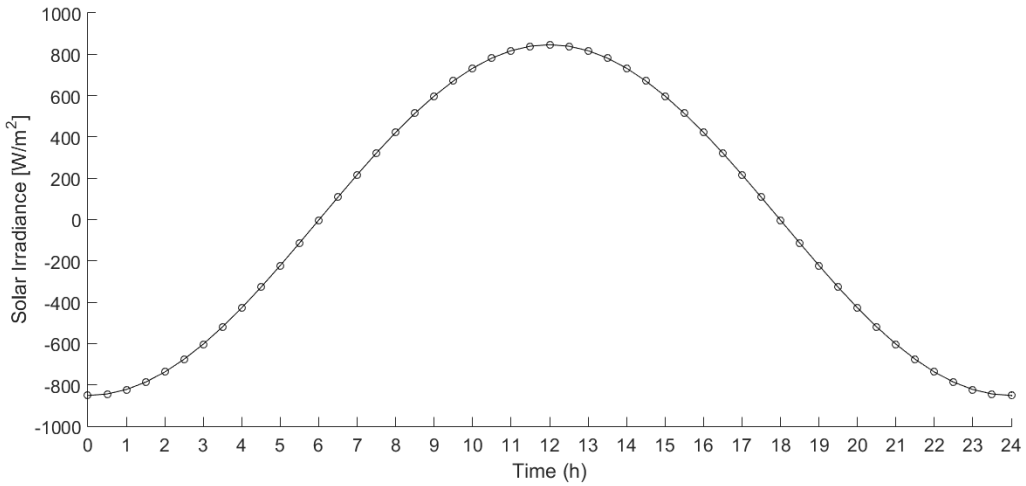

Figure 76 - Time vs Daily Irradiance (Castelo Branco)

Figure 76 depicts the solar irradiation model at the equinox for Castelo Branco (Portugal), the maximum value of solar irradiance (846 W/m^2) occurs aproximately at mid-day. At 6h15m the zenith angle of the sun stars incresing up to 90° and gets 0° again at 18h. The negative values of solar irradiance are related with the night time hours.

Taking into account the C60 solar cells efficiency (22.5%) and the Genasun GV-10 solar charger efficiency (0.98%), the azimuth and inclination of the wings during the flight [33], it was possible to obtain the SCC output power. In a second moment, from the propulsive systems results (required power for cruising) and considering a 111Wh battery, the endurance was calculated.

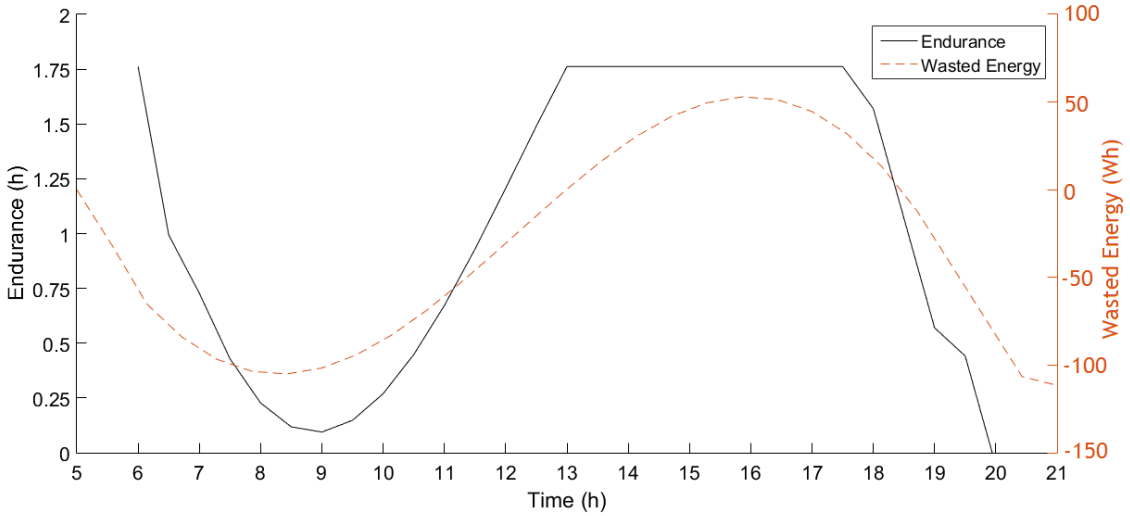

Figure 77 - Theoretical Estimation of the LEEUAV's Flight Endurance

Figure 77 shows the theoretical estimation of LEEUAV flight endurance for a typical mission profile. This mission profile starts with a take-off at 6h with a full charged battery, around 9h the battery will have spent 87,5% of its capacity and will start charging. At about 12h45 the battery completes its charge and will stay charged until 17h45, where the solar irradiation is no longer enough to compensate the required power for the flight. However, the remaining stored energy in the battery will let it to fly one hour and forty-five minutes more and land at 19h45. The final endurance result predicted is of 13h45.

The non-linearity of the endurance line at the beginning and at the end of the flight is related with the higher/lower power requirements considered for take-off (climb up to the cruise altitude) and landing respectively. Parallel to the endurance estimation calculation, an estimate of the wasted energy, i.e., the surplus energy that did not fit into the battery, was calculated. From the beginning of the flight until 12h45 there is no waste of energy, since the battery is charging. However, from this hour until 17h45 there is a considerable amount of energy (333Wh) wasted, which would give approximately more 5h of endurance, if a higher capacity battery was considered (without considering the weight increase of the new battery).

7.4 Flight Difficulties and Hazards

The present LEEUAV aircraft is the result of continuous improvements of the hazards and problems detected during the flight tests. This sections only covers a very small percentage of the total hazards found and corrective actions to fix and prevent them.

Table 9 - Flight difficulties and hazards during LEEUAV flight tests

Hazardous condition	Cause	Effect	Corrective action	Precaution	Flight No.
Spatial disorientation	FPV camera too close to the airframe	Low camera visibility	Raise the camera support	Flight in line of sight	A-2
Inconsistent telemetry data display	Inadequate refresh rates	Low stream of telemetry data	Change refresh rates	None	A-2
Power oscillations	ESC overheat	Power losses	Upgrade ESC	Land	A-1
Loss of yaw control	High torque applied on rudder	Rudder inoperability	Reinforce rudder control arms	Land	A-3
High temperature inside the UAV	High air temperature at the airfield	Decreased efficiency, risk of components failures	Open air intakes at the nose	None	A-1
Lack of tail boom bolt	Forgetfulness/inattentiveness	Risk of disintegration	Creation of a pre-flight checklist	Flight at low speeds and land	A-1

7.5 Error Analysis

Each sensor reading contains a random error that usually is known and specified by each sensor's manufacturer. This error tends to propagate along the calculation process, thus leading to a global error in the final result.

Although the global error is influenced by other variables such as polynomial approximation, components temperatures, time, etc. In this work, the global error calculation was based on the measurement of the reading errors of each component for the most important parameters used, namely the drag, airspeed, lift-to-drag ratio and required power.

For example, the total drag error comprises the error of each component used to calculate it, i.e., according to formula 26, the total drag error includes the measurement error of weighing (aircraft mass), the accuracy of Pixhawk's barometer sensor (rate of climb), the measurement error of the airspeed sensor (airspeed) and the accuracy of the GPS sensor (ground speed). The total drag error was calculated for all the points analysed and is defined by:

$$\Delta D = \frac{dD}{dm}\Delta m + \frac{dD}{dh}\Delta h + \frac{dD}{dv_{air}}\Delta v_{air} + \frac{dD}{dv_g}\Delta v_g \tag{31}$$

Where $\frac{dD}{dm}$, $\frac{dD}{dh}$, $\frac{dD}{dv_{air}}$ and $\frac{dD}{dv_g}$ are the drag's partial derivatives of mass, altitude, airspeed and ground speed respectively. The Δm, Δh, Δv_{air} and Δv_g are the accuracies (specified by their manufactures) of the components used on LEEUAV. A similar process was repeated for airspeed, lift-to-drag-ratio and required power. The results obtained are in table 10.

Table 10 - Measurement results, relative error and average uncertainty

Parameter	Measurement Error	Minimum relative error	Medium relative error	Maximum relative error	Average uncertainty
Drag (N)	0.556	0.057	0.244	0.979	11.12%
Airspeed (m/s)	2.380	0.232	0.250	0.281	21.64%
C_L/C_D	1.199	2.201E-4	0.068	0.213	7.99%
P_{req} (W)	10.884	0.057	0.112	0.173	15.55%

Having in mind the practical circumstances, the overall results of the errors calculated are fairly good, the highest value of average uncertainty belongs to the airspeed sensor and the minimum average uncertainty to the lift-to-drag ratio. In order to conclude about error results obtained, table 11 compares the results between the practical measurements (considering the error associated) and the theoretical results, for the cruise airspeed.

Table 11 - Comparison between practical and theoretical results.

Parameter	Measurement Error	Real measured value	Theoretical measured value	Real and theoretical values difference
Drag (N)	0.556	3.593	3.151	0.442
C_L/C_D	1.199	17.839	17.139	0.700
P_{req} (W)	10.884	28.178	24.711	3.467

The real and theoretical results difference is acceptable for the cruise airspeed, since all the real measured values plus the measurement error associated are higher than the difference between the real and theoretical values, for all the parameters. However, for airspeeds above 10m/s this does not happen, where the real measured values plus the measurement error boundaries do not attain the theoretical measured values.

Even before the global error is known, before applying the MATLAB algorithm to LEEUAV flight data, it was applied to Olharapo. Olharapo was a previous project developed at the Department of Aerospace Sciences (DCA) of University of Beira Interior related to instrumentation and flight tests to evaluate the aerodynamic performance of an Unmanned Aerial Vehicle. The results obtained with Olharapo flight logs, using the MATLAB algorithm covered in this work, prove to be very similar to the results obtained by Joaquim Sousa [58], validating the method for LEEUAV performance estimation.

7.6 Other observations

Although not described here, before the LEEUAV autonomous flight a similar autonomous flight was performed with a less complex foam RC model (Skywalker), where flight modes, speeds, flight paths, altitudes and aircraft attitudes were tested, analysed and adjusted.

There were some other tests also carried out, but due to their subjectivity they are not addressed above. Handling qualities, aeroelastic stability, airframe stress, wind influence, and structural integrity of the aircraft in flight are some of them. All the project requirements (section 6.2) were also successfully achieved during the flight tests.

During the flight tests, it was possible to foresee some additional ways to increase flight endurance by using altitude as energy storage, climbing during the day and descent at night time, using of thermal winds for altitude gain or upgrading the on-board battery.

Intentionally left blank

Chapter 8

8 Conclusion

8.1 Main Achievements

The presented thesis is a culmination of three-year partnership between three universities working on the LEEUAV project. This work has proposed to test and validate all theoretical calculations of the designed project of an electric unmanned aircraft. The main objectives of the proposed work were successfully achieved. This work allowed me to learn about the concepts inherent of unmanned aircraft as well as improve my knowledge about the RC aircraft world. The systems integration, including the choice and purchasing of the required electronic components required that I learn about and understand the "Why?" of each choice, ensuring the compatibility, applicability and reliability of all the systems applied in the LEEUAV.

Besides all the systems integration part, the practical phase of finishing the airframe structure and changing the wing tip of the LEEUAV required of me an acquirement of knowledge of CNC programing, including the 2-Axis laser cutting machine and the 3-Axis CNC milling cutter for hard materials, carbon fibre lamination techniques and procedures, welding electronic components and heat shrink film application.

After integrate all the systems and completing all the structure of the LEEUAV, the required missions to validate the airworthiness and utility of the LEEUAV were delineated and scheduled. Although the piloting of the LEEUAV flight tests was not been conducted by me, all ground and system operability tests were of my responsibility, including the monitorization of the flight variables. This work has therefore, enhanced my multitasking capacity and workload management, preparing me for the future phase of my life.

As soon as all the practical segment, including the flight tests, were completed, an evaluation of the agreement between theoretical and practical results was done, questioning for my interpretation and analysis ability. The error analysis permitted to estimate the experimental error related with the measuring accuracy of the LEEUAV's on-board sensors. The results were satisfactory since the estimated experimental error is in agreement with the magnitude of the error of the theoretical results.

8.2 Prospective Future Improvements

Since the pioneer, Fred Militky combined the two fields of solar cells and electric aircraft, solar aviation has been on the radar of researchers. The experience and knowledge gained during this thesis allows me to foresee continuous improvements in the solar Aviation field, not only in relation to the macroscopic view, but also in relation to small processes like materials used, manufacture techniques applied, reliability, diversity and functionality of on-board electronic components as well as the applicability of unmanned aerial systems on our daily lives.

Solar aircraft for the transportation of humans or heavy payloads are currently under development on a large scale although many electric aircraft producers had already proven that it is possible and safe. The present, maned, solar aircraft are associated with low weight, large wingspans or low flight autonomies due to the available technologies existent on the market.

In order to make the solar aircraft usable and serviceable there are some current challenges, which do not only affect the field of aeronautics but also many others fields where electric propulsion is applied, that have to be surpassed, namely:

- Increase of batteries energy density;
- Enhance the (FPV) video range and quality for control at very long distances;
- Improvements on solar cells efficiency and solar power harvesting;
- Improvement of sensibility and responsiveness of autonomous flight controllers.

In my personal opinion, I believe that as soon as these challenges have been met, we will be seeing a great improvement in the way we get around.

8.3 Suggested Future Work

The work developed in this thesis does not cover all the characterization of the LEEUAV. So, following a continuous improvement philosophy, there are some future works to be developed on this LEEUAV project, namely:

- Design and implement other solar panels integration (inside the wing structure), in order to reduce the total drag;
- Perform more flight tests in order to obtain sufficient flight information to assess, in its fullness, the aerodynamic efficiency and reliability of LEEUAV;
- Carry out more long solar flights in summer time and use altitude as energy storage and with high discharge rate Li-ion batteries;
- Characterize the LEEUAV aircraft in other not analysed flight phases.

References

[1] Anderson, J. (2011). *Introduction to Flight*. 7ª Edition. Columbus, Ohio. McGraw-Hill Education.

[2] U.S. Department of Energy. (2002). *History of Solar*. Available at: *http://www1.eere.energy.gov/solar/pdfs/solar_timeline.pdf [Accessed at 5 April, 2016]*

[3] Boucher R. J. (1984) *History of Solar Flight*. In Proc. of the 20th Joint Propulsion Conference, AIAA-84-1429, Cincinnati, Ohio, USA.

[4] Noth, A. (2008). *History of Solar*. Autonomous Systems Lab, ETH Zürich, Switzerland. Available at: http://www.sky-sailor.ethz.ch/docs/History_of_Solar_Flight_v1.2-A.Noth_2006.pdf [Accessed at 28 April, 2016]

[5] Urs, M. & Vezzini, A. (2015) *Electric flight – history – state of the art and first Applications*. Berne University of Applied Sciences BUAS, *Switzerland*. Available at: https://www.bfh.ch/fileadmin/data/publikationen/2015/D_35_Muntwyler_U.pdf [Accessed at 3 May, 2016]

[6] Jackson, P. (2005). *Jane's All the World's Aircraft 2004-2005*. London, Jane's Information Group.

[7] Schäper, W. (1999). *Wolfgang Schäper flog seinen 13. erfolgreichen.* ModellFlug Gruppe Markdorf e.V. Available at: http://www.mfg-markdorf.de/rekorde/index.htm [Accessed at 15 May, 2016]

[8] Stinton, D. (2001) *The Design of the Aeroplane*, 2ª ed. Oxford, UK, Blackwell Science.

[9] Raymond, E. (2016). *Sunseeker I.* USA. Solar Flight. Available at: http://www.solar-flight.com/projects/sunseeker-i/ [Accessed at 16 May, 2016]

[10] History of the Berblinger Competition - Ulm. Available at: http://www.berblinger.ulm.de/html/berblinger_prize [Accessed at 16 May, 2016]

[11] University of Stuttgart. (1996). Icaré 2. Stuttgart Available at: http://www.icare-solar.de/index.php/projekt [Accessed at 18 May, 2016]

[12] Gibbs, Y. (2014). *NASA Pathfinder Solar-Powered Aircraft*. Solar-Power Research at NASA Dryden. Washington. Available at: http://www.nasa.gov/centers/armstrong/news/FactSheets/FS-034-DFRC.html [Accessed at 28 May, 2016]

[13] Gibbs, Y. (2014). *NASA Armstrong Fact Sheet: Solar-Power Research*. NASA Publisher. Washington. Available at: https://www.nasa.gov/centers/armstrong/news/FactSheets/FS-054-DFRC.html [Accessed at 28 May, 2016]

[14] DLR Institute of Flight Systems. *History – Road Map of Events: 1994-1996 (Solitair)*. Available at: http://www.dlr.de/ft/en/desktopdefault.aspx/tabid-1388/1918_read-3385/ [Accessed at 1 Jun, 2016]

[15] Renewable Energy World. (2005). *Solar Plane Breaks Two-Night Flight Barrier*. Available at: http://www.renewableenergyworld.com/articles/2005/07/solar-plane-breaks-two-night-flight-barrier-34057.html [Accessed at 1 Jun, 2016]

[16] Amos, J. (2008). *Solar plane makes record flight (Zephyr 6)*. BBC News. UK. *Available at: http://news.bbc.co.uk/2/hi/science/nature/7577493.stm* [Accessed at 2 Jun, 2016]

[17] Solar-Impulse – The Adventure (2016). Available at: https://www.solarimpulse.com/adventure [Accessed at 3 Jun, 2016]

[18] Hodges, J. (2011). *DARPA Vulture Project*. NASA Researchers News. U.S. Available at: http://www.nasa.gov/centers/langley/news/researchernews/rn_nov11colloquium.html [Accessed at 3 Jun, 2016]

[19] Christensen, B. (2008). *DARPA Vulture Five Year Flying Wing*. Technovelgy. Available at: http://www.technovelgy.com/ct/Science-Fiction-News.asp?NewsNum=1491 [Accessed at 8 May, 2016]

[20] Solar Flight Company – Sunseeker II, Sunseeker Duo, Sun Star and Solar 6-seat transporter. USA. Available at: http://www.solar-flight.com/home/ [Accessed at 5 Jun, 2016]

[21] Airbus Defense and Space. (2015). *Zephyr, the High Altitude Pseudo-Satellite*. Available at: https://airbusdefenceandspace.com/our-portfolio/military-aircraft/uav/zephyr/ [Accessed at 5 Jun, 2016]

[22]Warwick, G. (2015). *Facebook's UAV Flies, Builds On Developments In Solar Power*. Aviation Week & Space Technology. Available at: http://aviationweek.com/technology/facebook-s-uav-flies-builds-developments-solar-power [Accessed at 5 Jun, 2016]

[23] Trimble, S. (2015). *Facebook unveils 42m wingspan Aquila UAV*. Washinton DC. Flight Global. Available at: https://www.flightglobal.com/news/articles/facebook-unveils-42m-wingspan-aquila-uav-415331/ [Accessed at 5 Jun, 2016]

[24] Garrun, D. (2015). *Solara 50 Atmospheric Satellite*. UK. Aerospace Tecnhology. Available at: http://www.aerospace-technology.com/projects/solara-50-atmospheric-satellite/ [Accessed at 5 Jun, 2016]

[25] Oettershagen, P., Melzer, A., Mantel, T., Rudin, K., Stastny, T., Wawrzacz, B., Hinzmann, B., Alexis, K., Siegwart, R. (2001). *Perpetual flight with a small solar-powered UAV: Flight results, performance analysis and model validation*. Autonomous Systems Lab Swiss Federal Institute of Technology Zurich, Zurich

[26] Silent Falcon Company – Silent Falcon UAV. USA. Available at: http://www.silentfalconuas.com/silent-falcon [Accessed at 30 Sep, 2016]

[27] Moir, I; Seabridge, A; Langton, R. (2010). *Unmanned Air Systems: UAV Design, Development and Deployment*. Wiltshire, UK. John Wiley & Sons Ltd.

[28] Centre for Telecommunications and Information Engineering, Monash University. *Remote Piloted Aerial Vehicles: An Anthology*. Melbourne, Australia. Available at: http://www.ctie.monash.edu.au/hargrave/rpav_home.html [Accessed at 8 Jun, 2016]

[29] Unmanned Aerial Vehicles Systems Association. (2016). *Civil and Commercial UAS Applications*. Wiltshire, UK. Available at: https://www.uavs.org/commercial [Accessed at 9 Jun, 2016]

[30] Frey, T. (2014). *192 Future Uses for Flying Drones*. Available at: http://www.futuristspeaker.com/business-trends/192-future-uses-for-flying-drones/ [Accessed at 9 Jun, 2016]

[31] Cândido, L. (2014). *Projeto de um UAV Solar de grande autonomia*. MSc Thesis. Structures and Vibrations Lab, University of Beira Interior (UBI), Portugal.

[32] Ferreira, T. (2014). *Hybrid Propulsion System of a Long Endurance Electric UAV*. MSc Thesis. Instituto Superior Técnico (IST), Portugal.

[33] Sousa, J. (2015). *Solar System for a Long Endurance Electric UAV*. MSc Thesis. Structures and Vibrations Lab, University of Beira Interior (UBI), Portugal.

[34] Duarte, A. (2016). *Development part of the Structure of a Long Endurance Electric UAV*. MSc Thesis. Structures and Vibrations Lab, University of Beira Interior (UBI), Portugal.

[35] Freitas, L. (2017). *Aerodynamic Analysis of a Forward-Backward Facing Step Pair on the Upper Surface of a Low-Speed Airfoil*. MSc Thesis. Universidade da Beira Interior (UBI), Portugal

[36] Moutinho, P. (2017). *Real-Time Estimation of Remaining Flight Time Based on the Total Energy Balance for UAV's*. MSc Thesis. Universidade da Beira Interior (UBI), Portugal

[37] International Civil Aviation Organization. (2011). *ICAO's circular 328 AN/190: Unmanned Aircraft Systems (UAS)*. Canada.

[38] Pontzer, A; Lower, M; Miller, J. (2010). *Unique Aspects of Flight Testing Unmanned Aircraft Systems*. Flight Test Technique Series, Vol. 27. Research and Technology Organisation of NATO.

[39] Noth, A. (2008). *Design of Solar Powered Airplanes for Continuous Flight*. PhD Thesis. Autonomous Systems Lab, Swiss Federal Institute of Technology (ETH) Zürich. Available at: http://www.sky-sailor.ethz.ch/docs/Thesis_Noth_2008.pdf [Accessed at 5 April, 2016]

[40] RC Lab Website. (2014). *The Basics of Electric Power: Brushless Motors*. Available at: http://www.rclab.info/2014/01/the-basics-of-electric-power-brushless.html [Accessed at 11 Jun, 2016]

[41] McGrady, C. (2016). *Brush or Brushless?*. Arrow Electronics. Available at: https://www.arrow.com/en/research-and-events/articles/which-dc-motor-is-best-for-your-application [Accessed at 11 Jun, 2016]

[42] German Energy Agency. (2016). *Technologies and applications - How a PV cell works*. Available at: http://www.renewables-made-in-germany.com/en/renewables-made-in-germany/technologies/photovoltaics/photovoltaics/technologies-and-applications.html [Accessed at 13 Jun, 2016]

[43] U.S. Department of Energy. (2016). *National Renewable Energy Laboratory (NREL) – Photovoltaics Research.* Available at: http://www.nrel.gov/pv/ [Accessed at 13 Jun, 2016]

[44] Home of Alternative and Renewable energy Tutorials. (2015). *Solar Cell I-V Characteristic Curve*.Available at: http://www.alternative-energy-tutorials.com/energy-articles/solar-cell-i-v-characteristic.html [Accessed at 13 Jun, 2016]

[45] Kimberlin, R. (2003). *Flight Testing of Fixed-Wing Aircraft. AIAA, Education Series. Virginia Polytechnic Institute and State University.* American Institute of Aeronautics and Astronautics, Inc., Reston, Virginia

[46] Wagner, L. (2007). *Overview of energy storage methods*. Strasbourg, France. MORA associates.

[47] Voelker, P. (2014). *Analysis of Lithium-Ion Battery Components.* Sunnyvale, USA. Thermo Fisher Scientific Inc. Available at: http://www.rdmag.com/article/2014/04/trace-degradation-analysis-lithium-ion-battery-components [Accessed at 14 Jun, 2016]

[48] Notten, P. (2006). *Rechargeable Batteries: Efficient Energy Storage Devices for Wireless Electronics*. AmIware Hardware Technology Drivers of Ambient Intelligence, Philips Research. Springer Netherlands. Eindhoven.

[49] Clancy, L. (1975). *Aerodynamics* (P*itman aeronautical engineering series)*. California. Pitman Publishing Ltd.

[50] Silva, N. (2014). *Parametric Design, Aerodynamic Analysis and Parametric Optimization of a Solar UAV*. MSc Thesis. Instituto Superior Técnico (IST), Portugal.

[51] Gadd, C. Scale and Giant Scale R/C – Servo Torque Calculator. USA. Available at: http://www.mnbigbirds.com/Servo%20Torque%20Caculator.htm [Accessed at 30 Sep, 2016]

[52]ArduPilot Dev Team. (2015). *Mission Planner Overview. Available at:* http://ardupilot.org/planner/docs/mission-planner-overview.html [Accessed at 15 Jun, 2016]

[53]Wilson's, J., Dávila, J., McNeil, T. (2000). *Decomposition of Functions Performed During a Commercial Transport Flight*. Covell Avionics. Available at: http://flightdeck.ie.orst.edu/ElectronicChecklist/HTML/mission.html [Accessed at 25 Jun, 2016]

[54] Godwin, O., Frazier, F., Durnin, R. (1965). *USAF Performance Flight Test Theory*. USAF Test Pilot School, Edwards AFB, California.

[55]Bridges, P., Cross, E., Boatwright, W. (1977). *Flight Test Evaluation of a Method to Determine the Level Flight Performance of a Propeller Driven Aircraft*. Society of Automotive Engineers.

[56] Massachusetts Institute of Technology (MIT) Open Course: IV Aircraft performance – Vehicle Drag. Available at: http://ocw.mit.edu/ans7870/16/16.unified/propulsionS04/UnifiedPropulsion4/UnifiedPropulsion4.htm [Accessed at 20 Jun, 2016]

[57] Yoon, J. (2001). *Adverse Yaw and Aircraft Turns*. Aerospace Web Article. Available at: http://www.aerospaceweb.org/question/dynamics/q0045.shtml [Accessed at 20 Jun, 2016]

[58] Sousa, J. (2014). *Avaliação em Voo das Características de uma Asa de Envergadura Variável*. MSc Thesis. Universidade da Beira Interior (UBI), Portugal.

[59] Albino, A. (2014). *Radiação solar: estudo e criação de plataforma de apoio à conceção de um sensor de radiação solar*. MSc Thesis. Universidade de Évora. Portugal.

Annex A – LEEUAV Specification Tables

LEEUAV General Definitions Table			
Type	Long Endurance Electric Solar Aircraft	**First Flight**	18th July of 2016
Control	Unmanned (Remoted Piloted)	**Owner**	University of Beira Interior
Airframe Materials	Carbon Fibre. Balsa Hood and Termoadherente fabric	**Mission Type**	Surveillance. Loiter. Monitoring
Wing Configuration	High Wing. No Dihedral. No Sweptback	**Commands Range**	80 km
Wing Airfoil	Designed by Prof. Pedro Gamboa (UBI)	**Endurance**	8 h
Horizontal Stabilizer Airfoil	NACA0010	**Landing Gear**	No
Vertical Stabilizer Airfoil	NACA0010	**Telemetry Range**	2 km
Tail Configuration	Inverted "T" Tail	**FPV Range**	10 km
Thrust Method	Pull	**Solar Panels Max. Efficiency**	22.5 %
Propulsive System Configuration	Single Brushless Out-runner Electric Motor	**Solar Panels Max. Power**	140 W
FPV Operating Frequency	1300 MHz	**Radio Control Operating Frequency**	433 MHz
Telemetry Operating Frequency	2400 MHz	**Battery Capacity**	10000mAh

LEEUAV Measured Flight Performance Table			
Take-off Speed* [m/s]	6.94	**Max. Flight Endurance* [h]**	6
Max. Vertical Speed* [m/s]	2	**Max. Flown Speed* [m/s]**	26
Cruise Speed* [m/s]	7.8	**Stall Speed* [m/s]**	6.5
Max. Landing Speed* [m/s]	10	**Take-off Distance* [m]**	10
Max. Flown Altitude* [m]	718	**Min. Landing Distance* [m]**	40
Max. Flown Range* [km]	3.4	**L/D***	17.43

*From flight tests results

LEEUAV Weight Breakdown Table

Main Weights (non-solar version weights)			
MTOW [N]	54.129 (46.088)	**Wing [N]**	23.602 (18.001)
Empty Weight [N]	47.118 (39.077)	**Battery Weight [N]**	7.980
Payload [N]	0 (8.041)	**Solar System Weight [N]**	8.041

Detailed Weight of LEEUAV Systems			
Component	**Unit Weight [N]**	**Quantity**	**% of total LEEUAV Weight**
Structure			47.533
Fuselage	4.169	1	7.704
Wing Central Panel	6.321	1	11.682
Left Wing Tip	5.543	1	10.011
Right Wing Tip	5.326	1	9.830
Tail Tube	2.520	1	4.657
Tail Support	0.331	1	0.612
Horizontal Stabilizer	1.048	1	1.937
Vertical Stabilizer	0.595	1	1.100
Electronics - Flight Control			8.298
Receiver	0.196	1	0.362
Receiver Antennas	0.137	2	0.506
Telemetry Transceiver	0.098	1	0.181
Telemetry Antenna	0.049	1	0.091
Flight Controller	0.372	1	0.687
On Screen Display	0.118	1	0.218
Camera	0.116	1	0.214
Video Transmitter	0.569	1	1.052
Video Antenna	0.118	1	0.218
Wing and Elevator Servos	0.123	5	0.909
Rudder Servo	0.235	1	0.434
UBEC	0.334	1	0.617
GPS	0.269	1	0.497
Airspeed Sensor	0.147	1	0.272
Wiring	0.980	-	1.811
Propulsion System			21.226
Propeller and Spinner	0.373	1	0.689
Motor	1.825	1	3.373
ESC	1.112	1	2.055
Battery	7.980	1	14.747
Power Module	0.196	1	0.362
Solar Energy System			14.516
Solar Charger	1.814	1	3.352
Solar Panels	5.883	1	10.872
Amperage Sensor	0.158	1	0.292
C.G. Positioning Ballasts			8.427

LEEUAV Geometry Definition Table			
Airframe		**Wing**	
Length [m]	2.557	**Wing Surface Area [m^2]**	1.490
Span [m]	4.525	**Solar Panel Area [m^2]**	0.792
Height [m]	0.334	**Mean Chord [m]**	0.330
Tail		**Wing Dihedral**	0
Horizontal Stabilizer Span [m]	0.700	**Wing Aspect Ratio**	13.71
Vertical Stabilizer Span [m]	0.280	**Wingtip**	Endplate
Horizontal Stabilizer Mean Chord [m]	0.175	**Tapering**	None
Vertical Stabilizer Mean Chord [m]	0.215	**Torsion at wing tip [˚]**	-4.5
Stabilizers Angle [˚]	90	**Wing Incidence Angle [˚]**	3

LEEUAV Systems and Components Table			
Spinner	Aluminium Spinner - Aeronaut	**Video Camera**	RunCam 600TVL
Propeller	13x8 Retractable Propeller - Aeronaut	**Telemetry Transceiver**	RM024 - Laird Technologies
Motor	Hyperion ZS 3025-10	**Video Transmitter**	-
ESC	75A - Castle Creation Phoenix Edge	**Receiver**	12Ch - Scherrer RX700LR V7
Flight Controller	Pixhawk	**Radio Control**	16Ch Royal SX - Multiplex
On Screen Display	AlceOSD 0v3	**Solar Cells**	C60 - Sunpower
Solar Charge Controller	Genasun GV-10	**Telemetry Antenna**	-
Step Up/Down Converter	-	**Video Antenna**	Skew Planar Wheel
Receiver Antennas	TSLRS	**Battery**	Range Video 3S3P. 2C. 18300 mAh
Universal Battery Eliminator Circuit	Turnigy 15A	**Rudder Servo**	Hitec HS-5125MG Servo
Aileron Servos	Corona 939MG Metal Gear Servo	**Airspeed Sensor**	3DR Digital Airspeed Sensor
GPS	Ublox NEO-M8N		

Annex B

Final Assembly Wiring Diagram

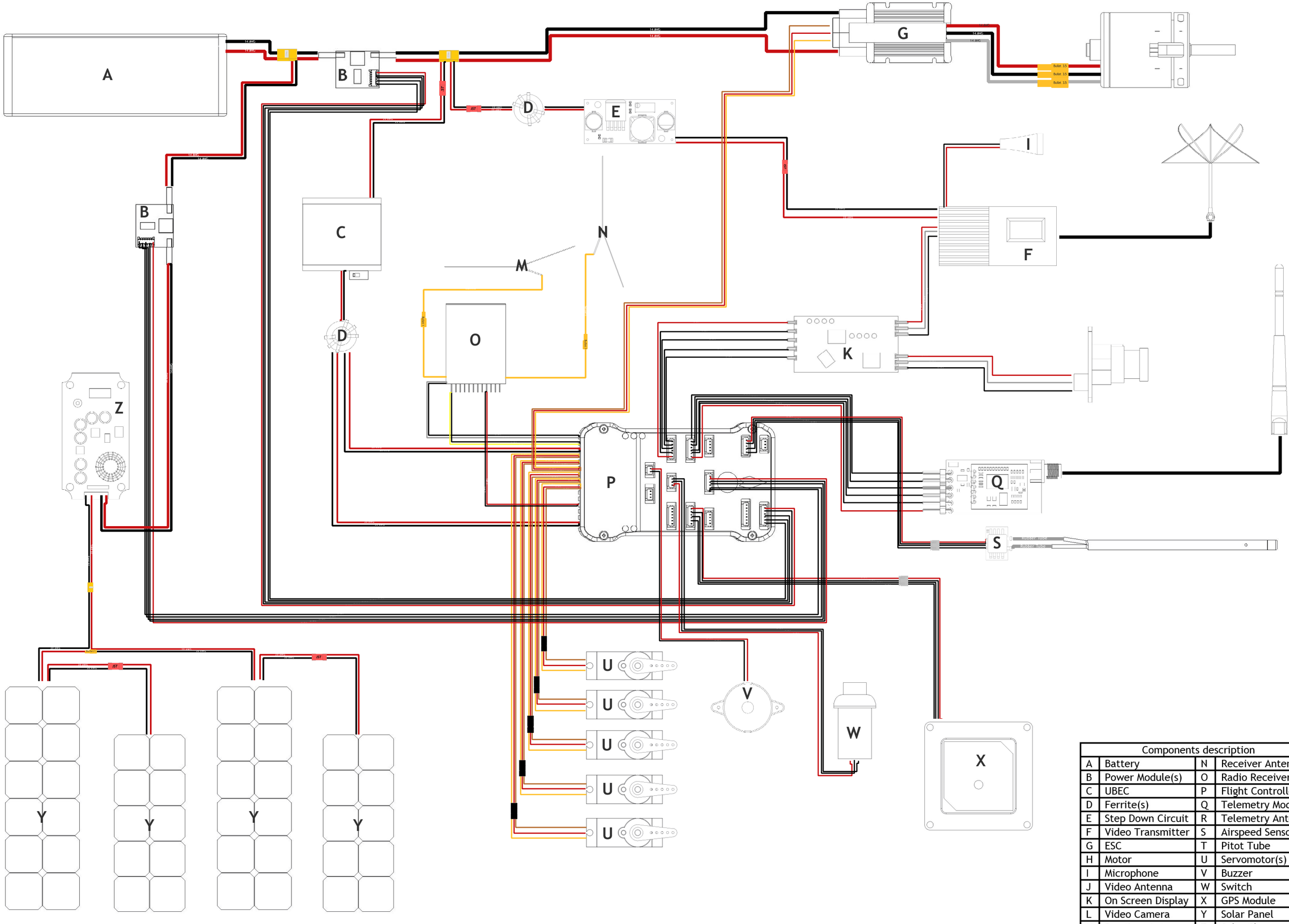

Components description			
A	Battery	N	Receiver Antenna
B	Power Module(s)	O	Radio Receiver
C	UBEC	P	Flight Controller
D	Ferrite(s)	Q	Telemetry Module
E	Step Down Circuit	R	Telemetry Antenna
F	Video Transmitter	S	Airspeed Sensor
G	ESC	T	Pitot Tube
H	Motor	U	Servomotor(s)
I	Microphone	V	Buzzer
J	Video Antenna	W	Switch
K	On Screen Display	X	GPS Module
L	Video Camera	Y	Solar Panel
M	Receiver Antenna	Z	Solar Charger

Annex C

LEEUAV Performance Analysis algorithm

```
%==========================================================================
%===              LEEUAV FLIGHT PERFORMANCE ANALYSIS
%===                    - A. Rodrigues, 2016 -
%===
%=== This code reads .txt log files from the Pixhawk flight controller and
%=== calculates the flight coefficients based on glidings (No thrusts).
%=== For more information about this algorithm see Chapter 6 and 7.
%==========================================================================

function []=Aerodynamic_Performance_Algorithm_LEEUAV()
% Flight Coefficients and Lift-to-Drag Ratio
clear all
clc

%% ----------------------------.TXT FILE LOAD-----------------------------
% Input .txt file
fprintf('Enter the name of the .txt Log file to analyse.\n')
fileID =-1;
errmsg='';
while fileID<0
    disp(errmsg);
    filename=input ('open file: ', 's');
    [fileID,errmsg]=fopen(filename);
end
% Open .txt file
fileID=fopen(filename);
% Verification step
if(fileID==-1)
    fprintf('ERROR opening the file %s \n',filename)
    return
  else
    fprintf('File opening OK!\n',fileID)
end

%% ---------------------- READ .TXT FILE ---------------------------------
% Initialize variables.
delimiter = ',';
% Format string for each line of text:
formatSpec = '%s%f%f%f%f%f%f%f%f%f%f%f%f%[^\n\r]';
% Open the text file.
fileID = fopen(filename,'r');
% Read columns of data according to format string.
dataArray = textscan(fileID, formatSpec, 'Delimiter', delimiter,↙
'MultipleDelimsAsOne', true, 'EmptyValue' ,NaN, 'ReturnOnError', false);
% Close the text file.
fclose(fileID);

%% --------------------VARIABLES ALLOCATION-------------------------------
% Allocate imported array to column variable names
name = dataArray{:, 1};
var2 = dataArray{:, 2};
var3 = dataArray{:, 3};
var4 = dataArray{:, 4};
var5 = dataArray{:, 5};
var6 = dataArray{:, 6};
```

```
var7 = dataArray{:, 7};
var8 = dataArray{:, 8};
var9 = dataArray{:, 9};
var10 = dataArray{:, 10};
var11 = dataArray{:, 11};
var12 = dataArray{:, 12};
var13 = dataArray{:, 13};
var14 = dataArray{:, 14};
% Clear temporary variables
clearvars filename delimiter formatSpec fileID dataArray ans;

%% --------------------------ARRAYS FORMATION-----------------------------
fprintf('\n--> Starting Arrays Formation')

%-----------------------------Airspd - ARSP---------------------------------
str1={'ARSP'};
A=strcmp(str1,name);                                          % ARSP Position
P=find(A==1);                                              % ARSP Identification
i=1;
while (1)
   if i<length(P)
    Val_Airspd(i)=var3(P(i));
    time_Airspd(i)=var2(P(i));
 i=i+1;
   else
       break
end
end
Airspd = horzcat(time_Airspd',Val_Airspd');                % Concatenation

%-----------------------------Gndspd - GPS----------------------------------
str1={'GPS'};
A=strcmp(str1,name);                                           % GPS Position
P=find(A==1);                                               % GPS Identification
i=1;
while (1)
   if i<length(P)
    Val_Gndspd(i)=var11(P(i));
    time_Gndspd(i)=var2(P(i));
    i=i+1;
   else
       break
   end
end
Gndspd = horzcat(time_Gndspd',Val_Gndspd');                % Concatenation

%-------------------------------Pitch - AHR2--------------------------------
str1={'AHR2'};
A=strcmp(str1,name);                                          % AHR2 Position
P=find(A==1);                                              % AHR2 Identification
i=1;
while (1)
   if i<length(P)
    Val_Pitch(i)=var4(P(i));
    time_Pitch(i)=var2(P(i));
```

```
 i=i+1;
   else
       break
   end
end
Pitch = horzcat(time_Pitch',Val_Pitch');                    % Concatenation

%------------------------------Altitude - BARO----------------------------
str1={'BARO'};
A=strcmp(str1,name);                                        % BARO Position
P=find(A==1);                                             % BARO Identification
i=1;
while (1)
   if i<length(P)
    Val_Alt_baro(i)=var3(P(i));
    time_Alt_baro(i)=var2(P(i));
 i=i+1;
   else
       break
   end
end
Alt_baro = horzcat(time_Alt_baro',Val_Alt_baro');            % Concatenation

%-----------------------Temperature - Airspeed---------------------------
str1={'ARSP'};
A=strcmp(str1,name);                                        % ARSP Position
P=find(A==1);                                             % ARSP Identification
while (1)
   if i<length(P)
    Temp(i)=var5(P(i));
 i=i+1;
   else
       break
   end
end
Temperature=mean(Temp);                                     % Concatenation

%------------------------------Pressure - BARO----------------------------
str1={'BARO'};
A=strcmp(str1,name);                                        % BARO Position
P=find(A==1);                                             % BARO Identification
i=1;
while (1)
   if i<length(P)
    Val_press(i)=var4(P(i));
    time_press(i)=var2(P(i));
 i=i+1;
   else
       break
   end
end
Press = horzcat(time_press,Val_press);                      % Concatenation
fprintf('\n--> Arrays Formation Complete\n')

%% ------------------------USER INPUTS-------------------------------------
```

```
% Number of Intervals to analyse
n=input('\n Enter the number of intervals to analyse:');
fprintf('\n------------------Export Fligth Data----------------------\n')
R=input('\nWrite 1 to Export L/D Partial Flight Data: \nWrite 2 to Export Complete↙
Flight Data:\n','s');
if strcmp(R,'1')
    dlmwrite('LD_Partial_Flight_Data.txt', 'Airspeed(m/s),Drag(N),Cd,Cl,L/D','',''); %↙
Write first line
elseif strcmp(R,'2')
    dlmwrite('LD_Complete_Flight_Data.txt', 'time(min),AccX(m/s2),Airspeed(m/s),↙
Ground_speed(m/s),Altitude_baro(m),Rho(kg/m3),Climb_Rate_baro(m/s),Ppot(W),Pkin(W),D↙
(N),Cd,Cl,L/D','',''); %Write first line
end
e=1;

% Aircraft Parameters
m=input('\nInsert the Airplane Mass [Kg]:');                % Aircraft Mass
Sref=input('\Insert the Reference Area of the Airplane [m^2]:');% Ref. Area
G=9.8067;                                          % Gravitational Acceleration
while e<=n

%% ----------------------------TIME INTERVAL--------------------------------
% Interval of Analysis
fprintf('\n--------------------Interval number %d ----------------------\n',e)
e=e+1;

% Time interval of glidings
ti=input('Enter start time of the interval of analysis [seg]:')*10^6;
tf=input('Enter end time of the interval of analysis [seg]:')*10^6;
interval=(tf-ti);

if interval > 0
    fprintf('The interval of analysis has: %d [seconds].\n', interval/(10^6))
else
    fprintf('The interval times are incorrect.\n')
end

%% ----------------------ARRAYS TIME RESIZING-----------------------------
% ----------------------Airspeed array adjustment-------------------------
i=1;
j=1;
while i<=length(Airspd)
if Airspd(i,1)>=ti & Airspd(i,1)<=tf
    New1_Airspd(j,1)= Airspd(i,1);
    New1_Airspd(j,2)= Airspd(i,2);
    i=i+1;
    j=j+1;
else
    i=i+1;
end
end
New1_Airspd;

% ---------------------Groundspeed array adjustment-----------------------
i=1;
```

```
j=1;
while i<=length(Gndspd)
if Gndspd(i,1)>=ti & Gndspd(i,1)<=tf
    New1_Gndspd(j,1)= Gndspd(i,1);
    New1_Gndspd(j,2)= Gndspd(i,2);
    i=i+1;
    j=j+1;
else
    i=i+1;
end
end
New1_Gndspd;

% ---------------------- Pitch array adjustment--------------------------
i=1;
j=1;
while i<=length(Pitch)
if Pitch(i,1)>=ti & Pitch(i,1)<=tf
    New1_Pitch(j,1)= Pitch(i,1);
    New1_Pitch(j,2)= Pitch(i,2);
    i=i+1;
    j=j+1;
else
    i=i+1;
end
end
New1_Pitch;

% ---------------------- Altitude array adjustment-----------------------
i=1;
j=1;
while i<=length(Alt_baro)
if Alt_baro(i,1)>=ti & Alt_baro(i,1)<=tf
    New1_Alt_baro(j,1)= Alt_baro(i,1);
    New1_Alt_baro(j,2)= Alt_baro(i,2);
    i=i+1;
    j=j+1;
else
    i=i+1;
end
end
New1_Alt_baro;

% ---------------------- Pressure array adjustment-----------------------
i=1;
j=1;
while i<=length(Press)
if Press(i,1)>=ti & Press(i,1)<=tf
    New1_Press(j,1)= Press(i,1);
    New1_Press(j,2)= Press(i,2);
    i=i+1;
    j=j+1;
else
    i=i+1;
end
```

```
end
New1_Press;

%% ----------------------ARRAYS INTERPOLATION-----------------------------
N=length(New1_Pitch);                          % Length of the smallest array
ini=max([New1_Airspd(1,1) New1_Gndspd(1,1) New1_Pitch(1,1) New1_Alt_baro(1,1)↙
New1_Press(1,1)]); % First instant time value
fin=min([New1_Airspd(end,1) New1_Gndspd(end,1) New1_Pitch(end,1) New1_Alt_baro(end,1)↙
New1_Press(end,1)]); % Last instant time value
R=1;                                       % Length of the new arrays factor

t = linspace(ini,fin,R*N)';                                % Time array (new)

% Airspd Array
New2_Airspd(:,1)=t(:,1);
New2_Airspd(:,2)=interp1q(New1_Airspd(:,1),New1_Airspd(:,2),t(:,1));
New2_Airspd;

% Gndspd Array
New2_Gndspd(:,1)=t(:,1);
New2_Gndspd(:,2)=interp1q(New1_Gndspd(:,1),New1_Gndspd(:,2),t(:,1));
New2_Gndspd;

% Pitch Array
New2_Pitch(:,1)=t(:,1);
New2_Pitch(:,2)=interp1q(New1_Pitch(:,1),New1_Pitch(:,2),t(:,1));
New2_Pitch;

% Altitude Array
New2_Alt_baro(:,1)=t(:,1);
New2_Alt_baro(:,2)=interp1q(New1_Alt_baro(:,1),New1_Alt_baro(:,2),t(:,1));
New2_Alt_baro;

% Pressure Array
New2_Press(:,1)=t(:,1);
New2_Press(:,2)=interp1q(New1_Press(:,1),New1_Press(:,2),t(:,1));
New2_Press;

%% --------------------CALCULATION OF OTHER ARRAYS-------------------------
% Calculation of Rate of Climb (Altitude variation-Barometer)
i=2;
CR_baro(:,1)=New2_Alt_baro(:,1);
while (i<length(New2_Alt_baro))
    CR_baro(i,2)=(New2_Alt_baro(i+1,2)-New2_Alt_baro(i-1,2))*1000000/((New2_Alt_baro↙
(i+1,1)-New2_Alt_baro(i-1,1)));
    i=i+1;
end
CR_baro;

% Calculation of Acceleration array (Airspeed variation-GPS)
i=2;
AccX_gndspd=New2_Gndspd(:,1);
while (i<length(New2_Gndspd))
    AccX_gndspd(i,2)=(New2_Gndspd(i+1,2)-New2_Gndspd(i-1,2))/((New2_Gndspd(i+1,1)-↙
New2_Gndspd(i-1,1))./1000000);
```

```
    i=i+1;
end
AccX_gndspd;

%% -------------------------FILTERING-----------------------------------
% CR_baro filter
CR_baro_filt(:,1)=CR_baro(:,1);
CR_baro_filt(:,2)=smooth(CR_baro_filt(:,1),CR_baro(:,2),0.5,'loess');

% AccX_gndspd filter
AccX_gndspd_filt(:,1)=AccX_gndspd(:,1);
AccX_gndspd_filt(:,2)=smooth(AccX_gndspd_filt(:,1),AccX_gndspd(:,2),0.5,'loess');

% Gndspd filter
New2_Gndspd_filt(:,1)=New2_Gndspd(:,1);
New2_Gndspd_filt(:,2)=smooth(New2_Gndspd_filt(:,1),New2_Gndspd(:,2),0.5,'loess');

% Airspd filter
New2_Airspd_filt(:,1)=New2_Airspd(:,1);
New2_Airspd_filt(:,2)=smooth(New2_Airspd_filt(:,1),New2_Airspd(:,2),0.5,'loess');

% Pitch filter
New2_Pitch_filt(:,1)=New2_Pitch(:,1);
New2_Pitch_filt(:,2)=smooth(New2_Pitch_filt(:,1),New2_Pitch(:,2),0.5,'loess');

%% Groundspeed correction for Pitch
New3_Gndspd_filt(:,1)=New2_Gndspd_filt(:,1);
New3_Gndspd_filt(:,2)=New2_Gndspd_filt(:,2).*(cos(deg2rad((New2_Pitch_filt(:,2)))));

%% ------------------------ARRAYS OPERATIONS-------------------------------
% Flight Powers Calculations
Ppot=m*G*CR_baro(:,2);                                    % Potential Power
Pkin=diag(m*(New2_Gndspd(:,2)*AccX_gndspd(:,2)'));          % Kinetic Power
Pwrsum=-(Ppot+Pkin);                                      % Sum of Powers

% Others
D=Pwrsum(:,1)./New2_Airspd(:,2);                                  % Drag
rho(:,1) = New2_Press(:,2)./(287.058*(Temperature+273.15));   % Air Density

% Flight Coefficients Calculation
Cd= D(:,1)./(0.5*Sref*rho.*New2_Airspd(:,2).^2);         % Drag Coefficient
Cl_Pitch=(m*G*cos(deg2rad(New2_Pitch(:,2)))).*(0.5*Sref*rho.*New2_Airspd(:,2).^2); %↙
Lift Coefficient

LD_Pitch=Cl_Pitch(:,1)./Cd(:,1);                        % Lift-to-Drag Ratio

%% -------------------OUTPUT VERIFICATION TABLE-----------------------------
Conc=horzcat(t(:,1)./60000000, AccX_gndspd_filt(:,2), New2_Pitch_filt(:,2),↙
New2_Airspd_filt(:,2), New3_Gndspd_filt(:,2), New2_Alt_baro(:,2), rho(:,1),↙
CR_baro_filt(:,2), Ppot, Pkin, D, Cd, Cl_Pitch, LD_Pitch);
uitable('Data', Conc, 'ColumnName', {'time(min)','AccX(m/s2)', 'Pitch(degrees)',↙
'Airspd(m/s)', 'Gndspd(m/s)', 'Altitude BARO(m)', 'Air density', 'CR BARO(m/s)', 'Ppot↙
(W)', 'Pkin(W)', 'Drag(N)', 'Cd', 'Cl_noPitch','L/D_noPitch'}, 'Position', [50 50 1250↙
600]);
```

```
%% ------------------------INTERPOLATION GRAPHS----------------------------
figure
% Altitude-BARO
subplot(2,2,1)
scatter(New1_Alt_baro(:,1)./60000000,New1_Alt_baro(:,2),[],'r')
hold
scatter(New2_Alt_baro(:,1)./60000000,New2_Alt_baro(:,2),[],'g')
xlabel('time (min)');
ylabel('Baro Altitude (m)');
title('Altitude Array Interpolation')
legend('Real Extracted Values','Values from Linear Interpolation')

% Airspeed-ARSP
subplot(2,2,2)
scatter(New1_Airspd(:,1)./60000000,New1_Airspd(:,2),[],'r')
hold
scatter(New2_Airspd(:,1)./60000000,New2_Airspd(:,2),[],'g')
xlabel('time (min)');
ylabel('Airspeed (m/s)');
title('Airspeed Array Interpolation')
legend('Real Extracted Values','Values from Linear Interpolation')

% Pitch-AHR2
subplot(2,2,3)
scatter(New1_Pitch(:,1)./60000000,New1_Pitch(:,2),[],'r')
hold
scatter(New2_Pitch(:,1)./60000000,New2_Pitch(:,2),[],'g')
xlabel('time (min)');
ylabel('Pitch (degrees)');
title('Pitch Array Interpolation')
legend('Real Extracted Values','Values from Linear Interpolation')

% Groundspeed-GPS
subplot(2,2,4)
scatter(New1_Gndspd(:,1)./60000000,New1_Gndspd(:,2),[],'r')
hold
scatter(New2_Gndspd(:,1)./60000000,New2_Gndspd(:,2),[],'g')
xlabel('time (min)');
ylabel('Groundspeed (m/s)');
title('Groundspeed Array Interpolation')
legend('Real Extracted Values','Values from Linear Interpolation')

% --------------------------FILTERING GRAPHS-----------------------------
figure
% Climb Rate
subplot(2,2,1)
plot(CR_baro(:,1)./60000000,CR_baro(:,2),'b-',CR_baro_filt(:,1)./60000,CR_baro_filt(:,↙
2),'r-')
xlabel('time (min)');
ylabel('CR (m/s)');
title('Climb Rate Filtering')
legend('CR Oiginal Data','CR Filtered Data')

% AccX
subplot(2,2,2)
```

```
plot(AccX_gndspd(:,1)./60000000,AccX_gndspd(:,2),'b-',AccX_gndspd_filt(:,1)./60000,↙
AccX_gndspd_filt(:,2),'r-')
xlabel('time (min)');
ylabel('AccX (m/s2)');
title('Acceleration Filtering')
legend('AccX Oiginal Data','AccX Filtered Data')

% Groundspeed
subplot(2,2,3)
plot(New2_Gndspd(:,1)./60000000,New2_Gndspd(:,2),'b-',New2_Gndspd_filt(:,1)./60000,↙
New2_Gndspd_filt(:,2),'r-')
xlabel('time (min)');
ylabel('Ground Speed (m/s)');
title('Ground Speed Filtering')
legend('Gndspd Oiginal Data','Gndspd Filtered Data')

% Airspeed
subplot(2,2,4)
plot(New2_Airspd(:,1)./60000000,New2_Airspd(:,2),'b-',New2_Airspd_filt(:,1)./60000,↙
New2_Airspd_filt(:,2),'r-')
xlabel('time (min)');
ylabel('Airspeed (m/s)');
title('Airspeed Filtering')
legend('Airspeed Oiginal Data','Airspeed Filtered Data')

%% --------------------EXPORT FLIGHT DATA--------------------------------
% Formation of the matrix to be exported (Partial Flight Data)
PFD=horzcat(New2_Airspd_filt(:,2), D, Cd, Cl_Pitch, LD_Pitch);
% Formation of the matrix to be exported (Complete Flight Data)
CFD=horzcat(t(:,1)./60000000, AccX_gndspd_filt(:,2), New2_Airspd_filt(:,2),↙
New2_Gndspd_filt(:,2), New2_Alt_baro(:,2), rho(:,1), CR_baro_filt(:,2), Ppot, Pkin, D,↙
Cd, Cl_Pitch, LD_Pitch);

% User Inputs
Check=input('\nWrite 1 to Export the Results:\nWrite 2 to Skip the Results:\n:');

% Export LD Flight Data
if (R == 1) && (Check == 1)
fileID = fopen('LD_Partial_Flight_Data.txt','a');
dlmwrite('LD_Partial_Flight_Data.txt', PFD, '-append')
elseif (R == 2) && (Check == 1)
fileID = fopen('LD_Complete_Flight_Data.txt','a');
dlmwrite('LD_Partial_Flight_Data.txt', CDF, '-append')
end
clearvars -except e n Airspd Gndspd Pitch Alt_baro Temperature Press R m Sref G
end

if R==1
fprintf('\n Partial Flight Data Exported to "LD_Partial_Flight_Data.txt" \n')
elseif R==2
fprintf('\n Complete Flight Data Exported to "LD_Complete_Flight_Data.txt" \n')
end

%% ------------------------RESULTS ANALYSIS--------------------------------
fprintf('\n--------------------Results Analysis---------------------- \n')
```

```
Q=input('\nPress 1 to analyse the Results:\nPress 2 to Finnish:\n');

if Q==1
clear all

% Temporary file read
filename='LD_Partial_Flight_Data.txt';
Matriz_total=dlmread(filename,',',1,0);
Matriz_total_ordenada = sortrows(Matriz_total,1);

% Variables allocation
Airspd= Matriz_total_ordenada(:,1);
Drag = Matriz_total_ordenada(:,2);
Cd = Matriz_total_ordenada(:,3);
Cl_Pitch = Matriz_total_ordenada(:,4);
LD_Pitch = Matriz_total_ordenada(:,5);
LD32_Pitch = Cl_Pitch.^(3/2)./Cd;

j=1;
dt=0.1;
for i=5:dt:26
row=mean(Matriz_total_ordenada(find(Matriz_total_ordenada(:,1)>=i &↙
Matriz_total_ordenada(:,1)<i+dt),:));
Resultado(j,:) = row;
j=j+1;
end
Resultado(isnan(Resultado(:,1)),:)=[];                    % Remove NaN lines
Resultado=sortrows(Resultado,1);                        % Sorting by airpseed

% --------------------------POLYNOMIAL CURVES-----------------------------
fprintf('\n--------------Flight Coefficient Graphs----------------------')
% Cl vs Cd approximation curve
g=input('\nInsert the polynomial order for the polar Cl vs Cd Curve aproximation:');
p = polyfit(Cl_Pitch,Cd,g) ;
pcurve=polyval(p,Cl_Pitch);

% L/D approximation curve
g=input('\nInsert the polynomial order for the polar L/D Curve aproximation:');
p = polyfit(Airspd,LD_Pitch,g) ;
pcurve1=polyval(p,Airspd);

% L^(3/2)/D approximation curve
g=input('\nInsert the polynomial order for the polar L/D Curve aproximation:');
p = polyfit(Airspd,LD32_Pitch,g) ;
pcurve2=polyval(p,Airspd);

% Airspeed vs D approximation curve
g=input('\nInsert the polynomial order for the polar Airspeed vs Drag Curve↙
aproximation:');
p = polyfit(Airspd,Drag,g) ;
pcurve3=polyval(p,Airspd);

%% ----------------------GRAPHICAL RESULTS -------------------------------
% Aerodynamic Flight Graphs
input('\nPress Enter to see Flight Coefficients Graphs')
```

```
figure
subplot(1,1,1)
scatter(Cl_Pitch,Cd,[],'r');
hold on
plot (Cl_Pitch, pcurve,'b');
hold off
xlabel('Lift Coefficient');
ylabel('Drag Coefficient');
title('Polar Curve');

figure
subplot(1,1,1)
scatter(Airspd,LD_Pitch,[],'r');
hold on
plot (Airspd, pcurve1,'b');
hold off
xlabel('Airspeed');
ylabel('Lift-to-Drag Ratio');
title('Lift-to-Drag Ratio');

figure
subplot(1,1,1)
scatter(Airspd,LD32_Pitch,[],'r');
hold on
plot (Airspd, pcurve2,'b');
hold off
xlabel('Airspeed');
ylabel('Cl^(3/2)/Cd');
title('Airspeed vs Cl^(3/2)/Cd');

figure
subplot(1,1,1)
scatter(Airspd, Drag,[],'r');
hold on
plot (Airspd, pcurve3,'b');
hold off
xlabel('Airspeed (m/s)');
ylabel('Drag (N)');
title('Drag vs Airspeed');

% Statistical Flight Graphs
fprintf('\n--------------Statistical Flight Graphs----------------------')
input('\nPress Enter to see Flight Statistical Graphs')

% Sample size - Graph
j=1;
dt=0.5;
for i=5:dt:26
C=find(Matriz_total_ordenada(:,1)>=i & Matriz_total_ordenada(:,1)<i+dt);
N(j,1)=nnz(C);                                  % Count all non-zero values
j=j+1;
end

% Bar Graph
```

```
X=5:dt:26;
figure
subplot(1,1,1)
bar(X,N,'FaceColor',[0 0.447058823529412 0.741176470588235],'BarWidth',0.7);
xlabel('Airspeed (m/s)');
ylabel('N° of Samples');
title('Number of Samples per Airspeed Value');

%% ----------------------EXPORT FINAL RESULTS-------------------------------
fprintf('\n\n--------------Export Fligth Data Results---------------\n')
R=input('\n Write Y to Export Flight Data Results\n','s');

if strcmp(R,'Y')
dlmwrite('Results.txt', 'Airspeed(m/s),Drag(N),Cd,Cl,L/D','','') %Write first line
dlmwrite('Results.txt', Resultado, '-append')                    %Export table
fprintf('\n Flight Data Exported to "Results.txt" \n')
end

elseif Q==2
input('Press Enter to Finnish')
end
clear all
clc
end
```

```
%==========================================================================
%===              LEEUAV FLIGHT PERFORMANCE ANALYSIS
%===                    - A. Rodrigues, 2016 -
%===
%=== This code reads .txt log files from the Pixhawk flight controller and
%=== calculates the Propulsive System Efficiency based on loiter condition
%=== (Speed variation). For more information about this algorithm see
%=== Chapter 6 and 7.
%==========================================================================

function []=Propulsive_System_Performance_LEEUAV()
clear all
clc
%% ----------------------.TXT FILE LOAD-----------------------------------
% Input .txt file
fprintf('Enter the name of the .txt Log file to analyse.\n')
fileID =-1;
errmsg='';
while fileID<0
    disp(errmsg);
    filename=input ('open file: ', 's');
    [fileID,errmsg]=fopen(filename);
end
% Open .txt file
fileID=fopen(filename);
% Verification step
if(fileID==-1)
    fprintf('ERROR opening the file %s \n',filename)
    return
  else
    fprintf('File opening OK!\n',fileID)
end
%% ------------------------ READ .TXT FILE-------------------------------
% Initialize variables.
delimiter = ',';
% Format string for each line of text:
formatSpec = '%s%f%f%f%f%f%f%f%[^\n\r]';
% Open the text file.
fileID = fopen(filename,'r');
% Read columns of data according to format string.
dataArray = textscan(fileID, formatSpec, 'Delimiter', delimiter,↙
'MultipleDelimsAsOne', true, 'EmptyValue' ,NaN, 'ReturnOnError', false);
% Close the text file.
fclose(fileID);

%% --------------------VARIABLES ALLOCATION-------------------------------
name = dataArray{:, 1};
var2 = dataArray{:, 2};
var3 = dataArray{:, 3};
% Clear temporary variables
clearvars filename delimiter formatSpec fileID dataArray ans;

%% -------------------------ARRAYS FORMATION-----------------------------
fprintf('\n\n-------------------Arrays Formation--------------------------\n')
```

```
%-----------------------------Airspd - ARSP---------------------------------
str1={'ARSP'};
A=strcmp(str1,name);                                        % ARSP Position
P=find(A==1);                                             % ARSP Identification
i=1;
while (1)
   if i<length(P)
    Val_Airspd(i)=var3(P(i));
    time_Airspd(i)=var2(P(i));
 i=i+1;
   else
       break
end
end
Airspd = horzcat(time_Airspd',Val_Airspd');                % Concatenation

%-----------------------------Power - ENE---------------------------------
str1={'ENE'};
A=strcmp(str1,name);                                         % ENE Position
P=find(A==1);                                              % ENE Identification
i=1;
while (1)
   if i<length(P)
    Val_Pwr(i)=var3(P(i));
    time_Pwr(i)=var2(P(i));
 i=i+1;
   else
       break
end
end
Pwr = horzcat(time_Pwr',Val_Pwr');                          % Concatenation

%% ----------------------------USER INPUTS---------------------------------
% Number of Intervals to analyse
n=input('Enter the number of intervals to analyse:');
R=input('\n Write Y to Export Flight Data Results\n','s');
if strcmp(R,'Y')
dlmwrite('Power_Results.txt', 'Airspeed(m/s),Electric Power(W)','','')   %Write first↙
line
end
e=1;
while e<=n
%% ---------------------------TIME INTERVAL---------------------------------
% Interval of analysis
fprintf('Interval number.\n')
disp(e)
e=e+1;
% Loi
ti=input('Enter start time of the interval of analysis [seg]:')*10^6;
tf=input('Enter end time of the interval of analysis [seg]:')*10^6;
interval=(tf-ti);
if interval > 0
    fprintf('The interval of analysis has: %d [minutes].\n', interval/(60*10^6))
else
    fprintf('The interval times are incorrect.\n')
```

```
end

%% ----------------------ARRAYS TIME RESIZING-----------------------------
% ----------------------Airspeed array adjustment-------------------------
i=1;
j=1;
while i<=length(Airspd)
if Airspd(i,1)>=ti & Airspd(i,1)<=tf
    New1_Airspd(j,1)= Airspd(i,1);
    New1_Airspd(j,2)= Airspd(i,2);
    i=i+1;
    j=j+1;
else
    i=i+1;
end
end
New1_Airspd;

% -------------------Electric Power array adjustment--------------------
i=1;
j=1;
while i<=length(Pwr)
if Pwr(i,1)>=ti & Pwr(i,1)<=tf
    New1_Pwr(j,1)= Pwr(i,1);
    New1_Pwr(j,2)= Pwr(i,2);
    i=i+1;
    j=j+1;
else
    i=i+1;
end
end
New1_Pwr;

%% --------------------EXPORT FLIGHT DATA--------------------------------
% Airspeed - Electric Power Matrix
Resultado=horzcat(mean(New1_Airspd(:,2)),mean(New1_Pwr(:,2)))

% Export Flight Power Data Results
fileID = fopen('Power_Results.txt','a');
dlmwrite('Power_Results.txt', Resultado, '-append')
clearvars -except e n Airspd Pwr fileID
end
fclose(fileID);
fprintf('\n Flight Data Exported to "Power_Results.txt" \n')

%% ------------------------ARRAYS OPERATIONS-----------------------------
% Read Power_Results.txt file
fileID=fopen('Power_Results.txt');
delimiter2 = ',';
Results=dlmread('Power_Results.txt',delimiter2, 1, 0); % Variables allocation
Results_ord=sortrows(Results,1);                        % Sort by airspeed

Results_nosystems(:,1)=Results_ord(:,1);
Results_nosystems(:,2)=Results_ord(:,2)-11.7528;     % Remove systems power
```

```
%% ----------------------GRAPHICAL RESULTS -------------------------------
% Airspeed vs Electric Power Graph
% Polynomial Curves
p=polyfit(Results_ord(:,1),Results_ord(:,2),2);
y=polyval(p,Results_ord(:,1));
q=polyfit(Results_nosystems(:,1),Results_nosystems(:,2),2);
z=polyval(q,Results_nosystems(:,1));

figure
subplot(1,1,1)
plot (Results_ord(:,1),y,'r');
hold on
plot (Results_nosystems(:,1),z,'c');
plot(A,y(B),'r*');
scatter(Results_ord(:,1),Results_ord(:,2),[],'b');
scatter(Results_nosystems(:,1),Results_nosystems(:,2),[],'g');
line([A A], [0 Results_ord(B,2)],'Color',[1 1 0]);
hold off
xlabel('Airspeed (m/s)');
ylabel('Electric Power (W)');
title('Airspeed vs Electric Power');
legend('Electric Power With Systems','Electric Power Without Systems')

%% Converting to h/MJ
Pwrcs=1./(Results_ord(:,2)*3600/1000000);  % h/MJ (with systems)
Pwrss=1./(Results_nosystems(:,2)*3600/1000000); % h/MJ (without systems)

% Polynomial Curves
p=polyfit(Airspd,Pwrcs,3);
pcurve5=polyval(p,Airspd);
q=polyfit(Airspd,Pwrss,3);
pcurve6=polyval(q,Airspd);

figure
subplot(1,1,1)
plot (Airspd,pcurve5,'r');
hold on
plot (Airspd,pcurve6,'b');
hold on
scatter(Airspd,Pwrcs,[],'r');
hold on
scatter(Airspd,Pwrss,[],'b');
hold off
xlabel('Airspeed (m/s)');
ylabel('Specific Endurance (h/MJ)');
title('Airspeed vs Specific Endurance');
legend('Time spent per MJ consumed - With Systems','Time spent per MJ consumed -↙
Without Systems');

%% Airspeed vs Electric Power/Airspeed Graph
Results_ord2(:,1)=Results_ord(:,1);
Results_ord2(:,2)=Results_ord(:,2)./Results_ord(:,1);
Results_nosystems2(:,1)=Results_nosystems(:,1);
Results_nosystems2(:,2)=Results_nosystems(:,2)./Results_nosystems(:,1);
```

```
% Polynomial Curves
p=polyfit(Results_ord2(:,1),Results_ord2(:,2),2);
y=polyval(p,Results_ord2(:,1));
q=polyfit(Results_nosystems2(:,1),Results_nosystems2(:,2),2);
z=polyval(q,Results_nosystems2(:,1));

figure
subplot(1,1,1)
plot (Results_ord2(:,1),y,'r');
hold on
plot (Results_nosystems2(:,1),z,'c');
plot(A,y(B),'r*');
scatter(Results_ord2(:,1),Results_ord2(:,2),[],'b');
scatter(Results_nosystems2(:,1),Results_nosystems2(:,2),[],'g');
line([A A], [0 Results_ord2(B,2)],'Color',[1 1 0]);
hold off
xlabel('Airspeed (m/s)');
ylabel('Electric Power/Airpseed');
title('Airspeed vs Electric Power/Airspeed');
legend('Electric Power/Airspeed With Systems','Electric Power/Airspeed Without↙
Systems','Maximum Range Point')


%% Converting to km/kJ
PwrVcs=1./(PwrVcs*1000/1000); % km/kJ - with systems
PwrVss=1./(PwrVss*1000/1000); % km/kJ - without systems

% Polynomial Curves
p=polyfit(Airspd,PwrVcs,3);
pcurve7=polyval(p,Airspd);
q=polyfit(Airspd,PwrVss,3);
pcurve8=polyval(q,Airspd);

figure
subplot(1,1,1)
plot (Airspd,pcurve7,'r');
hold on
plot (Airspd,pcurve8,'b');
hold on
scatter(Airspd,PwrVcs,[],'r');
hold on
scatter(Airspd,PwrVss,[],'b');
hold off
xlabel('Airspeed (m/s)');
ylabel('Specific Range (km/kJ)');
title('Airspeed vs Specific Range');
legend('Travelled Distance per kJ - With Systems','Travelled Distance per kJ - Without↙
Systems');

%% ----------------PROPULSIVE SYSTEM EFFICIENCY----------------------------
% Read .txt file
fileID = fopen(filename,'r');
Matrix=dlmread(filename,delimiter, 1, 0);

% Variables Allocation
```

```
Airspd=Matrix(:,1);
Preq=Matrix(:,5);
Pe=Matrix(:,6);
Div=Preq./Pe;

i=1;
for j=1:5:length(Preq)
   Preq1(i,1)=Preq(j,1);
   Airspd1(i,1)=Airspd(j,1);
   Pe1(i,1)=Pe(j,1);
   Div1(i,1)=Div(j,1);
   i=i+1;
end

% Airspeed vs Pe and Preq Graph
figure
subplot(1,1,1)
plot (Airspd,Preq,'r');
hold on
plot (Airspd,Pe,'b');
hold on
scatter(Airspd1,Preq1,[],'b');
scatter(Airspd1,Pe1,[],'b');
hold off
xlabel('Airspeed (m/s)');
ylabel('Power');
title('Airspeed vs Power');
legend('Required Aerodynamic Power','Required Electric Power');

% Airspeed vs Propulsive System Efficiency Graph
figure
subplot(1,1,1)
plot (Airspd,Div,'r');
hold on
scatter(Airspd1,Div1,[],'b');
hold off
xlabel('Airspeed (m/s)');
ylabel('Propulsive System Efficiency');
title('Airspeed vs Propulsive System Efficiency');

clear all
end
```

Annex D

Article

Airframe Assembly, Systems Integration and Flight Testing of a Long Endurance Electric UAV

UNIVERSIDADE
BEIRA INTERIOR

Airframe Assembly, Systems Integration and Flight Testing of a Long Endurance Electric UAV

Afonso Rodrigues

Department of Aerospace Sciences, Universidade da Beira Interior. 6201-001 Covilhã. Portugal

Abstract

Following current trends towards UAV innovative designs, LEEUAV, a prototype of 4.5 meters' wingspan and ultralight structure partially covered by solar cells was designed to fulfil a continuous flight mission of at least 8 hours at the equinox. The present paper aims to synthetize the main steps of the assembly, systems integration and flight testing procedures. In order to validate the LEEUAV's airworthiness concept several flight tests were performed and their respective data (static and total pressure, air temperature, ground speed and pitch angle) was collected for further analysis, using a flight controller with multiple sensors on board. The results obtained allowed to study the general performance of the aircraft, the main defects, agreement with the theoretical results as well as perform an aerodynamic analysis, through a reading and processing flight data algorithm in MATLAB software.

Keywords

Solar UAV, Solar Energy, Sustainable Flight, LEEUAV, Aeronautical Industry, Photovoltaic Cells, Electric Propulsion, Concepts Validation, Aerodynamic Performance.

1 Introduction

The demand for more efficient means of transport is an increasingly widespread reality due to the need to preserve the environment for the sustainability of future generations. It is known that the long-term consumption of energy derived from fossil fuels will become unsustainable.

Presently, the highly dependence of fossil fuels is being reduced through the application of other more sustainable ways, as is the case of electric propulsion. Regarding the aviation market, the electric propulsion technology is currently under development since the existing state-of-the-art batteries are still not enough to power a manned aircraft for a decent period of time.

However, since 1957[1] that the electric propulsion has been used in unmanned aircraft vehicles (UAV) but always with low flight endurance results. The ability for an aircraft to fly during an extended period of time has become a key issue and a target of research all over the world. At the present, external sources of power are required to reach such flight endurance, using for example solar powered platforms or refuelling the aircraft.

Using photovoltaic modules to collect energy from the sun, during the day time, allows solar aircraft to use part of the energy to fly and store the surplus of energy for the night flight[2].

Using cutting-edge technology some recently solar powered airplanes are being designed to fly near space, i.e., above the common atmospheric flight region and below the spacecraft flight region (approximately 20–100 km)[3]. Future solar UAVs projects claim they will be able to fly continuously for months, or even years, depending on the reliability of the airplane system and sunlight conditions, which is impossible for traditional, fossil-fuelled airplanes. Solar-powered airplanes can function as complement to low-altitude satellites, with the advantage of having a relatively low altitude, free deployment, high resolution, high frequency of coverage, and low cost.

Both manned and unmanned aviation are taking an increasingly important place in our society, meeting the needs of civilian and military areas. In the future, we will see applications of UAVs in areas of agriculture, inspection, security, marketing, emergency, business, science and transport[4].

LEEUAV was decided on a consortium meeting of Aeronautics and Space of Associated Laboratory for Energy, Transports and Aeronautics (LAETA)[5], having in mind the ultimate goal of creating a vehicle capable of flying for at least 8 hours at the equinox with low power requirements and carrying a payload of up to 1kg. The mission profile also requires a short take-off and landing distance, high

flight altitude (at least 1000 meters) and a descent without power.

This work follows the need to search, test and validate new techniques and practices in aviation area such as the use of solar energy in UAVs. Aiming to validate the concept of an unmanned airplane that gets most of its energy from solar irradiance, the main goals are: learn about the concepts inherent of unmanned solar flight aircraft; Finnish the LEEUAV airframe and systems integration; Plan LEEUAV missions; Perform flight and ground tests; Analyse LEEUAV's aerodynamic performance; Compare the theoretical results with practical results; Draw conclusions about results achieved.

2 LEEUAV Characteristics

The final stages of the multidisciplinary preliminary design of LEEUAV prototype, have resulted in a built-up monoplane aircraft with high wing configuration, without wings supports and large aspect ratio, without wing sweep nor dihedral. Regarding the airframe, the fuselage is fully made of carbon fibre reinforced with some plywood internal supports, the wing is constituted by three panels, one at the centre with constant chord and two tapered panels at the outward tips. Both the fuselage and wing are covered with heat shrink film. The outward panels of the wing have 4.5 degrees of negative twist and an endplate to prevent wing tip stall during tight turns of the aircraft.

The LEEUAV has a conventional tail configuration, with the horizontal stabilizer distanced from the vertical, to facilitate the spin recovery. The rudder and elevator are made of balsa also covered by heat shrink film. The propulsive system configuration is pusher and has a single electric motor attached to the folding propeller that is located at the front of the aircraft. Despite not having a landing gear, for take-off the LEEUAV uses a small ground bogey with wheels to facilitate land manoeuvres.

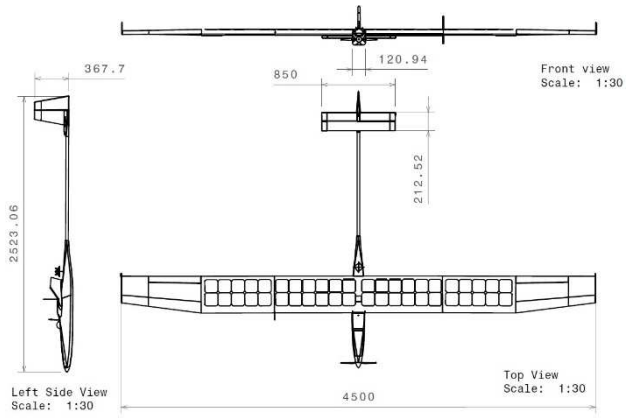

Figure 1 - 3D Drawing views of LEEUAV

From previous works[6-10] the final design and main specifications of the LEEUAV are presented in table 1 and the three drawing views are below in figure 1.

Table 1 - LEEUAV prototype final design specifications

Dimensions	Wingspan [m]	4.525	Weights	Empty weight [N]	47.118
	Length [m]	2.557		MTOW [N]	54.129
	Height [m]	0.334		Payload* [N]	9.81
	Mean chord [m]	0.330		Structure weight [N]	47.533
	Wing root chord [m]	0.350	Performance	Take-off distance [m]	8.100
	Wing tip chord [m]	0.250		Endurance* [h]	8
	Wing area [m^2]	1.490		Maximum speed [m/s]	21.10
	Aspect Ratio [AR]	13.50		Stall speed [m/s]	6.94

3 Systems Integration

The LEEUAV is an integrated unmanned aerial system (UAS) which can be subdivided into multiple subsystems according to their functionality. From a macroscopic point of view, these subsystems may be grouped in two main categories:

- Ground control station (GCS): It is a land control centre where the aircraft is controlled and monitored during its flight, where all the flight information about aircraft attitude, on-board sensors and video stream is directed;
- Aircraft: It is a flying device which carries all the components for the desired mission, including all sensors for data recording and antennas for data streaming to the GCS. It also has an on-board FPV system to allow flight out of line of sight.

In order to comply with the mission requirements, LEEUAV has a set of on-board equipment that allows to fly it safely and autonomously. Moreover, the auto-flight navigation system has several sensors including accelerometer, gyroscopes, airspeed, compass and barometer which were used to analyse the LEEUAV's aerodynamic performance.

Starting with the flight control system, a Pixhawk autonomous flight controller from 3D Robotics[15] was chose. The open source firmware, optional hardware, lightweight and versatility are some of the features of this device. The servomotors used to control the ailerons, rudder and elevator are

connected to the Pixhawk's rail which in turn is connected to a dedicated power supply (universal battery elimination circuit) providing a stable 5V of output. To power up Pixhawk's internal circuits a dedicated power module from 3D Robotics was connected between the Li-Po battery and Pixhawk.

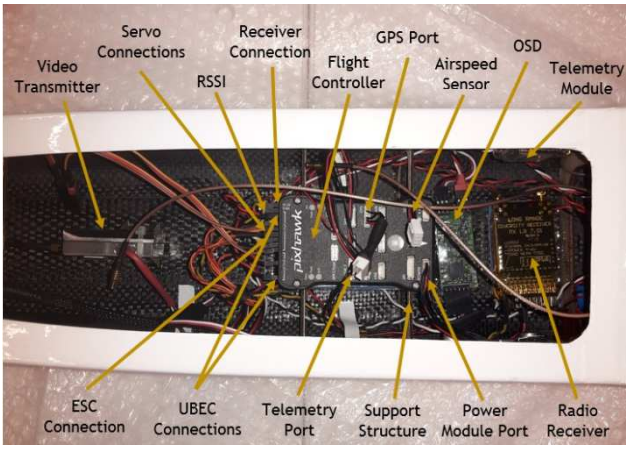

Figure 2 - LEEUAV flight controller connections

Regarding the communication system, this is composed by three independent systems, the first-person view (FPV), telemetry and radio control system. The FPV system intends to simulate the human presence inside the aircraft using an on-board video camera and a transmitter module to stream the video image to the GCS. The FPV system wiring includes a connection between the video camera and an on-screen display (OSD) circuit board, the last has the function to superimpose the aircraft sensor's data (altitude, airspeed, home distance, radio signal strength, coordinates, battery voltage and current consumption) in the video image. For the OSD gets the flight information it also need to be connected with one of the flight controller output telemetry ports. The OSD output is after connected to the video transmitter which is also connected to a step-up/down circuit board whose function is to provide a stable voltage of 12V.

The telemetry consists of stream the flight controller state and on-board sensor's information to a laptop on GCS through a dedicated 2.4GHz communication protocol. The physical disposal of the telemetry components is simply constituted by a telemetry transceiver module connected to the telemetry port on the flight controller. To receive the input commands of the GCS, inside the aircraft there is a Scherrer RX700LR V7[16] receiver with dual diversity antenna system connected to the flight controller RC port, using PPM signals.

In the GCS, a LCD without blue screen function is connected to a video diversity controller which in turn is connected with two video transmitting antennas, one omnidireccional (skew planar wheel radial antenna) for low range and one directional helical antenna for long range. The telemetry is received with a patch antenna directly connected to the laptop using Mission Planner software created by Michael Oborne[17]. To control de aircraft in manual mode or to change flight control parameters in flight a 12-channel Royal SX transmitter from Multiplex[18], connected to an external module (Tx700 PRO Long Range[16]) operating at a frequency of 433MHz and amplifying the signal, was used.

With respect to the navigation system which includes the GPS (Ublox NEO-M8N from Drotek[19]) and an airspeed sensor from 3D Robotics, they were both connected to the Pixhawk respective ports, as depicted in figure 2. The GPS was placed in the upper side of the wing in order to avoid carbon fibre interferences and the airspeed sensor was positioned on the leading edge of the right wing so that is not disturbed by the propeller's airflow.

The propulsion system is responsible to provide thrust leading the energy stored in the battery to the electric motor. In Luís Cândido work [7] suitable propulsion system for LEEUAV was designed and proposed, this propulsion system comprises an 75A electronic speed controller (from castle creations[20]) connected to an 1150W ZS 3025-10 electric motor (from Hyperion[21]) which in turn is connected with a 16x8 inches folding propeller. The ESC is also connected with the flight controller and the aircraft's battery.

Figure 3 - LEEUAV solar panel fixation method

Lastly, to power all the on-board devices there is an electric system made up of a 10000mAh 3-cells lithium-ion battery, 44 C60 solar cells from Sunpower[22], a current sensor to measure the incoming solar energy and a lightweight solar charge controller from Genasun[23] to properly adjust the solar panels' output voltage to charge the battery. The integration of the solar cells onto the wing was made with a double-sided adhesive tape between the solar cells and the wings' heat shrink film, to smooth the edges of the solar panels a transparent adhesive tape was used (figure 3). Once fixated, the solar panels output cable was connected to the SCC and after connected to the current sensor which in turn charges the battery.

4 Flight Testing

With regard to the LEEUAV's mission goals and performance analysis, several flight tests were performed in Castelo Branco aerodrome and Terlamonte airstrip (Portugal). The ultimate goals established at Aeronautics and Space of Associated Laboratory for Energy, Transports and Aeronautics (LAETA) consortium meeting have resulted:

- Take-off in a very short distance (8 m) or Launched by hand (3 m);
- Climb to 1000 m above ground level for a cruise altitude, in 10 minutes;
- Sustainable-flight of 8 hours at equinox with a flight cruise speed (>7 m/s);
- Descend from cruise altitude during 29 minutes to ground level without power;
- Landing in the field.

The 1kg of payload allows LEEUAV the ability to carry different on-board sensors, cameras, probes, among other data recording systems to perform different missions during the cruise flight phase.

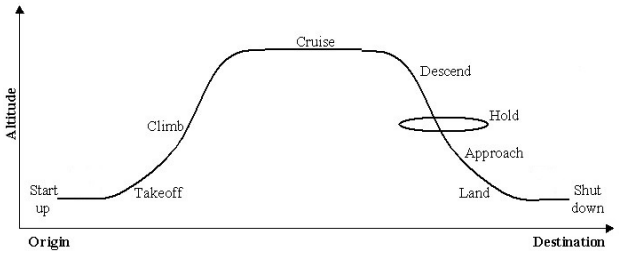

Figure 4 - LEEUAV typical mission profile

As depicted in figure 4, the LEEUAV's mission profile comprises 5 main phases. On take-off, the aircraft leaves the ground and starts to climb to the cruise altitude, where it stands for the most part of the mission time, when the battery's power is low it starts to descent to the approach altitude and lands.

Before defining the flight tests for performance analysis, it is vital to highlight the importance of the ground tests performed before each flight. Hazards found during the first flights such as Inconsistent telemetry data display, ESC power oscillations, lack of tail boom bolt, etc. have forced to create a before-flight checklist that includes all the ground tests to be performed. Some examples are: check the control surface arms and servos, the flight controller modes, the airframe damages, solar panels and antennas fixation, propulsion and communication systems operability and centre of gravity positioning. Three other highly relevant aspects taken into account during the flight tests were the wind speed, solar irradiation level (for solar flight purposes) and safety procedures such as the flight inside a clean airspace away from urban spaces. The maximum wind speed permitted to safely flight the aircraft must not be higher than 15km/h.

Regarding the flight controller programing and flight data retrieval, a fixed-wing aircraft firmware and a several aircraft parameters were loaded and configurated, namely, minimum and maximum rate of climb, throttle setting, airspeed, altitude, pitch, yaw, roll angles and rates. Other parameters related to the mission were also configurated, such as cruise speed, altitude, return-to-home (RTL) altitude, loiter radius and flight modes (manual, fly-by-wire, auto, RTL).

To retrieve the flight data from the flight controller an open source software (Mission Planner) was used. The information contained in a flight log is vast, requiring an after-flight screening for particular analysis.

Figure 5 - LEEUAV during the flight test campaign

A total of 9 flights experiments were realized summing more than 10.4 hours in air. The flights took place at Castelo Branco aerodrome and in Terlamonte (Covilhã) aisptrip in Portugal, each one of them with different purposes.

This first flight was very important and the most critical, once that the integrity and stability of the aircraft was tested for the first time. The ability for circuit manoeuvres (pitch, roll and yaw) was the second goal. As soon as the LEEUAV's airworthiness was proved the performance flight tests for concept validation were done. The most important tests to validate the aircraft comprises the integrity, balance, trimming, manoeuvres, systems operability, flight performance, autonomous flight, take-off and landing qualities and of course the main goal of this work the maximum endurance. In table 2 are some of the flight tests and its goals.

Table 2 - LEEUAV's flight tests goals

Test No.	Flight Pattern	Goals
A-1	Visual	Integrity, trimming, balance, circuit manoeuvres, wind gust effects and take-off/landing qualities
A-2	FPV	Auto-tune and Systems Operability
A-3	FPV	Autonomous flight
A-4 **A-5**	FPV	Flight Performance (Aerodynamics)
A-6	FPV	Flight Performance (Power)
A-7	FPV	Range and Endurance

Despite the numerous flight performance areas suitable to be evaluated and due to the reduced time available, it was decided to conduct the study to obtain the most important performance indicators of an aircraft, the aerodynamics coefficients and required power for level flight.

So, this section aims to determine the practical lift-to-drag ratio or aerodynamic efficiency (L/D) of the LEEUAV based on the retrieved flight data from the on-board sensors. Although existing other methods for aerodynamic performance analysis, the Mechanical Energy Method was adopted[11,12].

Considering a steady-state gliding flight condition, where the forces acting in the airplane are only lift (L), drag (D) and weight (W) and considering the aircraft as a dissipative mechanical system, where the main energy variations are potential (E_{pot}), kinetic (E_{kin}) and dissipative (E_{Dis}).

$$E_{pot} = mgh \tag{1}$$

$$E_{kin} = \frac{1}{2}mv^2 \tag{2}$$

$$E_{Dis} = \int Dv\,dt \tag{3}$$

Knowing that power is an energy variation along time and converting for the specific case of an aircraft:

$$P_{pot} = \frac{d}{dt}(E_{pot}) = \frac{d}{dt}(mgh) = mg\frac{d(h)}{dt} = mgRC \tag{4}$$

$$P_{kin} = \frac{d}{dt}(E_{kin}) = \frac{d}{dt}\left(\frac{1}{2}m{v_G}^2\right) = \frac{1}{2}m2v_G\dot{v_G} = mv_Ga_G \tag{5}$$

$$P_{Dis} = \frac{d}{dt}(E_{Dis}) = \frac{d}{dt}(Dv_{Air}dt) = Dv_{Air} \tag{6}$$

Whereas there are not any other force acting in the aircraft, the sum of the three powers above is zero, and the drag force can be calculated for a given airspeed.

$$P_{potencial} + P_{kinetic} - P_{Dissipative} = 0 \tag{7}$$

$$mgRC + mv_Ga_G - Dv_{Air} = 0 \tag{8}$$

$$D = \frac{mgRC + mv_Ga_G}{v_{Air}} \tag{9}$$

So that the Mechanical Energy Method can be applied the LEEUAV has to fly in a pre-determined pattern without using motor (gliding). To correctly determine the LEEUAV's drag force and considering the theoretical safe airspeed range (6-25m/s)[7], several gliding flights with different airspeeds were performed. The flight mission pattern consists of climbing to a pre-determined altitude (300-500m), apply a suitable trim to achieve the desired airspeed and set the throttle level to zero, gliding the aircraft during a period of time not less than 60 seconds. The process was repeated at least 3 times for each gliding speed in order to minimize the sensors errors and wind disturbances.

Different methods like Prop-Feathered Sinks, Glide Polars and Speed-Power methods[11,12] could also be used to calculate the lift-to-drag ratio, but they require to know the propeller characteristic curves (Ct vs J or Cp vs J or eta vs J) or the decomposition of true airspeed vector in its components (u,v,w), which further requires an Alpha-Beta sensor probe.

To apply the Mechanical Energy Method described above using the retrieved information of the on-board sensors a MATLAB algorithm was created. This algorithm loads the flight controller log file and screens the desired flight data for performance analysis, after it allocates the flight data in arrays, the information is filtered and interpolated, posteriorly with some user inputs of the aircraft specifications (weight, reference area, etc.) the graphical results are shown.

5 Results

The first flight took place in Castelo Branco aerodrome on 18th July of 2016 and LEEUAV's flight performance was qualitatively in line with the predictions and requirements of the project. The integrity of the low-speed LEEUAV's flight was in accordance with the requirements. All the fixations and fittings, including wing bolts for wing-fuselage attachment, tail boom fixation bolt and groove, tail support, wing outer panels - central panels connections and motor support prove to be adequate and reliable to ensure a safe and good flight. The

trimming was firstly adjusted on ground by visual alignment of the control surfaces with fixed surfaces and after during a straight level flight.

Regarding balance, during the pre-flight tests, 465g of small weights were applied near the nose of the fuselage ensuring a C.G. position between 20-22% of the wing chord. Unfortunately, this is not a desired solution, once it is carrying more weight and thus reducing the available payload.

Despite the LEEUAV good results with regard to the integrity, the manoeuvrability was not so good. Due to the large aspect ratio of the wing and the small area of the ailerons the roll movement was very limited specially at low speeds, something that had already been detected in previous flight tests of the current wing. Both pitch and yaw movements were considered suitable for this type of aircraft.

At the end of the flight a malfunction on the ESC was detected which force to land the aircraft. After some analysis, it was concluded that ESC had overheated during that hot summer day flight and the solution adopted was to replace the ESC with a better one.

At the same place, on 28th July, the second flight test, intended to perform more flight manoeuvres capabilities and systems operations, was not successful. A severe hazard related with the aircraft assembly was detected when the aircraft was already flying. Since the structural integrity of LEEUAV was in doubt, the landing was forced. In turn, this emergency landing caused a LEEUAV nose crash and some other broken structures in the wings and tail.

After repairing the LEEUAV broken structures, the A-2 flight (on 9th November) started with an auto-tune flight. As soon as the flight controller was configured, systems operability tests were started.

This second part of the A-2 flight allowed to check all systems operability, namely the control, FPV and telemetry systems. This high relevance flight, allowed to detect some unexpected configuration aspects through some flight hazards such as spatial disorientation and inconsistent telemetry data display.

With the auto-tune done, LEEUAV was ready to perform an autonomous flight. In Terlamonte on 12th November, a pre-set 45min flight plan, established by several waypoints with different altitudes, positions as well as airspeed variations was loaded into the Pixhawk. This flight was also an opportunity to check and correct some pre-defined parameters such as loiter radius, minimum and maximum flight speeds, maximum pitch, roll and yaw angles, maximum line of sight distance, RTL behaviour and climb/descent rates.

Regarding the results, the loiter radius should not be smaller than 200m; the flight envelope speeds must in the range [7,20]m/s; the maximum pitch, roll and yaw angles were well predefined, and their values were [-20º,+20º], [-35º,+35º] and [-20º,+20º] respectively; the maximum line of sight distance is 800m in a clear weather day; the RTL parameters should be 200m for the radius and 8m/s of airspeed; the climb/descent rates are limited by the throttle setting which cannot exceed the 60A of current defined by the motor producer and the maximum aircraft speed 20m/s regarding the descent rate.

On 11th, 12th and 17th of November the aerodynamic tests of the non-solar version of LEEUAV were performed. Despite the calm weather, different days have different weather conditions, so these flights allow to minimize the sensor errors (temperature/wind). Regarding the sample size, in figure 6 is shown the total acceptable values of each 0.5m/s airspeed interval of points analysed. Concerning the non-solar version, the airspeed confidence intervals are [6.5,7], [8.5,10], [11,11.5] and [12,15] where it is possible to assure more accurate results for the graphs of figures 7, 8, 9 and 10. The airspeed range of more confidence is by far the [8.5,10] in which there is a mean value of 1750 points per 0.5m/s airspeed interval.

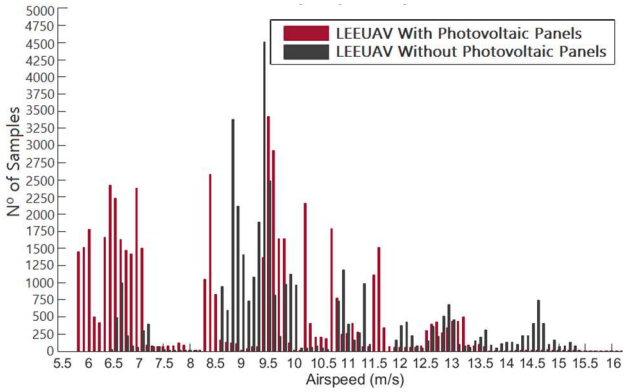

Figure 6 - Number of acceptable points per airspeed value

On the other hand, on 24th of November the 3-hour LEEUAV flight (with photovoltaic panels) have resulted in 22 acceptable gildings, where the more confidence intervals are [6,7], [8.5,9], [9.5,10] and [10.5,13]. The most reliable airspeed interval is [6,7] (mean value of 1500 points), so more accuracy in the results for these airspeeds is expected.

In MATLAB, after loading each flight log file and resizing the arrays to the time intervals of each glide, applying equation 9, it was possible to relate the drag value for each 0.1m/s airspeed interval.

The smallest value of drag obtained was 2.59N and occurs at the minimum tested airspeed of 6.60m/s for LEEUAV without photovoltaic panels. Conversely, for LEEUAV with photovoltaic panels

installed the average drag value increases 0.95N, confirming the expectations, the minimum drag value obtained was 3.54N for an airspeed of 6.88m/s.

Having the drag values for each airspeed and considering: $D = \frac{1}{2}\rho V^2 S C_D$ it was possible to determine the correspondent drag coefficients (C_D) values. In order to obtain the drag polar for this aircraft, the lift coefficient (C_L) for each tested airspeed was calculated: $C_L = W/\left(\frac{1}{2}\rho V^2 S\right)$

The air density (ρ) values used to calculate the aerodynamic coefficients have considered the day temperature and static air pressure recorded by the flight controller, during the flight time.

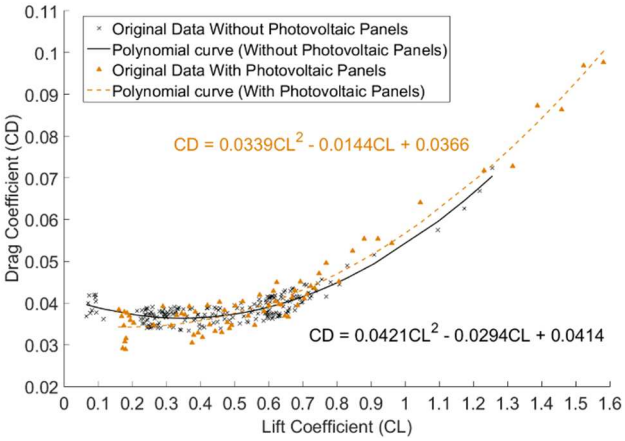

Figure 7 - LEEUAV with and without solar panel drag polar

The second-degree polynomial approximation curves for each polar of the figure 7 allowed to determine the values of the lift and drag coefficients for tested airspeeds. In turn, it was possible to obtain the lift-to-drag ratio (C_L/C_D) and the endurance-airspeed ($C_L{}^{3/2}/C_D$) curves.

The lift-to-drag ratio curve allows to find the airspeed for best range from an aerodynamic point of view, i.e., without considering the propulsive system.

In figure 8 is shown the (C_L/C_D) curve for LEEUAV with and without photovoltaic panels respectively. As expected, there is a reduction in the L/D curve after the panels had been applied, this fact is related with the step created on the upper surface caused by the solar cells fixation on the wing and the additional drag caused by the photovoltaic panels wiring connections and soldering points.

The setback of placing solar cells on the upper surface of an airplane wing, since the solar cells have a finite thickness, is that, they create a localized thickening or an offset in the airfoil, with a forward-facing step (FFS) at the beginning of the solar cell array and a backward-facing step (BFS) at its end. These steps cause separation of the flow: in the FFS flow, two regions of separation occur, one upstream and one downstream, and in the BFS flow, one separated region develops downstream of the step. The first flow separation, upstream the FFS, does not generate a significant amount of turbulence, but in the separation after the sharp corner of the FFS results in a significant increase of turbulence. Flow separation after the BFS also generates high turbulence levels, yet lower than those generated after the FFS[13].

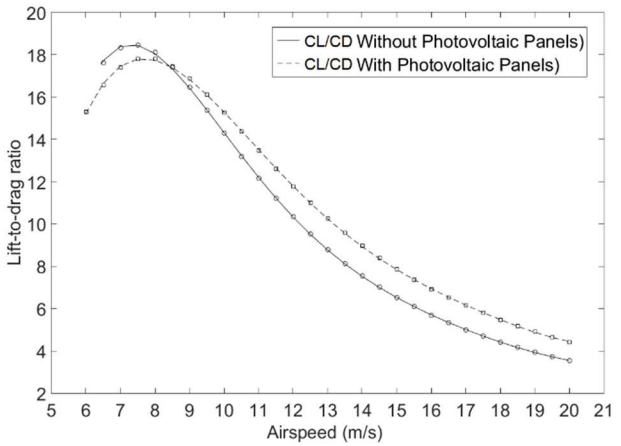

Figure 8 - Lift-to-drag ratio of LEEUAV (with and without photovoltaic panels)

Without photovoltaic panels, the LEEUAV maximum aerodynamic efficiency is 18.45 and occurs at 7.4m/s. After applying the photovoltaic cells, the aerodynamic efficiency decreases 1.02 for a value of 17.43 and it is achieved at 7.8m/s.

Another important fact is the shift of the lift-to-drag ratio curve which increments the best gliding range airspeed from 7.4 to 7.8m/s. This 0.4m/s shift is related with the increased weight (+0.720kg) of the aircraft after applying the photovoltaic system.

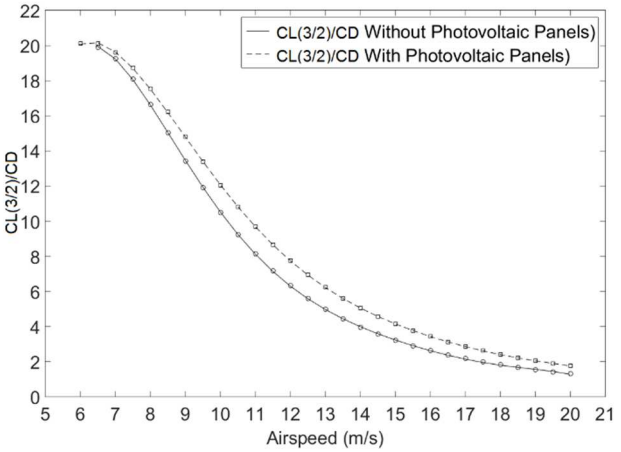

Figure 9 - $C_L{}^{(3/2)}/C_D$ vs Airspeed of LEEUAV (with and without photovoltaic panels)

As depicted in figure 9, the best airspeed which maximizes non-powered flight endurance occurs on

the minimum tested airspeed, near the stall and for both of the LEEUAV versions (with and without solar panels). For LEEUAV without photovoltaic panels the best endurance airspeed is 6.60m/s and for the solar version is 5.99m/s. Although the airspeeds below 6.5m/s of non-solar version were not tested, the best endurance airspeed is clearly under this value, however it would be dangerous to test it.

The LEEUAV performance analysed so far only considered an aerodynamic point of view, i.e., without considering the propulsive system. To analyse the LEEUAV propulsive system efficiency, an on-board power meter sensor was used. The PM stays between the battery and on-board components, calculating the amount of electric power that the aircraft is consuming by measuring current and voltage.

When the throttle is set to zero it is possible to know the electric energy required for systems operation, which has the average value of 11.75W.

In order to plot the electric power required for each airspeed, A-6 autonomous flight was done. This flight was composed by 300m radius circular flight path varying the flight speed from 7 to 15m/s with an increment of 0.5m/s. To reduce the wind disturbances, for each analysed airspeed there were performed two complete loiter circles, with an average value of 2.86 minutes each.

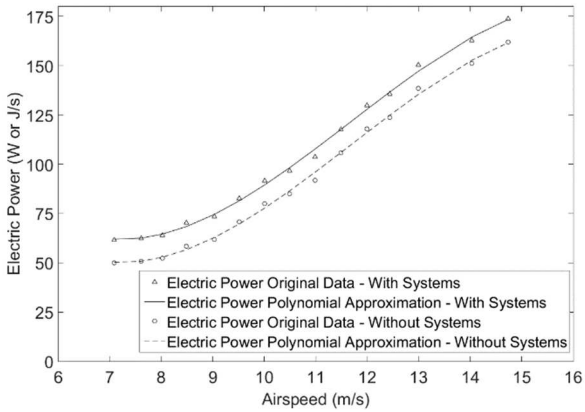

Figure 10 - Electric Power(with and without systems) vs Airspeed

In figure 10 is plotted the electric power curve for LEEUAV with photovoltaic panels. Each point is the average value of the electrical power consumed for each airspeed tested. The lowest power consumption has the value of 61.65W and occurs in the lowest airspeed tested of 7.09m/s, being this the best airspeed for maximum endurance. Removing the systems contribution, the minimum electric power required for the same airspeed is 49.90W. It is noteworthy the significant increase in the required electrical power for airspeeds superior than 8.5m/s.

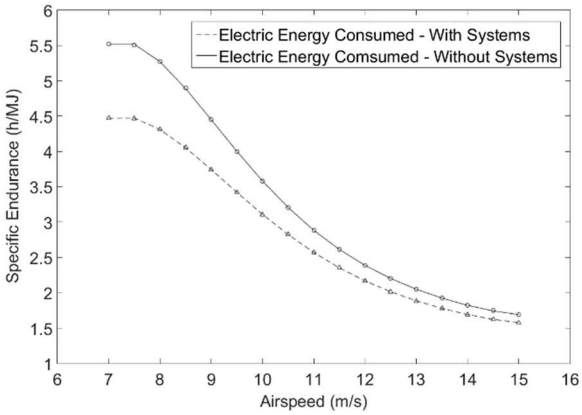

Figure 11 - Specific Endurance vs Airspeed

Converting the electric energy consumed per second (J/s) to hour (h/MJ), it allows to determine how many hours the LEEUAV flies per MJ consumed. According to figure 11 the airspeed that maximizes the flight time per MJ consumed is 7m/s. Another important characteristic to highlight is the decreased distance between the two curves along the airspeed. This fact is explained by the increasing difference between the power used by the propulsive system and the power of the systems with the increasing airspeed. If there were no systems on-board, at the lowest airspeed, the LEEUAV would be able to fly one more hour for the same MJ of energy.

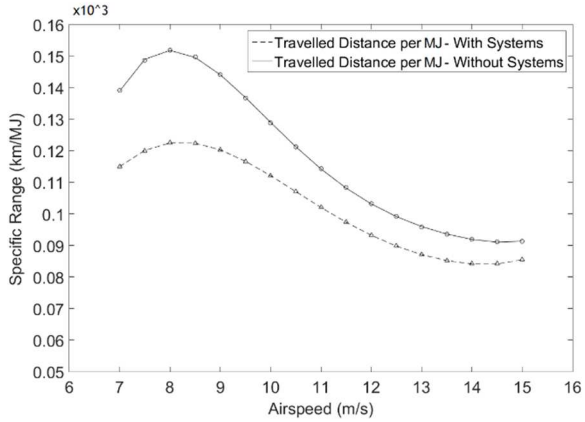

Figure 12 - Specific Range vs Airspeed

Dividing the electric power by the correspondent airspeed value and converting it to (km/kJ) it was possible to obtain the specific range where the distance travelled for each MJ of energy consumed is 150km at 8m/s.

It is also relevant to compare the required power (P_{req}), from the aerodynamic point of view, with the required electric power (P_e), from propulsive system point of view. In figure 13 is plotted the electric power (without systems) and the required power from the drag force times the airspeed (equation 6) for the solar powered UAV.

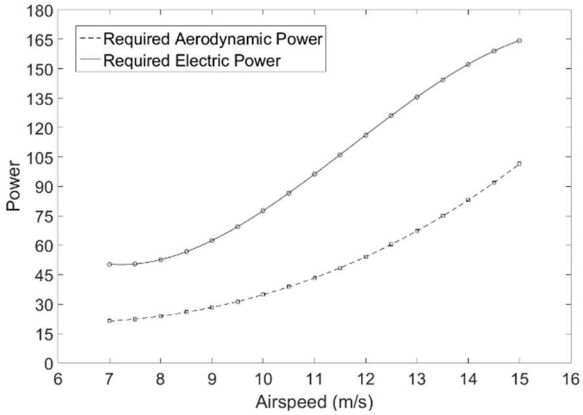

Figure 13 - Electric and Required Power vs Airspeed

The P_{req} curve shows the required power to fly in a cruise condition, where thrust equals the LEEUAV drag force. The P_e is the electric power withdrawn from the battery to the propulsive system and it is always higher than the required power, which is in accordance with the results shown in figure 13.

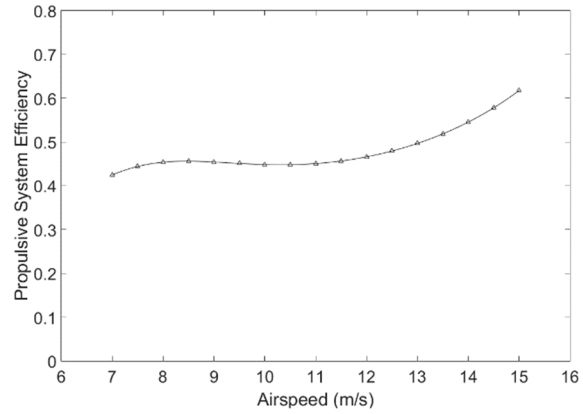

Figure 14 - Propulsive System Efficiency vs Airspeed

The propulsive system efficiency ($\eta_{ESC}\eta_{motor}\eta_{prop}$) can also be extracted by dividing the (P_{req}) by (P_e) and plotting the P_{req}/P_e vs Airspeed (figure 14). This efficiency comprises all the propulsive system components, namely, power module, ESC, electric motor and propeller. So, figure 14 shows the global efficiency of the propulsive system which for cruise speed is near 45%, getting higher for higher airspeeds. The efficiency increase at the end of the curve (for higher speeds) is unusual, but it is due to the negative curvature of the electric power curve (figure 12) at these speeds. This may be caused by measurement errors (sensors) or averages during the data handling.

In order to evaluate the agreement between the theoretical and practical results a comparison of the main aerodynamic and propulsive system indicators was made.

The graphical comparison depicted in figures 15-18 below considered the average value of the air density measured during the flight tests (1.12kg/m^3) and an aircraft weight of 54N, regarding the theoretical results. The presented theoretical results also consider the drag caused by external accessories such as antennas, control arms, camera's canopy, etc. and solar panels influence.

Starting with the aerodynamic efficiency indicators, in figure 15 is depicted the drag and required power curves comparison. The first aspect that stands out is the superior real values of the required power and drag curves when compared to the theoretical results. Considering the cruise speed, there is a difference of 0.44N between the drag curves and 3.47W between the required power curves, this difference is in order of magnitude of the estimated experimental errors and it increases for higher speeds.

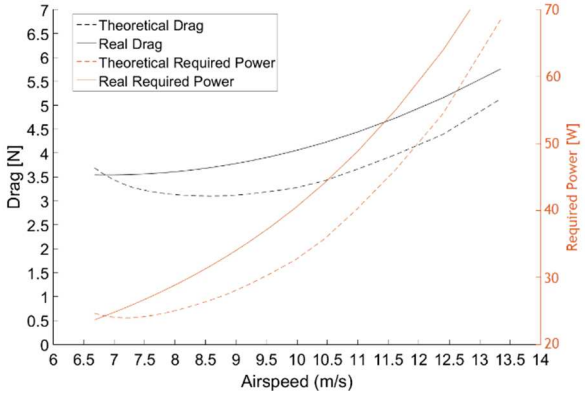

Figure 15 - Power (Real and Theoretical values) vs Airspeed

With respect to the aerodynamic efficiency (L/D), the results are somewhat in concordance with theoretical marks for the cruise speed (7.8m/s). For lower speeds the real values of the aerodynamic efficiency proved to be more optimist, this fact could be justified by the measured error associated with the instability of the flight near the stall speeds. Regarding the $C_L^{3/2}/C_D$ curves the results are similar to the C_L/C_D curve where exists an increasing discrepancy is for lower speeds (figure 16).

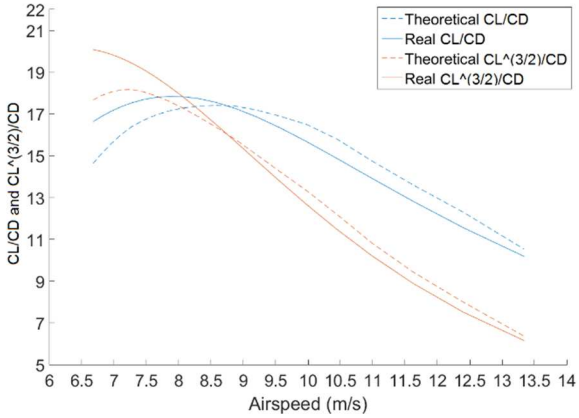

Figure 16 - C_L/C_D vs $C_L^{3/2}/C_D$ vs Airspeed

The propulsive system results depicted in figures 17 and 18 only consider the power used by the electric motor (without on-board systems) and also consider the influence of solar panels and the external accessory's drag. Both the theoretical estimations for the specific range and endurance were obtained considering the same conditions referred above (1,12kg/m^3 air density, 54N of weight, accessories drag) and a 111Wh battery (without external energy of the solar panels).

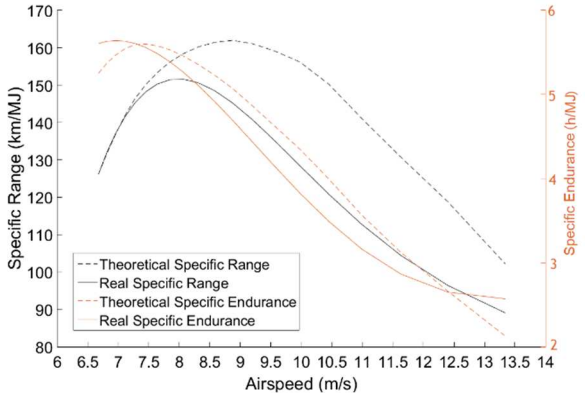

Figure 17 - Specific Range vs Specific Endurance vs Airspeed

The specific range results depicted in figure 17 are, in a certain way, disappointing. For speeds above the cruise speed there is a huge discrepancy between the theoretical and real results, this fact is probably related with the decrease of the propulsive system efficiency for high speeds. Considering a 10m/s LEEUAV's flight for the same amount of energy the aircraft should be able to fly more 27,76km. Similar to the specific range results, the specific endurance is also lower than expected for high speeds, where for the same amount of energy the LEEUAV flies 31,34 minutes less (at 10m/s) than the theoretical results.

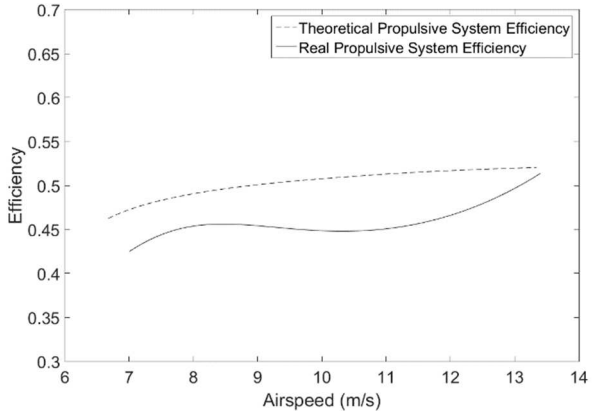

Figure 18 - Propulsive System Efficiency vs Airspeed

The difference between the specific range and endurance curves of figure 17 is a consequence of the poor propulsive system efficiency for high speeds. In this figure 18 is possible to highlight the difference between the theoretical and real measured propulsive system efficiencies. This fact is related with the ESC-motor-propeller efficiencies. However, a deeper study of this system, considering other components (motor, propeller), would be desirable.

6 Conclusions

This work proposed to test and validate all theoretical calculations of the design stage of a long endurance electric unmanned aircraft. The main objectives of this work were successfully achieved. The 10.4hour flight tests of LEEUAV allow to validate the concept and the initial mission requirements, proving its airworthiness.

The flight data retrieved from LEEUAV's on-board sensors allowed to determine the main aerodynamic efficiency indicators such as the C_L, C_D and lift-to-drag ratio. After analysis of the results achieved, the comparison between the theoretical design values of the flight performance prove the reliability of the Mechanical Energy Method used.

The influence of the solar panels thickness in the flight performance was notorious, however the overall aerodynamic performance was very good. Despite the weather conditions at the time of the flight tests did not permit to test the maximum real flight endurance, according to the theoretical estimation, based on the measured power requirements, LEEUAV will be able to fly more than 13h at equinox, in certain conditions.

Although the error analysis is not presented in this article, the estimated experimental error is in agreement with the magnitude of the error of the theoretical results.

Regarding the LEEUAV's future improvements, a higher capacity battery to avail the surplus of solar energy produced during the flight and flight tests experiments with other suitable propellers are some of the recommended enhancements/tasks.

Acknowledgements

I would like to thank my thesis advisor Doctor Pedro Gamboa and my fellows Pedro Santos, Alexandre Duarte and Pedro Moutinho for their contribution to the work here presented.

References

[1] Noth, A. (2008). *History of Solar*. Autonomous Systems Lab, ETH Zürich, Switzerland. Available at: http://www.skysailor.ethz.ch/docs/History_of

_Solar_Flight_v1.2-A.Noth_2006.pdf [Accessed at 28 April, 2016]

[2] Boucher R. J. (1984) History of Solar Flight. In Proc. of the 20th Joint Propulsion Conference, AIAA-84-1429, Cincinnati, Ohio, USA.

[3] Airbus Defense and Space. (2015). Zephyr, the High Altitude Pseudo-Satellite. Available at: https://airbusdefenceandspace.com/our-portfolio/military-aircraft/uav/zephyr/ [Accessed at 5 Jun, 2016]

[4] Frey, T. (2014). 192 Future Uses for Flying Drones. Available at: http://www.futuristspeaker.com/business-trends/192-future-uses-for-flying-drones/ [Accessed at 9 Jun, 2016]

[5] LAETA - Associated Laboratory for Energy, Transports and Aeronautics composed by Centre for Aerospace Science and Technology (CCTAE), Aeronautics and Astronautics Research Centre (AEROG), Institute of Mechanical Engineering (IDMEC) and Institute of Science and Innovation in Mechanical and Industrial Engineering (INEGI)

[6] Duarte, A. (2016). *Development part of the Structure of a Long Endurance Electric UAV*. MSc Thesis. Structures and Vibrations Lab, University of Beira Interior (UBI), Portugal.

[7] Cândido, L. (2014). *Projeto de um UAV Solar de grande autonomia*. MSc Thesis. Structures and Vibrations Lab, University of Beira Interior (UBI), Portugal.

[8] Freitas, L. (2017). *Aerodynamic Analysis of a Forward-Backward Facing Step Pair on the Upper Surface of a Low-Speed Airfoil*. MSc Thesis. Universidade da Beira Interior (UBI), Portugal

[9] Sousa, J. (2015). *Solar System for a Long Endurance Electric UAV*. MSc Thesis. Structures and Vibrations Lab, University of Beira Interior (UBI), Portugal.

[10] Ferreira, T. (2014). *Hybrid Propulsion System of a Long Endurance Electric UAV*. MSc Thesis. Instituto Superior Técnico (IST), Portugal.

[11] Godwin, O., Frazier, F., Durnin, R. (1965). *USAF Performance Flight Test Theory*. USAF Test Pilot School, Edwards AFB, California.

[12] Bridges, P., Cross, E., Boatwright, W. (1977). *Flight Test Evaluation of a Method to Determine the Level Flight Performance of a Propeller Driven Aircraft*. Society of Automotive Engineers.

[13] Albino, A. (2014). *Radiação solar: estudo e criação de plataforma de apoio à conceção de um sensor de radiação solar*. Universidade de Évora, Évora, (Portugal).

[14] Marta, A; Gamboa, P. (2014). *Long Endurance Electric UAV for Civilian Surveillance Missions*. LAETA, CCTAE, Instituto Superior Técnico, Universidade da Beira Interior, Lisboa, Covilhã (Portugal).

LEEUAV's Components

[15] Pixhawk flight controller. (2016). 3D Robotics.

[16] Scherrer RX700LR V7 and Tx700 PRO Long Range. (2016). TSLRS. Denmark.

[17] Oborne, M. Mission Planner software. (2016).

[18] Royal SX 16 Elegance. (2014). Multiplex. Germany.

[19] Ublox NEO-M8N. (2016). Drotek. France

[20] Phoenix Edge 75A Electronic Speed Controller. (2016). Castle Creations. USA.

[21] ZS 3025-10 electric motor. (2016). Hyperion. Hong Kong.

[22] C60 Monocrystalline Silicon Solar Cells. (2016). Sunpower. USA.

[23] GV-10 MPPT Solar Charge Controller. (2016). Genasun. USA.